NTNU – Trondheim
Norwegian University of
Science and Technology

Assessment of Hull Response due to Impact from Falling Object

Andreas Bergstad

Marine Technology
Submission date: June 2014
Supervisor: Bernt Johan Leira, IMT

Norwegian University of Science and Technology
Department of Marine Technology

NTNU
Norwegian University of Science and Technology
Department of Marine Technology

Master's Thesis, Spring 2014

Stud. Techn. Andreas Bergstad

Assessment of Hull Response due to Impact from Falling Object

Vurdering av skrogrespons relatert til støt fra fallende objekt

The objective of this thesis is to assess the resistance of deck structures in ship hulls with respect to impacting objects with particular application to falling containers. This implies that the energy absorption and the deformation of the deck structure need to be analysed. Generally nonlinear finite element methods are required in addition to procedures for estimation of absorbed energy. Furthermore, adequate representation of the material non-linearity at a local level also needs to comprise criteria that define when the transition from large plastic deformations to fracture will occur.

The following subjects are to be examined:

1. Current rules for design of hull components with respect to impact loading are to be reviewed with focus on deck structural members. The general rules from DNV shall be used as a basis.

2. The basic properties of the model for impact analysis shall be described. This includes giving a review of criteria which define the transition from large plastic deformations to fracture of the material (i.e. so-called fracture criteria).

3. Methods for assessment of impact energy and associated structural response shall be reviewed. The ability to quantify this energy shall be demonstrated through a numerical study based on modelling a part of an example deck structure. Sensitivity studies concerning boundary conditions and mesh refinement shall be included. The analysis is to be carried out using the computer program ABAQUS.

4. Parametric studies concerning the modelling of a deck structure and its resistance are to be performed. The effect of changing material parameters will be studied. A comparison study with respect to modelling the falling container as rigid in contrast with deformable, is to be executed.

The work scope may prove to be larger than initially anticipated. Subject to approval from the supervisor, topics may be deleted from the list above or reduced in extent.

In the thesis the candidate shall present his personal contribution to the resolution of problems within the scope of the thesis work.

NTNU
Norwegian University of Science and Technology
Department of Marine Technology

Theories and conclusions should be based on mathematical derivations and/or logic reasoning identifying the various steps in the deduction.

The candidate should utilise the existing possibilities for obtaining relevant literature.

The thesis should be organised in a rational manner to give a clear exposition of results, assessments, and conclusions. The text should be brief and to the point, with a clear language. Telegraphic language should be avoided.

The thesis shall contain the following elements: A text defining the scope, preface, list of contents, summary, main body of thesis, conclusions with recommendations for further work, list of symbols and acronyms, references and (optional) appendices. All figures, tables and equations shall be numerated.

The supervisor may require that the candidate, in an early stage of the work, presents a written plan for the completion of the work.

The original contribution of the candidate and material taken from other sources shall be clearly defined. Work from other sources shall be properly referenced using an acknowledged referencing system.

The thesis shall be submitted in an electronic version:

- Signed by the candidate
- The text defining the scope included
- Drawings and/or computer prints which cannot be bound should be organised in a separate folder.

Supervisor: Professor Bernt J. Leira

Contact person at Wärtsilä Ship Design Norway AS: MSc Roger Johnsen

Deadline: June 10th 2014

Trondheim, May 28th 2014

Bernt J. Leira

Preface

This master's thesis was written during the spring semester of 2014 to satisfy the final requirement of the specialisation programme in Marine Structures of the Department of Marine Technology, the Norwegian University of Science and Technology. Some preliminary work was carried out in the project during the autumn of 2013. Professor Bernt J. Leira proposed the scope of the thesis and supervised the work. The initial topic was developed in collaboration with Wärtsilä Ship Design Norway AS, Fitjar, represented by my co-supervisor MSc Roger Johnsen.

First of all I want to thank Professor Leira for offering a challenging project and for pointing me in the right direction along the way. I also want to thank MSc Johnsen for developing an interesting and relevant topic for my master's thesis. I am also grateful to Professor Jørgen Amdahl and Professor Sören Ehlers for helping me with some key topics through a couple of informative discussions.

I also acknowledge my fellow students at office A1.027 who promoted a good working environment and meaningful discussions. They also made the writing experience enjoyable.

The study has been a slow but maturing learning experience during which I have improved my working methods significantly. My confidence has increased significantly with regards to my specialisation. I also value the much needed brush up of my English writing skills.

Finally I want to thank my lovely Iselin for being my muse.

Trondheim, June 10th 2014

Andreas Bergstad

Abstract

The present study assesses ship hull response of a platform supply vessel due to impact from falling objects. This is carried out primarily by investigating the critical energy absorption and localised deformation to penetration of the deck structure subjected to impact by a falling container. This is made possible by conducting contact simulations with the nonlinear finite element solver Abaqus/Explicit., i.e. explicit time integration of elemental equations of motion by use of the central difference method. Absorbed energy is quantified by integrating the obtained deck resistance/contact force with respect to the deformed distance/indentation. For simplicity the container is assumed infinitely rigid, i.e. kinetic energy from impact is solely absorbed by the deck.

A comparison is made between two steel configurations (conventional ship building steel and Hardox steel) to investigate the possibilities for improved strength, as this can decrease the risk of damage infliction to a liquefied natural gas fuel tank located beneath deck.

Det Norske Veritas rules and standards for application in accidental limit state design are reviewed with particular interest in recommended procedures for dimensioning hull structural members to withstand impact loads. The principle of shared energy dissipation between two colliding bodies is presented analytically. Dimensioning load from a dropped object can be determined, e.g. based on the maximum load capacity of an eventual deck crane. Recommended further, is the application of nonlinear finite element analysis.

A variety of simplified fracture models are reviewed, with specific interest in their ability to predict ductile failure of metal alloys. Dependence of stress triaxiality, plastic stress-strain relation, geometry and size, and strain rate is investigated in relation to the different models.

Nonlinear material behaviour is defined in the finite element model, including true stress-strain relations, strain rate dependence and fracture criteria. The onset of fracture is modelled by introducing an empirical element length-related constant strain fracture criterion in the material definition for conventional steel. Applications of fracture criteria for Hardox steel were not discovered. This led to the narrow definition of one constant value for strain to fracture, as specified in the obtained material parameters. Adjusting yield strength due to

strain rate dependence is included by application of the Cowper-Symonds constitutive equation. Parameter variations of strain rate coefficients clearly show large uncertainties in the estimated resistance force-indentation relation.

Analytical methods for estimation of resistance in plastic collapse and crushing of structural members are applied in comparison with numerical results. Satisfying results are found in the absorbed energy estimates provided by simplified methods concerning in-plane crushing of web girders. Although not completely accurate, these methods provide physical understanding on how to increase the crushing resistance of girders by increasing web thickness. This is namely because the plastic moment capacity is quadratic dependent on the plate thickness.

Hardox steel provides significantly increased capacity in energy dissipation to penetration. However, the specific degree of increase should be verified by further simulations. Experiments of different scale can be compared with numerical analyses, in the aim of discovering a well suited fracture criterion and specifying coefficients applicable in the Cowper-Symonds equation.

Sammendrag

Abstract in Norwegian

Denne studien tar for seg skrogrespons av et plattformforsyningsskip, påvirket av en fallende last. Hovedsaklig studeres kritisk energiopptak og lokaliserte deformasjoner ved penetrering av dekk, utsatt for støtbelastning fra en fallende konteiner. Dette er gjort mulig ved utførelse av kontaktsimuleringer med bruk av den ikkelineær elementmetoden i analyseprogrammet Abaqus/Explicit. Dette programmet løser de elementvise bevegelseslikningene ved bruk av eksplisitt tidsintegrasjon (sentral differanse). Energiopptak blir kvantifisert ved å integrere dekkets motstandskraft ved støt, med hensyn på deformert dybde. For enkelhets skyld blir konteineren antatt å være ikke-deformerbar, da den totale kinetiske energien blir absorbert av dekket.

Sammenlikning av to ulike stålkombinasjoner er blitt utført (konvensjonelle ståltyper og Hardox-stål) for å studere muligheten for økt dekksstyrke, og minsket risiko for skade på underliggende tank som inneholder flytende naturgass.

Det Norske Veritas sine regler og standarer er gjennomgått. Dette er gjort med inngående fokus på anbefalte metoder til bruk i dimensjonering av skrogelementer, for å motstå støtbelastning fra et fallende objekt. Delt energiopptak mellom to kolliderende legemer blir presentert analytisk. Dimensjonerende last for fallende objekt kan fastsettes, f.eks. basert på maksimum lastkapasitet til en eventuell dekkskran. Videre blir det gitt anbefalning til bruk av ikkelineær elementanalyse.

Ulike bruddkriterier presenteres og vurderes ut i fra deres tolkning av brudd som følge av flytning i duktile metaller (mikroskopisk sprekkdannelse). Dette gjøres ved å se på metodenes relasjon til ulike parametre, f.eks. spenningstilstand, forhold mellom plastisk spenning og tøyning, geometri og størrelse, og tøyningsrate.

Ikkelineær materialoppførsel er definert i elementmodellen. Her inkluderes målte relasjoner mellom spenning og tøyning for gitte platetykkelser (basert på innsmalning av det spennede tverrsnitt ved plastisk tøyning), effekt av tøyningsrate og bruddkriterier. Bruddutvikling i konvensjonelle ståltyper modelleres ved bruk av et empirisk utviklet bruddkriterie, der

bruddtøyningen avhenger av elementlengde. Sammenliknbare anvendelser av bruddkriterier er ikke funnet for Hardox-stål. Dette fører til en smal definisjon av bruddkriteriet, da kun én enkelt verdi for bruddtøyning er mottatt. Effekten på flytspenning av tøyningsrate er inkludert ved bruk av Cowper-Symonds-likningen. Store usikkerheter i resultater er vist ved variasjon av parametre i denne likningen.

Dekksmotstand er estimert ved hjelp av forenklede analytiske metoder, som baserer seg på plastisk kollaps og sammenbretting av strukturelementer. Samsvar er observert i forhold til numeriske løsninger, spesielt i bruk av forenklede formler for motstandskraft ved sammenfolding (i planet) av plater og bjelkesteg. Selv om metodene ikke gir sikre resultater, kan de derimot gi økt forståelse for hvordan plastisk bøyemotstand i flytelinjene blir forbedret ved økt platetykkelse. Dette skyldes kvadratisk avhengighet av platetykkelse.

Hardox-stål gir signifikant økning i dekkskapasitet relatert til kritisk energiopptak ved penetrering. Det er likevel ikke mulig å verifisere i hvor stor grad denne økningen er. Ut i fra usikkerhetene de medfører, anbefales det å finne et godt egnet bruddkriterie samt definere gode parametre for å beskrive effekten av tøyningsrate. Dette kan gjøres mulig ved hjelp av gjennomgående sammenlikninger mellom eksperimentelle og numeriske simuleringer, spesielt fokusert mot korrekt definering av ikkelineære materialegenskaper.

Contents

Figures

Tables

Abbreviations

LNG	Liquefied natural gas
DNV GL	Det Norske Veritas & Germanischer Lloyd
DNV	Det Norske Veritas
ALS	Accidental limit state
UKCS	United Kingdom Continental Shelf
PSV	Platform supply vessel
FEM	Finite element method
CAE	Complete Abaqus Environment
FE	Finite element
FEA	Finite element analysis
NLFEM	Nonlinear finite element method
CDM	Continuum damage mechanics
RVE	Reference volume element
GTN	Gurson-Tvergaard-Needleman
CAD	Computer aided design
CL	Centreline
BL	Baseline
BC	Boundary condition
HBW	Brinell hardness number
ASTM	American Society for Testing and Materials

SSAB	Swedish Steel AB
FLD	Forming limit diagram
FLSD	Forming limit stress diagram
NV A	Norske Veritas A (steel grade)
DOF	Degree of freedom
S4R	Conventional stress/displacement shell (S), number of nodes (4) Reduced integration (R)
S3R	Conventional stress/displacement shell (S), number of nodes (3) Reduced Integration (R)
CPU	Central processing unit

Symbols

E_K	Kinetic energy
m_o	Mass of dropped object
v	Impact velocity
g	Gravitational acceleration
h	Drop height from impact area
E_S	Total dissipated energy
$E_{S,O}$	Dissipated energy in dropped object
$E_{S,I}$	Dissipated energy in impacted structure
R_O	Impact load on dropped object
R_I	Impact load on impacted structure
w_O	Indentation of dropped object
w_I	Indentation of impacted structure
P	Contact load
k	Plate stiffness
m_i	Mass of plate within hinge circle
σ_y	Yield stress
σ_u	Ultimate tensile stress
t_p	Plate thickness
d	Inner diameter of drill collar at threaded end
r	Smallest distance from impact point to plate boundary

c	Non-dimensional factor for calculating plate stiffness
τ_{cr}	Critical shear stress
ρ_p	Mass density of plate material
w_f	Lateral tensile fracture displacement of stiffened plate in yield hinges
d_c	Characteristic dimension
c_1	2 for clamped ends, 1 for pinned ends
c_f	Flexibility factor
c_w	Displacement factor
ε_{cr}	Critical strain (corresponding to σ_u)
c_{pl}	Plastic zone length factor
W	Section modulus of beam (stiffener or girder including effective plate flange)
W_P	Plastic section modulus of beam
ε_y	Yield strain
κl	The smaller distance from impact point to adjacent joint
H	Non-dimensional plastic stiffness (Sec. 2) – or folding wave length (Sec. 5)
c_s	Non-dimensional spring stiffness
σ_{cr}	Critical stress (corresponding to ε_{cr})
w_c	Characteristic deformation
A	Cross-section area
E	Young's modulus of beam material
D_p	Diameter of pipe section

k_{eq} Equivalent elastic, axial stiffness

k_{node} Axial stiffness of the nodes considering the member removed (in direction of member neutral axis)

l Length of member

σ^* Stress triaxiality

σ_H Hydrostatic stress

σ_{eq} Equivalent von Mises stress

σ_i Principal stresses, i = 1 – 3

ε_{eq} Equivalent strain

ε_f Fracture strain

D_i Fracture constants, i = 1 – 5

$\dot{\varepsilon}^*$ Dimensionless plastic strain rate

T Temperature

T^* Homologous temperature

$\dot{\varepsilon}_{eq}$ Equivalent strain rate

$\dot{\varepsilon}_0$ 1.0 s^{-1}

$\dot{\varepsilon}_i$ Principal strain rates, I = 1, 2, 3

R Void radii

R_0 Initial void radii

α_{RT} Rice-Tracey constant

ε_{coa} Strain at coalescence

ε_{nuc} Strain at nucleation

E_{eff}	Effective modulus
E	Young's modulus
A_{eff}	Effective resisting area
A_0	Initial area
σ_{eff}	Effective stress
α	Damage exponent that characterises the growth phases of the RVE
D_{cr}	Critical Damage to failure
D_0	Initial damage
ε_{th}	Uniaxial threshold strain
p	Effective accumulated plastic strain
K	Material constant (Ramberg – Osgood power law)
n	Material hardening exponent (Ramberg – Osgood power law)
ν	Poisson's ratio
q_i	Calibration constants i = 1, 2, 3
f	Porosity
f^*	Porosity evolution
σ_m	Macroscopic mean stress
f_c	Porosity at void coalescence
f_f	Porosity at fracture
f_u^*	Porosity evolution at zero stress when stiffness of material is lost
Δt^i	Time increment at time step i

$\boldsymbol{u}^i$	Response at time step *i*
$\dot{\boldsymbol{u}}^i$	Velocity at time step *i*
$\ddot{\boldsymbol{u}}^i$	Acceleration at time step *i*
$\boldsymbol{M}$	Mass matrix
$\boldsymbol{F}$	External force vector
$\boldsymbol{I}$	Internal force vector
ω_{max}	Maximum element eigenvalue (for calculation of stable time increment)
ρ	Mass density
σ_{prop}	Plateau stress (true stress)
σ_{y2}	Stress-strain curve parameter (true stress)
ε_{py}	Plastic yield strain
ε_{py2}	Stress-strain curve parameter
σ_y^D	Dynamic yield stress
C	Cowper – Symonds coefficient
q	Cowper – Symonds coefficient
μ	Friction coefficient
δ	Indentation
M_0	Plastic moment capacity
E_i	Internal energy dissipation
E_e	External energy
P_{cr}	Critical collapse force

$P(\delta)$ Instantaneous resistance force

P_m Mean crushing force

σ_0 Flow stress

E_{tot} Total dissipated energy

N_0 Membrane force capacity

A_d Deformed area

λ Effective crushing factor

t_{px} Equivalent plate thickness in longitudinal direction

t_{py} Equivalent plate thickness in transverse direction

Software

Abaqus/CAE	Finite element analysis (FEA) software (Dassault Systémes, 2014)
Sesam GeniE	Program for computer aided design (CAD) and analysis of marine structures (DNV GL, 2014)

1 Introduction

Liquefied natural gas (LNG) is the fuel of the future according to the *Annual Report 2013* presented by Det Norske Veritas & Germanischer Lloyd (DNV GL, 2014). Stricter emission limits and economic efficiency requirements lead to increasing numbers of LNG-fuelled ships. DNV GL predicts a growth of up to 1000 LNG-fuelled ships by the year 2020. This also introduces new risks with regards to on-board safety. The storage temperature for LNG is -163 °C. At this temperature and liquid state, the volumetric percentage is at a level of 0.167 % compared to its gaseous state (Blikom, 2013). Leakage may cause serious damage, primarily by;

- Cryogenic effects, i.e. freezing temperatures, causing steel to become brittle, and breakage in turn causing harm to the crew and cargo. Also,
- Liquid evaporates (primarily methane) and blends with air into a flammable mixture (5 – 15 % gas) which is easily ignited. In the worst case scenario, contained gas may create explosions.

To avoid external damage that may cause leakage, LNG fuel is stored in a separate tank or membrane tank beneath the deck of a ship. Rules exist to define the location and requirements of an LNG fuel tank, e.g. Det Norske Veritas (DNV) Rules for Classification of Ships Pt. 6 Ch. 13 (DNV, 2014).

Even though proper safety measures are observed, extreme load scenarios and human error can lead to catastrophe. Loads and accidents of this nature are commonly referred to as accidental limit state (ALS) and include the following scenarios (Moan, 2003);

- Fire or explosion;
- Ship collision;
- Grounding;
- Dropped objects;
- Unintended load distribution on deck;
- Sudden change of pressure difference, e.g. in a pressure vessel.

The particular focus in this thesis was on the accidental load scenario of a dropped object. Dropped objects or falling loads comprise;

- Any object dropped from a crane or other lifting equipment;
- Man over board accident;
- Crane fall;
- Accidental drop of lifeboat.

For the UK continental shelf (UKCS) alone the reported annual frequency of dropped objects per vessel or installation in the period 1990 - 2007 was 1.1 (Oil & Gas UK, HSE, 2009). Apart from possibly damaging the structure and cargo underneath, dropped object accidents may lead to serious injuries and fatalities to the crew.

The object will be exemplified by a standard 20 foot container impacting an example ship deck. Quantifying the deck's capacity to absorb kinetic energy when deformed by the container is the main aim of this thesis. How the resistance to penetration is affected by using Hardox steel (SSAB, 2014) is of particular interest. The deck model is based on that of a platform supply vessel (PSV) of design VS 4411, by Wärtsilä Ship Design Norway AS. The vessel type is displayed in Figure 1. This ship is powered by a dual-fuel machinery system that allows for combustion of light fuel oil, low pressure natural gas (regasified LNG) and various other liquid fuels (Wärtsilä, 2013).

Figure 1: VS 4411 LNG PSV (Wärtsilä, 2013)

In order to address the objectives, structural analyses were carried out to assess the response of the deck to the impact of the falling container. This might have comprised experimental, analytical and numerical methods, and analyses of past accidents. This project was however limited to numerical and analytical approaches.

The finite element method (FEM) was applied for the numerical simulations. Abaqus was the chosen program, primarily because of its ability to handle nonlinear problems. In addition to the graphical interface provided to the user, a large variety of analyses can be carried out in the Abaqus/CAE package (Dassault Systémes, 2014). Abaqus/CAE provides implicit (Abaqus/Standard) and explicit (Abaqus/Explicit) solution techniques, which is convenient when studying dynamic problems with nonlinear response. The main results presented in this thesis were generated from assessing the resistance force in relation to indentation of a finite element (FE) model generated in Abaqus.

When applying the FEM in structural analysis, the modelling and parameter definition is critical. The three following concepts are the ground pillars of a traditional finite element analysis (FEA) of structures with linear-elastic material behaviour and small deformations (Fish & Belytschko, 2007);

- Equilibrium of each element (in terms of internal forces);
- Compatibility of deformations (no gaps or overlaps between elements after deformation);
- Constitutive law: Hooke's law for elastic stress-strain relation.

These, however, are too restricted when considering impact problems with large deformations. Nonlinear responses introduce new problems of geometrical and constitutive nature (Chapter 12 of Moan (2003)). When deformations are large, the geometry of a structure changes, i.e. nonlinear geometrical behaviour is observed. To predict the structural response correctly, the reference geometry needs to be updated incrementally. In dynamic analyses, erroneous results may arise if the response over time is calculated with an insufficient number of time increments.

Assessing nonlinear material behaviour is also essential when determining the response of a structure. Elastic-plastic material properties should be defined by applying;

- An initial yield criterion (yield stress vs. strain);
- A hardening rule where the yield condition is modified due to the history of plastic flow (commonly used are *kinematic* and *isotropic* hardening rules);
- A flow rule that updates the plastic stiffness (tangent modulus) by using an incremental stress-strain relationship.

The correct elastic-plastic behaviour of a material can be obtained from tensile tests. The results can be displayed by either of the following; engineering stress-strain relation, calculated using the initial geometry of the tensile specimen as reference, or a true stress-strain relation, which is calculated by updating the reference geometry as the cross-section of the tensile specimen reduces. Effectively, a true stress-strain curve describes the elastic-plastic material behaviour in an instantaneous manner. The true stress-strain formulation was therefore used in the FE analysis.

To assess possible errors in the FE solution, convergence tests based on mesh refinement and time increment size were carried out.

Parametric studies were carried out for variables that can influence the resistance and energy absorption of the deck. The following factors were considered relevant;

- Transient effects (strain rate) on yield strength;
- Friction due to relative sliding between colliding bodies;
- Impact velocity;
- Boundary conditions (BC’s);
- Fracture strain

Correct modelling of fracture is essential when dealing with nonlinear response of impact loaded structures. Fracture mechanics were therefore reviewed, and simplified criteria for predicting the onset of fracture were investigated.

A comparison study was executed, assessing the critical impact energy absorption to penetration of the deck. Four different impact locations were tested. The effects of modelling the container as deformable were studied. Finally the deck was tested with two different steel configurations; conventional shipbuilding steel vs. Hardox steel.

Analytical methods were also reviewed and tested with a simple deck model for comparison with numerical results. Plastic hinge theory was applied to assess the critical load to collapse. Other simplified methods were also tested, based on the assumed plastic deformation mechanisms of structural members. The main focus was on in-plane loaded plates and girders and perpendicular loaded plates. The methods were used to analytically predict the resistance force in relation to indentation. This was further used to calculate energy dissipation in the deck structure. Hong & Amdahl (2008) presented an extensive review of a variety of simplified methods. Material representation in these models is however poor due to the assumption of elastic-perfectly plastic material, so the results are only expected to provide an indication of the load-response relation.

Relevant DNV GL rules and standards in the design of hull components were reviewed. Primarily rules intended for dimensioning deck structural members to resist impact loading.

2 Relevant Rules and Standards

Rules that are applicable for the structural design of an impact loaded were reviewed, specifically rules relevant to dropped objects. DNV Offshore Standards and Recommended Practices are relevant and contain, among others, rules for the structural design of offshore ships and ALS design.

2.1 Current Rules

The relevant rules for design of impact loaded ship structures are:

- Offshore Standards
    - *DNV-OS-A101: Safety Principles and Arrangements* (DNV, 2013a)
    - *DNV-OS-C102: Structural Design of Offshore Ships* (DNV, 2012b)
- Recommended Practice
    - *DNV-RP-C204: Design Against Accidental Loads* (DNV, 2010)
    - *DNV-RP-C208: Determination of Structural Capacity by Non-linear FE analysis Methods* (DNV, 2013b)

According to DNV Offshore Standards, all accidental loads that are relevant and have an annual frequency of occurrence greater than 10^{-4} needs to be taken into account in the safety design (DNV, 2013a). According to statistics from the UKCS alone, the annual frequency of dropped loads occurring per floating offshore structure was 1.1 in the years 1990-2007 (Oil & Gas UK, HSE, 2009). If dropped objects are relevant accident scenarios in the design of a vessel, the maximum impact energy must be calculated in addition to the energy absorption capability of the hull structure.

2.2 Requirements

The specific requirements concerning accidental loads are given in *DNV-OS-A101* (DNV, 2013a).

2.2.1 Crane and lay down area

The placement of the crane and the arrangement of the lay down area is an important element of the design, and a major safety concern, i.e.:

- The crane load should not be handled close to pressurized hydrocarbon equipment and containers, safety equipment and hazardous inventories. If this cannot be avoided, special protective measures should be adopted.
- Necessary constraints should be used to secure loose loads to prevent uncontrolled movement, especially on floating structures.
- The lay down area should be located at safe distance from any hazardous areas.
- Tough barriers should be placed around the lay down area in to prevent damage to nearby equipment.

2.2.2 Dimensioning accidental load

The maximum crane load capacity (if present) should be used to calculate the kinetic energy E_K of the dropped object in an impact analysis. This is estimated accordingly (for parameter descriptions see Symbols);

$$E_K = \frac{1}{2} m_o v^2, where\ v = \sqrt{2gh} \quad (1)$$

2.2.3 Design against dropped load

The structural members of the deck need to be designed so that the load bearing capacity of the whole ship is intact after an accidental load has occurred. For dropped loads the structural integrity of the whole ship is normally not compromised, but local damage and consequences of such may lead to catastrophic results. The impact energy from the dropped load will mostly dissipate in the structure as strain energy, which invokes high plastic strains. Methods for

quantifying resistance (energy dissipation) and design of structural members are discussed in the next Section.

2.3 Recommended Design Methods

DNV-RP-C204 (DNV, 2010) was used as reference in the following.

2.3.1 Structural resistance

Impact energy from the falling load for the case of a dropped object can be estimated by Eq. (1). The resistance of the structure can be quantified by the dissipation of elastic and plastic strain energy. The structural resistance can be represented by a load (R)-deformation (w) curve (as shown in Figure 2) for both the object and the impacted structure, where the areas under the curves are the dissipated strain energies.

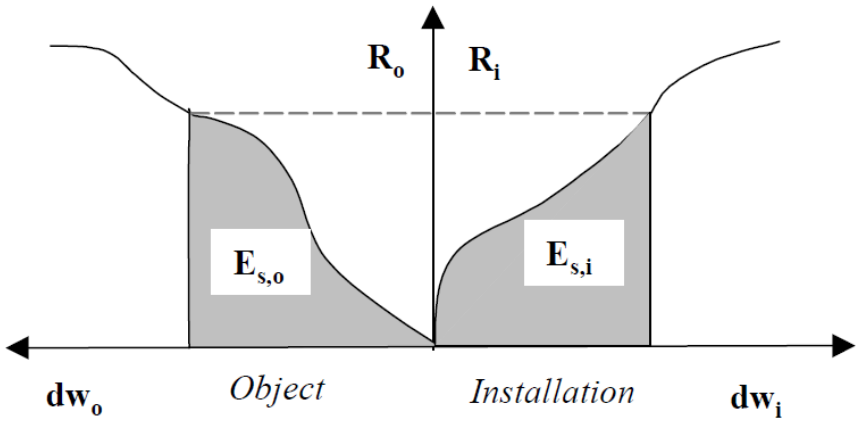

Figure 2: Resistance force vs. indentation for installation and dropped object (DNV, 2010)

An analytical expression can be defined for the total dissipated energy E_S, by integration of the force-indentation curves (subscripts I and O denote the installation and object respectively).

$$E_S = E_{S,I} + E_{S,O} = \int_0^{w_{I,max}} R_I dw_I + \int_0^{w_{O,max}} R_O dw_O \qquad (2)$$

In an impact simulation (e.g. using the FEM), the object could be conservatively assumed as infinitely rigid. This would introduce a high level of safety in the design, dimensioning the installation to absorb all energy in a collision.

2.3.2 Dimensioning of plates and stiffeners

In Sections 4 and 6 of *DNV-RP-C204* (DNV, 2010) methods for dimensioning plates and stiffeners with simple formulas are presented. Different impact spots on the deck must be considered (e.g. in top of or between girder(s) and/or stiffener(s)), in addition to the impact energy and the ultimate material limits. The simple method for pipes dropped on stiffened plates will be presented here. The dissipated strain energy can be defined by the following equation (for parameter descriptions see Symbols).

$$E_S = \frac{P^2}{2k}\left(1 + 0.48\frac{m_i}{m_o}\right)^2 \tag{3}$$

The plate stiffness *k* is expressed by;

$$k = \frac{1}{2}\pi\sigma_y t\left(\frac{1 + 5\frac{d}{r} - 6c^2 + 6.25\left(\frac{d}{2r}\right)^2}{(1+c)^2}\right) \tag{4}$$

The contact force *P*;

$$P = \pi dt\tau, \tau \leq \tau_{cr} \tag{5}$$

The critical shear stress τ_{cr};

$$\tau_{cr} = \sigma_u\left(0.42 + 0.41\frac{t}{d}\right) \tag{6}$$

The plate mass m_i enclosed by a plastic hinge circle;

$$m_i = \rho_p \pi r^2 t \tag{7}$$

And the constant *c* can be expressed by;

$$c = -\exp\left(-2.5\left(1 - \frac{d}{2r}\right)\right) \tag{8}$$

By these equations it is possible to describe how the energy will dissipate as strain energy in a stiffened plate subjected to a dropped object. The position of the dropped object will decide the value of *r* as shown in Figure 3.

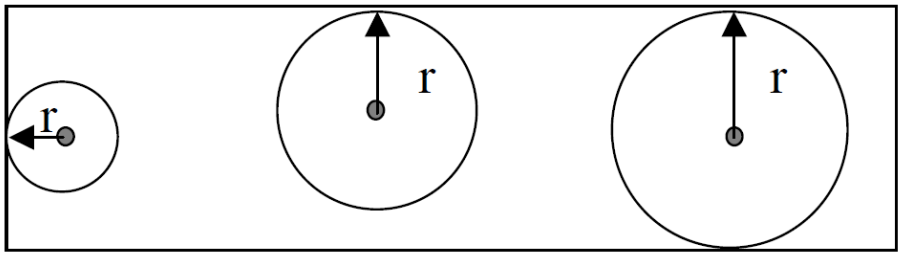

Figure 3: Distance r from impact area to plate boundaries (DNV, 2010)

In Section 6 of the same document, methods for dimensioning the stiffeners and girders (using the effective width of the plate between the stiffeners as a flange) are presented with different load conditions and boundary conditions. This will not be presented in detail in this thesis.

2.3.3 Fracture criterion

DNV have also developed a simplified method for calculating a tensile fracture criterion in yield hinges, which is documented in Section 3 of *DNV-RP-C204* (DNV, 2010). Rupture initiates when the plastic strain reaches a certain limit. The associated lateral displacement w_f at failure for a stiffened plate can be calculated by the following formulae (for parameter descriptions see Symbols);

$$\frac{w_f}{d_c} = \frac{c_1}{2c_f}\left(\sqrt{1 + \frac{4c_w c_f \varepsilon_{cr}}{c_1}} - 1\right) \tag{9}$$

The displacement factor c_w is;

$$c_w = \frac{1}{c_1}\left(c_{pl}\left(1-\frac{1}{3}c_{pl}\right)+4\left(1-\frac{W}{W_p}\right)\frac{\varepsilon_y}{\varepsilon_{cr}}\right)\left(\frac{\kappa l}{d_c}\right)^2 \tag{10}$$

The plastic zone length factor c_{pl} is;

$$c_{pl} = \frac{\left(\frac{\varepsilon_{cr}}{\varepsilon_y}-1\right)\frac{W}{W_p}H}{\left(\frac{\varepsilon_{cr}}{\varepsilon_y}-1\right)\frac{W}{W_p}H+1} \tag{11}$$

The axial flexibility factor c_f is;

$$c_f = \left(\frac{\sqrt{c_s}}{1+\sqrt{c_s}}\right)^2 \tag{12}$$

The non-dimensional plastic stiffness H is;

$$H = \frac{1}{E}\left(\frac{\sigma_{cr}-\sigma_y}{\varepsilon_{cr}-\varepsilon_y}\right) \tag{13}$$

The non-dimensional spring stiffness c_s;

$$c_s = \frac{4c_1 k_{eq} w_c^2}{\sigma_y A l} \tag{14}$$

The characteristic plastic deformation w_c;

$$w_c = \frac{D_p}{2}\ (tubular\ beam) = \frac{1.2W_P}{A}(Stiffened\ plate) \tag{15}$$

Finally the equivalent elastic stiffness k_{eq} is found by;

$$k_{eq} = \left(\frac{1}{k_{node}}+\frac{l}{2EA}\right)^{-1} \tag{16}$$

A table of critical strains (at σ_u) for conventional steel types can be seen in Table 1.

Table 1: Critical strain and non-dimensional plastic stiffness, bi-axial stress state (DNV, 2010)

Steel grade	ε_{cr}	*H*
S 235	20 %	0.0022
S 355	15 %	0.0034
S 460	10 %	0.0034

The concepts described above may also be applied in different nonlinear finite element method (NLFEM) software to study the capacity of a structure subjected to extreme load conditions. Of particular interest is the dimensioning dropped load, and method for assessing the critical energy absorption to failure. DNV GL presents recommended guidelines in *DNV-RP-C208* (DNV, 2013b) to carry out a nonlinear FEA in a sufficient manner.

3 Modelling of Ductile Failure

Basic fracture mechanisms were reviewed with the aim to show how these can be practically applied to define a variety of simplified fracture criteria. Modelling the response of a structure becomes increasingly complicated and nonlinear after the stresses in the structure surpass the ultimate material limits. Modelling plastic deformations in a material is a challenge in itself. When the plastic strains become too large, a new challenge arises when the initiation and propagation of fracture governs the material response. The NLFEM is a frequently applied tool to model and analyse failure response. However, choosing a fracture criterion can be a challenge. An understanding of fracture mechanisms at a microscopic level is essential to define the onset of fracture.

3.1 Fracture Mechanics

Most metal alloys fail by ductile fracture when the plastic deformations become too high. The fracture is initiated by microscopic voids that increase in size and then unite to develop a crack (Alsos, et al., 2009). The process from nucleation to fracture is shown in Figure 4. This type of plastic crack initiation is typical for a ductile fracture, characterized by large fracture toughness where the crack grows due to a critical level of strain ahead of the crack (Berge, 2006).

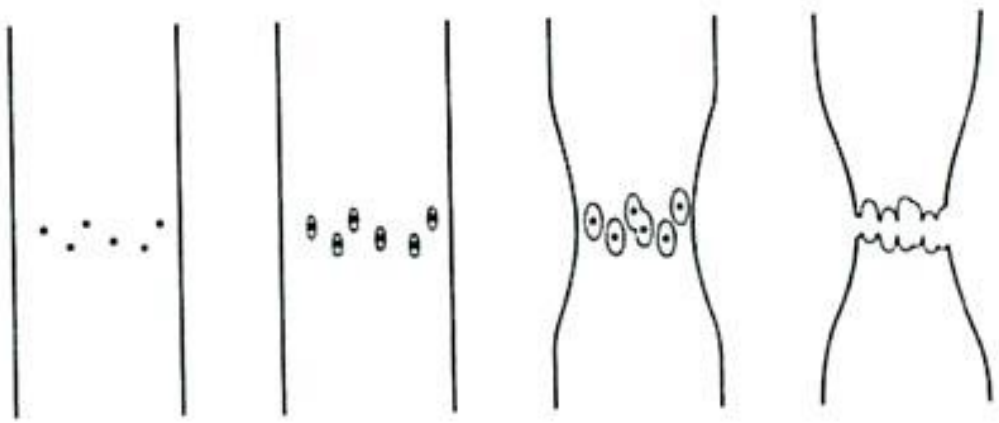

Figure 4: Void nucleation, growth and coalescence in a ductile fracture (Weck, n.d.)

In FE models of large structures it is computationally too expensive to model void growth at such a small scale. Many attempts have been made to model the onset and propagation of fracture by defining a damage variable *D* (Rice & Tracey, 1969; Tvergaard & Needleman, 1984; Johnson & Cook, 1985; Bonora, 1997). This factor is dependent on the stress and strain state, and fracture mechanism of the material.

3.2 Fracture Criteria

Nonlinear response must be accounted for in the design of a structure, e.g. should it be subjected to ALS-loads such as ship on ship/installation, explosions or dropped containers. Large plastic deformations to fracture of structural members must be included in the response. The risk of subsequent collapse should be assessed in relation to environmental loads and extreme loads at a later stage.

As mentioned above, the fracture in most metal alloys is ductile. This includes fractures in steel members used in ships and offshore structures. To successfully model ductile fracture in an efficient manner, different fracture criteria are needed. Ductile fracture depends on key factors such as; stress triaxiality, plastic strain, geometry and size, and strain rate. Fracture criteria depend differently on these factors, related to how they're defined. This can range from simple empirical model definition (e.g. from a series of tensile tests) to models based on the physical nature of the fracture. Törnqvist (2003) sorted a number of different fracture criteria into four categories; empirical criteria, void growth models, continuum damage models and porosity based models. He further presented an extensive review of these four categories in his PhD thesis *Design of Crashworthy Ship Structures*. These will be discussed shortly after a brief description of the stress triaxiality parameter.

3.2.1 Stress triaxiality

The level of triaxiality can be given by a factor that describes the multiaxial stress state in tension or compression. It can be calculated by Eq. (17).

$$\sigma^* = \frac{\sigma_H}{\sigma_{eq}} = \frac{\frac{1}{3}(\sigma_1 + \sigma_2 + \sigma_3)}{\sqrt{\frac{1}{2}((\sigma_1 - \sigma_2)^2 + (\sigma_2 - \sigma_3)^2 + (\sigma_1 - \sigma_3)^2)}} \tag{17}$$

Here σ_1, σ_2 and σ_3 are the principal stresses, σ_H is the hydrostatic stress and σ_{eq} is the equivalent von Mises stress (Johnson & Cook, 1985).

3.2.2 Empirical criteria

Many empirical fracture criteria have been developed that depend on a certain stress, strain or plastic work/volume to fracture. The simplest criteria can only be applicable to specific situations, and can for instance be based on experiments of a special structure (e.g. a stiffened plate) and material. Examples of such are presented in the following.

Ehlers (2010a) executed tensile tests and punch tests to determine the stress-strain relation to fracture for mild steel. Local deformations were obtained using an optical measurement system. The test specimens were grouped into facets with different pixel sizes. Fracture strains could then be measured based on the reference geometry of these pixels. This resulted in an empirical fracture model (shown in Figure 5) depending on element (pixel) size, to be used in nonlinear FEA.

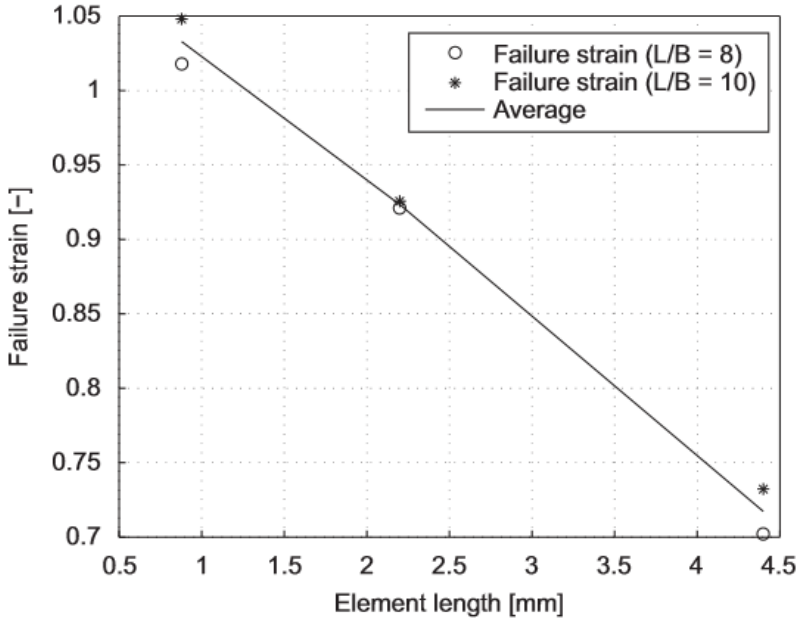

Figure 5: Failure strain vs. element length for different specimen sizes (Ehlers, 2010a)

A more complicated fracture criterion was developed by Johnson & Cook (1985), and is expressed in Eq. (18).

$$D = \int \frac{d\varepsilon_{eq}}{\varepsilon_f} \tag{18}$$

The fracture strain ε_f depends on strain rate, triaxiality σ^*, homologous temperature T^* and the dimensionless plastic strain rate $\dot{\varepsilon}^*$ in the following way;

$$\varepsilon_f = [D_1 + D_2 \exp(D_3\sigma^*)\,][1 + D_4 \ln(\dot{\varepsilon}^*)][1 + D_5 T^*] \tag{19}$$

D_i (for i = 1-5) are constants that need to be calibrated between results from experiments and FEA by varying the temperatures, stress states, etc. The dimensionless plastic strain rate can be expressed by this equation:

$$\dot{\varepsilon}^* = \frac{\dot{\varepsilon}_{eq}}{\dot{\varepsilon}_0} = \frac{\sqrt{\frac{2}{9}((\dot{\varepsilon}_1-\dot{\varepsilon}_2)^2+(\dot{\varepsilon}_2-\dot{\varepsilon}_3)^2+(\dot{\varepsilon}_1-\dot{\varepsilon}_3)^2)}}{1.0s^{-1}} \tag{20}$$

The homologous temperature T^* can be expressed by;

$$T^* = \frac{T - T_{room}}{T_{melt} - T_{room}} \tag{21}$$

When the damage parameters are determined, it is possible to use the Johnson-Cook model to define the onset of fracture in FEA software such as Abaqus (Dassault Systèmes, 2012).

3.2.3 Void growth models

These criteria are logically based on the growth of microscopic voids. As described by Törnqvist (2003), the Rice-Tracey and McClintock models are some of the most known void growth models. Discussed here is the Rice-Tracey model, which has shown to give satisfying results for damage prediction. Rice & Tracey (1969) observed that the relative void growth per unit applied strain has an exponential growth with respect to the transverse stress. Fracture initiates when the voids coalesce. This is assumed to happen when the void radii reaches a certain limit for R, shown in Eq. (22).

$$\ln\left(\frac{R}{R_0}\right) = \int_{\varepsilon_{nuc}}^{\varepsilon_{coa}} \alpha_{RT} \exp\left(\frac{3\sigma_H}{2\sigma_{eq}}\right) d\varepsilon_{eq} \tag{22}$$

where ε_{coa} and ε_{nuc} are the equivalent strains at void coalescence and nucleation respectively. α_{RT} is a material constant, which for mild steel was calculated to be 0.283 by Rice and Tracey . Others have predicted the parameter to be 0.427 (Törnqvist, 2003). In Figure 6, the spherical void expansion is shown for a specific strain rate field (in the x_3 – direction)

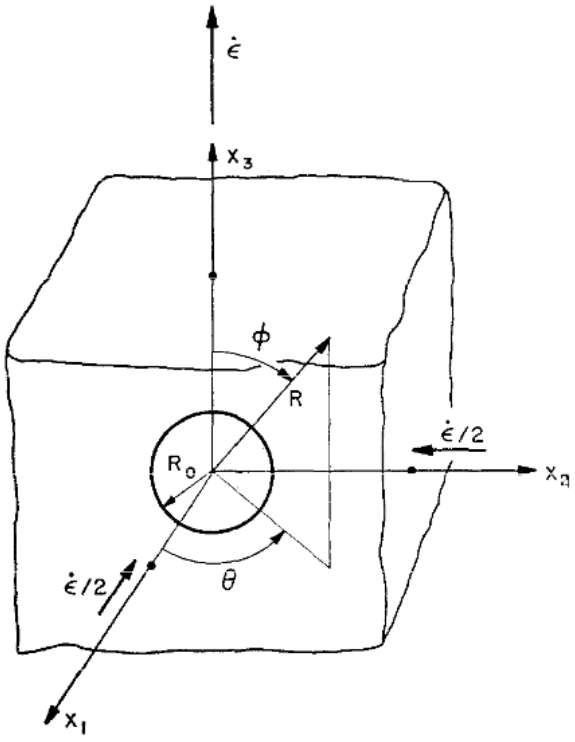

Figure 6: Spherical void in a remote simple tension strain rate field (Rice & Tracey, 1969)

3.2.4 Continuum damage models

Different continuum damage mechanics (CDM) models have been developed and are reviewed thoroughly by Törnqvist (2003). Presented here is the nonlinear CDM model developed by Bonora (1997).

The CDM models are based on damage due to the reduction of material resistance when it is loaded. This is based on the assumption that microscopic voids are evenly spread out in the material. The material damage D can then be expressed by the effective elastic modulus E_{eff}, as shown in Eq. (23), alternatively by the effective area A_{eff} as shown in Eq. (24).

$$D = 1 - \frac{E_{eff}}{E} \tag{23}$$

, or the effective area of the specimen;

$$D = 1 - \frac{A_{eff}}{A_0} \tag{24}$$

This is deterioration is illustrated in Figure 7.

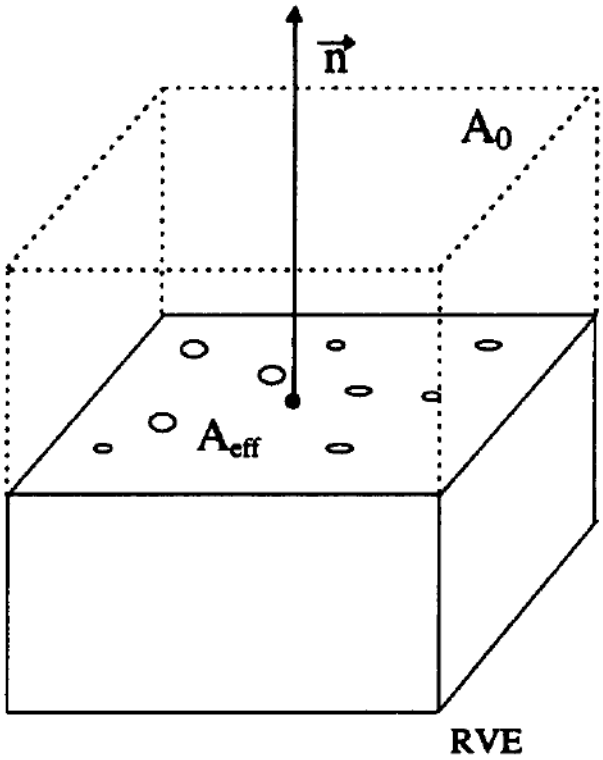

Figure 7: Damage evolution in a reference volume element (RVE) (Bonora, 1997)

Based on the above it is possible to describe the effective stress σ_{eff} in the element, using Eq. (25):

$$\sigma_{eff} = \frac{F}{A_{eff}} = \frac{F}{A_0(1-D)} = \frac{\sigma}{(1-D)} \tag{25}$$

This parameter accounts for material degradation by adjusting the load bearing area due to deformation (similar to the true stress). This introduces an important part of the model in that the strain at void evolution under the true stress state is assumed to be equivalent to the strain

of the undamaged body under the effective stress (strain equivalence). This means that it is possible to use the constitutive equations for the undamaged material, applying the effective stress instead of the nominal stress to describe the damage evolution.

Reference is made to Bonora (1997) for full deduction of the damage evolution law. The final expression is presented in Eq. (26);

$$dD = \frac{\alpha(D_{cr} - D_0)^{\frac{1}{\alpha}}}{\ln(\varepsilon_f) - \ln(\varepsilon_{th})} f\left(\frac{\sigma_H}{\sigma_{eq}}\right)(D_{cr} - D)^{\frac{\alpha-1}{\alpha}}\frac{dp}{p} \tag{26}$$

D_{cr} is the critical damage at failure, D_0 is the initial damage, ε_f is the uniaxial strain at failure, ε_{th} is the uniaxial plastic strain threshold, D is the damage parameter and α is a damage exponent that characterises the growth phases of the RVE under the accumulated strain p. The accumulated strain has the following relation to the effective equivalent von Mises stress:

$$\sigma_{eff,eq} = \frac{\sigma_{eq}}{1 - D} = Kp^{\frac{1}{n}} \tag{27}$$

K and n are material constants for hardening. The triaxiality function is;

$$f(\sigma^*) = \frac{2}{3}(1 + \nu) + 3(1 - 2\nu)(\sigma^*)^2 \tag{28}$$

The stress triaxiality σ^* is calculated by Eq. (17), and ν is the Poisson's ratio. Thus the damage evolution will be highly dependent on the triaxiality.

3.2.5 Porosity based models

The porosity models are similar to the CDM models, but base the damage criteria on the volume fraction of the voids in the material. This fraction f has a range from 0 where the yield function is a standard von Mises function, to 1 where the yield surface is minimized to a point (Törnqvist, 2003). An example of a porosity based model is the modified Gurson model, referred to as the Gurson-Tvergaard-Needleman (GTN) by Törnqvist (2003). Tvergaard and Needleman modified the expression from the basis of one void to account for the growth of multiple voids. Tvergaard (1981) firstly adjusted the model with constants to calibrate with experiments, and Tvergaard & Needleman (1984) adjusted the volume fraction expression to

account for the natural evolution of voids; separating the expression in nucleation and coalescence behaviour. This resulted in the following expression;

$$F = \left(\frac{\sigma_{eq}}{\sigma_y}\right)^2 + 2q_1 f^* \cosh\left(q_2 \frac{3\sigma_m}{2\sigma_y}\right) - 1 - (q_3 f^*)^2 \tag{29}$$

Here σ_m is the macroscopic mean stress, q_1, q_2 and q_3 are the calibration constants added by Tvergaard (1981), while f^* is the porosity evolution expressed by Tvergaard & Needleman (1984);

$$f^* = \begin{cases} f & f \leq f_c \\ f_c + \dfrac{f_u^* - f_c}{f_f - f_c}(f - f_c) & f > f_c \end{cases} \tag{30}$$

where f is the porosity, f_c is the porosity at void coalescence, f_f is the porosity at fracture and f_u^* is equal to f^* at zero stress when the material has lost all its stiffness.

4 Numerical Method

The simulations carried out for this thesis were dynamic and the response nonlinear. This required the use of a numerical analysis method to study the structural resistance of the given deck structure impacted by a falling container. The NLFEM was the obvious choice. Abaqus/CAE (Dassault Systémes, 2014) was applied due to its graphical interface and ability to solve nonlinear problems. However the program does pose weaknesses for the geometrical modelling of the deck structure. A more suitable program for this is the DNV software Sesam GeniE (DNV GL, 2014). This is an excellent program to make 3D plate models that can be exported to numerous other programs, in this case as an ASIS SAT-file. The *Sesam^{TM} User Manual GeniE Vol. III* (DNV, 2013c) was used as reference for the design and exportation of the model.

4.1 Geometrical Model

4.1.1 Deck structure

To make the analysis relevant and realistic, co-supervisor Johnsen (2014, pers. comm., 29 January) from Wärtsilä Ship Design provided drawings of a platform supply vessel (PSV). The deck structure above the LNG fuel tank was the area of interest. 3D models were made in Sesam GeniE, which could accurately represent the structure in close vicinity of the LNG tank. The container model was also made in Sesam GeniE.

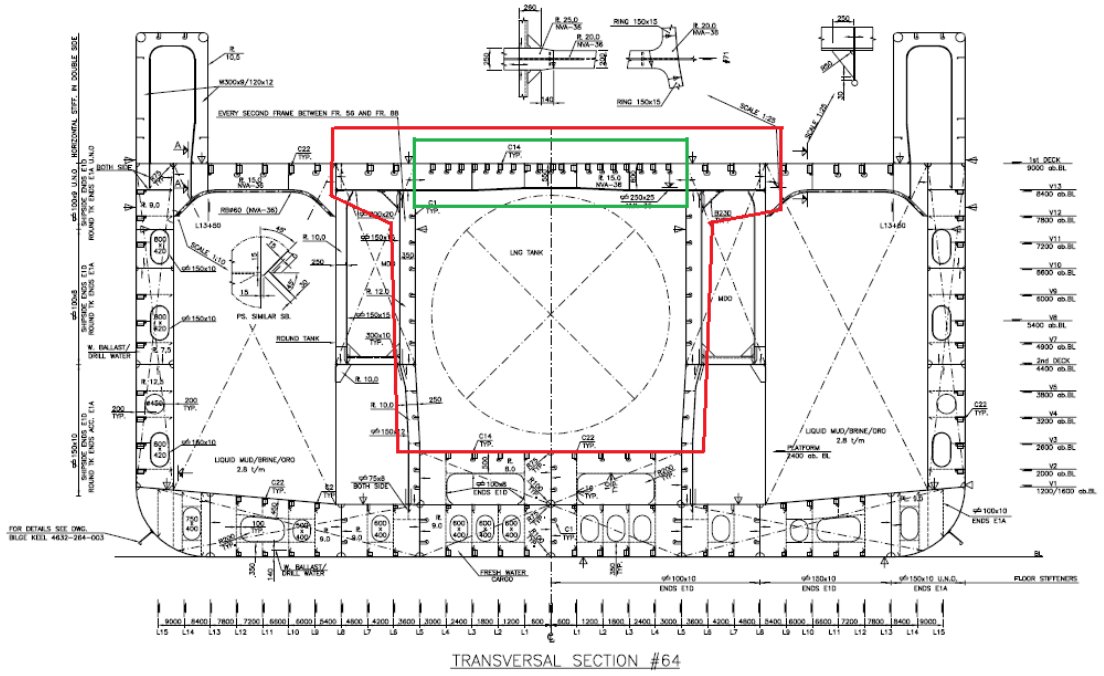

Figure 8: Extent of geometrical models designed in Sesam GeniE

The mid ship section drawing in Figure 8 shows a typical web frame for the PSV. The relevant scantlings used for the 3D design are listed in Appendix B, while the section scantlings as-built can be studied in the structural drawings shown in Appendix D. The structural details were represented well with plate element, only reducing the ability to model bulb stiffeners and cut-outs (around longitudinal stiffeners). The principal particulars for the PSV are listed in Table 2.

Table 2: Principal particulars

Length over all	89.2 m
Length betw. perp	80.4 m
Breadth mld.	19.0 m
Depth	9.0 m
Scantling draught	7.6 m
Transv. frame spacing	0.60 m
Block coeff.	0.79
Design speed	15.3 knots

4.1.2 Model 1

Sesam GeniE is a program developed by DNV GL, applicable for design and analysis of marine structures. In the present thesis it was used because of its computer aided design (CAD) possibility only. Model 1 was first made (within red lines in Figure 8) to represent the deck over the LNG tank. Some of the surrounding structure (deck and bulkheads) was included to examine if any global reactions to an impacting object were observed. The section scantlings of the model are listed in Appendix B. The extent of the model is described in the following;

- Longitudinal extent: frame #58 to #88.
- Transverse extent: up to 4800 mm from centreline (CL).
- Vertical extent: from platform 2400 mm above baseline (BL) to main deck 9000 mm above BL.

A half model was made to be mirrored about the centreline (as shown in Figure 9)

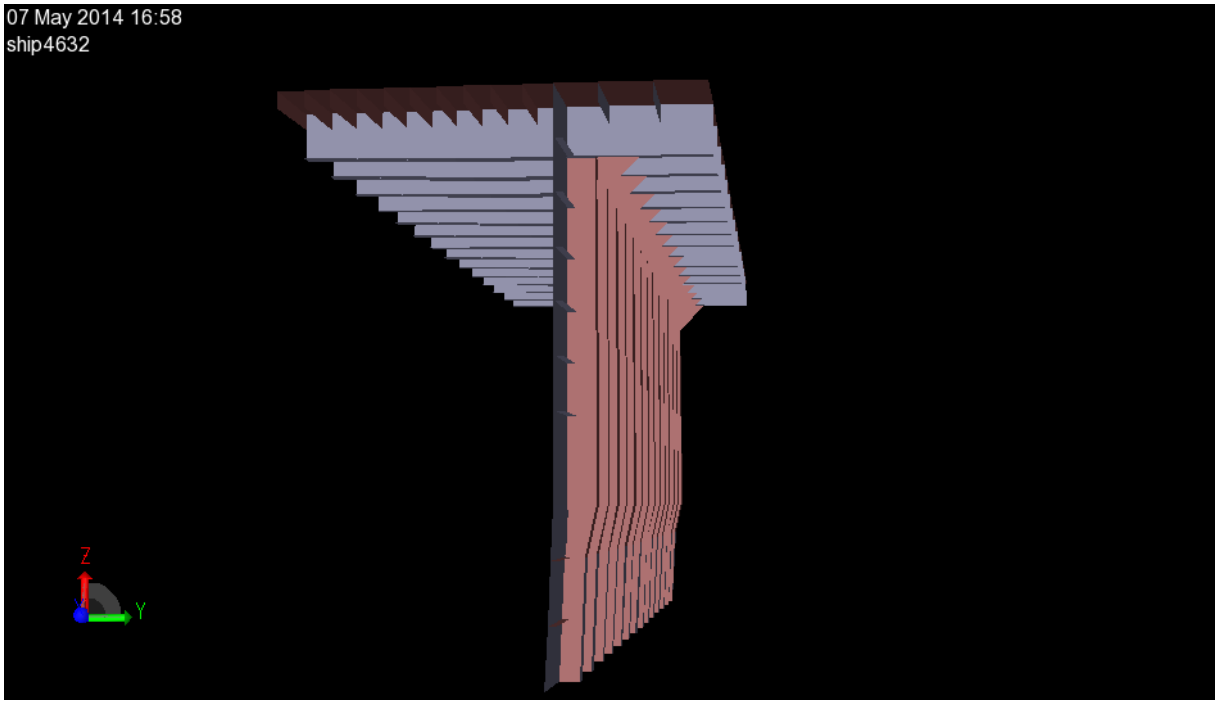

Figure 9: Model 1 as designed in Sesam GeniE

This model was exported to Abaqus/CAE as a ASIS SAT-file for parameter definition and analysis.

4.1.3 Model 2

A second model was made to investigate if the model extent would affect the results. This was studied in the sensitivity analysis regarding boundary conditions (BC's). Only the part of the deck covering the LNG-fuel tank was included in the model (as shown within the green lines in Figure 8). The section scantlings of the model are listed under *inner deck* in Appendix B. The extent of Model 2 is listed;

- Longitudinal extent: frame #58 to frame #88;
- Transverse extent: 3100 mm from CL;
- Vertical extent: 8400 mm above BL to 9000 mm above BL.

Just like for Model 1, only half the model was made to save time. Model 2 is displayed in Figure 10.

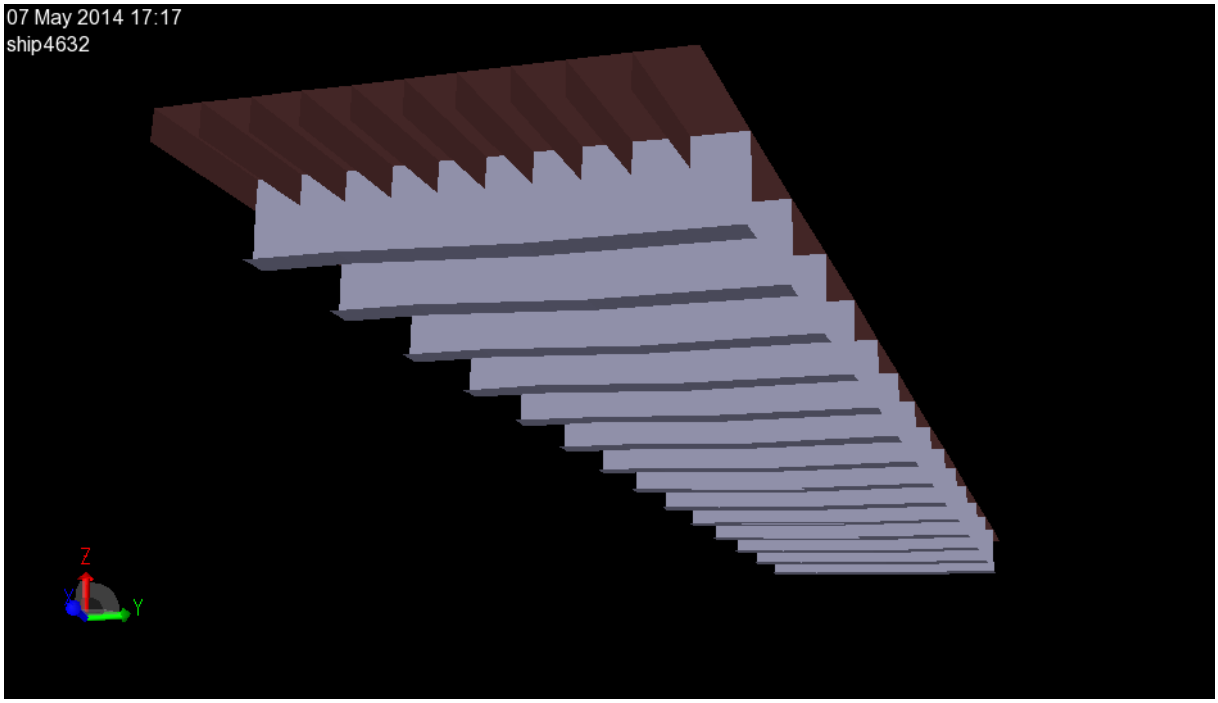

Figure 10: Model 2 as designed in Sesam GeniE

4.1.4 Container model

Also the dropped container was modelled using Sesam GeniE. The dimensions correspond to a 20 foot standard container. The inner dimensions are shown in Table 3.

Table 3: 20 foot standard container, dimensions (FOREIGN TRADE ON-LINE™, 2013)

Dimension	Value
Length [m]	5.89
Width [m]	2.33
Height [m]	2.38
Tare mass [kg]	2,229
Max. cargo [kg]	21,727

This model was also built with plate elements, and easily exported to Abaqus. The container model is shown in Figure 11.

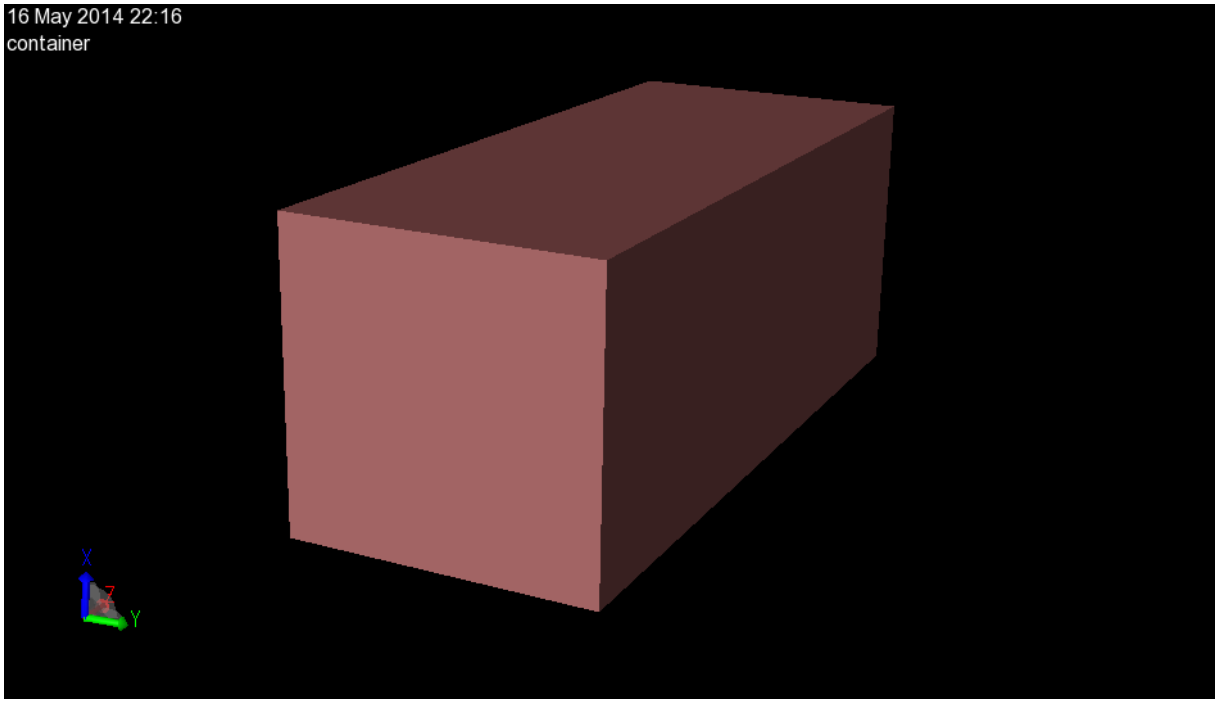

Figure 11: Container model in Sesam GeniE

4.1.5 Simplifications

The models were designed as true to the original structures as possible using plate elements in the design. HP bulb stiffeners were omitted from the modelling due to difficult geometry. A conservative simplification was made by using flat bar-stiffeners with equal thickness and height as the original stiffeners. In the initial state, the edges of Model 1 and Model 2 were given fixed boundary conditions. The LNG fuel tank was not included in the modelling, but the distance from the outer shell to the deck was considered when assessing deck deformations.

4.2 FE-Solver

Abaqus was chosen to execute the numerical analysis by nonlinear FEA of the deck response due to an impacting object. Using the NLFEM for dynamic impact analysis introduces two possible time integration methods; explicit time integration (using Abaqus/Explicit) and implicit time integration (using Abaqus/Standard). Chapter 12 of *TMR 4190 Finite Element Modelling and Analysis of Marine Structures* by Moan (2003) and the *Abaqus Theory Manual* (Dassault Systèmes, 2012) were used as reference.

An explicit solution method is commonly used for high-speed dynamic events, where the response is large and nonlinear. The response for the new time step $t + \Delta t$, is solved entirely based on displacements, velocities and accelerations from previous time steps. The central difference time integration method is used in Abaqus/Explicit, and shown in the following;

$$\ddot{\boldsymbol{u}}^{i} = \boldsymbol{M}^{-1}\left\{\boldsymbol{F}^{i} - \boldsymbol{I}^{i}\right\} \tag{31}$$

$$\dot{\boldsymbol{u}}^{i+\frac{1}{2}} = \dot{\boldsymbol{u}}^{i-\frac{1}{2}} + \frac{\Delta t^{i+1} + \Delta t^{i}}{2}\ddot{\boldsymbol{u}}^{i} \tag{32}$$

$$\boldsymbol{u}^{i+1} = \boldsymbol{u}^{i} + \Delta t^{i+1}\dot{\boldsymbol{u}}^{i+\frac{1}{2}} \tag{33}$$

The subscript *i* labels the current time step, $\boldsymbol{M}$ is the mass matrix, $\boldsymbol{F}$ is the external load vector and $\boldsymbol{I}$ is the internal load vector (from damping, restoring and inertial loads). $\boldsymbol{u}, \dot{\boldsymbol{u}}$ and $\ddot{\boldsymbol{u}}$ are the displacement, velocity and acceleration vectors respectively. The equations above show one incremental loop of the central difference method. Velocities for the new time step can be calculated by linear interpolation of the mean velocities;

$$\dot{\boldsymbol{u}}^{i+1} = \dot{\boldsymbol{u}}^{i+\frac{1}{2}} + \frac{1}{2}\Delta t^{i+1}\ddot{\boldsymbol{u}}^{i+1} \tag{34}$$

The initial conditions needed are the velocity and acceleration at t = 0. Also needed is $\dot{\boldsymbol{u}}^{-\frac{1}{2}}$. The following start condition is set;

$$\dot{\boldsymbol{u}}^{+\frac{1}{2}} = \dot{\boldsymbol{u}}^{0} + \frac{1}{2}\Delta t^{1}\ddot{\boldsymbol{u}}^{0} \tag{35}$$

This is substituted into Eq. (32) for i = 0 to get;

$$\dot{\boldsymbol{u}}^{0} + \frac{1}{2}\Delta t^{1}\ddot{\boldsymbol{u}}^{0} = \dot{\boldsymbol{u}}^{-\frac{1}{2}} + \frac{\Delta t^{1} + \Delta t^{0}}{2}\ddot{\boldsymbol{u}}^{0} \tag{36}$$

$$\dot{\boldsymbol{u}}^{-\frac{1}{2}} = \dot{\boldsymbol{u}}^{0} - \frac{1}{2}\Delta t^{0}\ddot{\boldsymbol{u}}^{0} \tag{37}$$

This is executed on an element level if we assume that the element mass matrices and damping matrices are lumped (no coupling effects). As a result of this, the explicit method is very efficient with respect to computational resources (easily invertible matrices). It is however very important to use sufficiently small time increments to achieve a stable solution. Abaqus/Explicit uses the highest eigenvalue ω_{max} of the element to calculate the stable time increment as follows;

$$\Delta t \leq \frac{2}{\omega_{max}} \tag{38}$$

This procedure is repeated for each element, where the minimum value is chosen for the whole model. Time increments are calculated automatically in Abaqus/Explicit, but can also be controlled manually by the user (by scaling the calculated time step). The *Abaqus Theory Manual* (Dassault Systèmes, 2012) was used as reference concerning details on how the stable time increment is calculated. As stated in the *Abaqus Analysis User's Manual* (Dassault Systèmes, 2012), the explicit analysis method has the following properties:

- Can handle very small dynamic response times, and allows very discontinuous processes for large models;
- Allows for large deformations and rotations;

- It can analyse assembled parts with very general contact definitions;
- A linear geometrical deformation theory can be used if small deformations and rotations are assumed;
- Adiabatic stress analysis can be used if generation of heat is assumed for inelastic dissipation;
- Allows for quasi-static analysis of models with complicated contact definitions;
- Allows for element deletion to model rupture.

An implicit solution method is commonly used for low-speed dynamic and quasi-static loading events. The response is calculated using a finite difference method with respect to time. The velocities and accelerations from the new time step $t + \Delta t$, in combination with known values from previous time steps are used to calculate the response at the time step $t + \Delta t$. An implicit solution is always stable, but is very time and memory consuming due to equation solving. In Abaqus/Standard, the equation solver used for quasi-static events is the backward Euler method. For dynamic events, an extension of the Newmark β – method is used. Since the implicit time integration method is not used, the reader is referred to the *Abaqus Theory Manual* (Dassault Systèmes, 2012) for details on how these equation solvers are applied.

The nature of the simulation being studied in this thesis made the choice of method easy. The explicit solver was chosen, so Abaqus/Explicit was used to execute the nonlinear FEA. Uncertainties in the stable time increment solver were investigated as a convergence study, by scaling the automatically calculated time increments with the factors 0.50 and 0.25.

4.3 Material Parameters

4.3.1 Elastic-plastic material properties

The material properties given to the initial configuration were based on the steel quality used for the PSV-deck. This included the steel grades NV-NS (S235) and NV-36 (S235). DNV (2013b) has proposed engineering and true stress-strain parameters for these steel grades based on tests of different plate thicknesses. They recommend using the true stress-strain

properties as input for FEA. Values for plate thicknesses t < 16 mm were applied in the material definition (listed in Table 4).

Table 4: Material properties for different strength NV A steel grades (DNV, 2013b)

Steel	**S235**	**S355**
E [GPa]	210	
ν [−]	0.3	
ρ $\left[\frac{kg}{m^3}\right]$	7850	
σ_{prop} $[MPa]$	211.7	320
σ_y $[MPa]$	236.2	357
σ_{y2} $[MPa]$	243.6	366.1
σ_u $[MPa]$	432.6	541.6
ε_{py} [−]	0.004	0.004
ε_{py2} [−]	0.0198	0.0197
ε_{cr} [−]	0.1817	0.1391

In the initial configuration, the transverse girders were made of NV-36 (S355) steel (as shown in Transversal Section #64, Appendix D). The remaining structure was built using NV-NS (S235) steel. In addition to these commonly used steel grades, one unusual steel type (for application in ship design) was tested and compared.

Swedish Steel AB (SSAB) produces a range of very tough steel types, e.g. Hardox steels. These are popularly applied for equipment used for mining, recycling, road building and in quarries (SSAB, 2014). In these segments, their steel is used for its tough and wear resistant qualities. It is therefore interesting to investigate how these qualities can increase the impact resistance of a ship deck, and decrease the risk of damaging the LNG tank underneath. Hardox 400 steel, with a typical yield stress of 1000 MPa, was used in the present study.

The numbering reflects hardness according to the Brinell scale, where the nominal hardness of the material is 400 HBW (H – hardness, B – brinell and W – the material of the indenter, tungsten (wolfram) carbide). (Reference is made to ASTM International (2014) for description and method for determining the Brinell hardness number) More information on the material properties of the steel type can be found in the Data Sheet (SSAB, 2011). The true stress-strain relation was obtained by contacting a Hardox representative MSc. G. Eriksson-Helle (2014, pers. comm., 24 March). The values are tabulated in Appendix A. Properties for the density and Poisson's ratio had to be assumed (equal to NV-NS and NV-36), due to lack of information obtained. To compare the three steel materials used in the present analyses, the true stress vs. true strain relations are plotted in Figure 12.

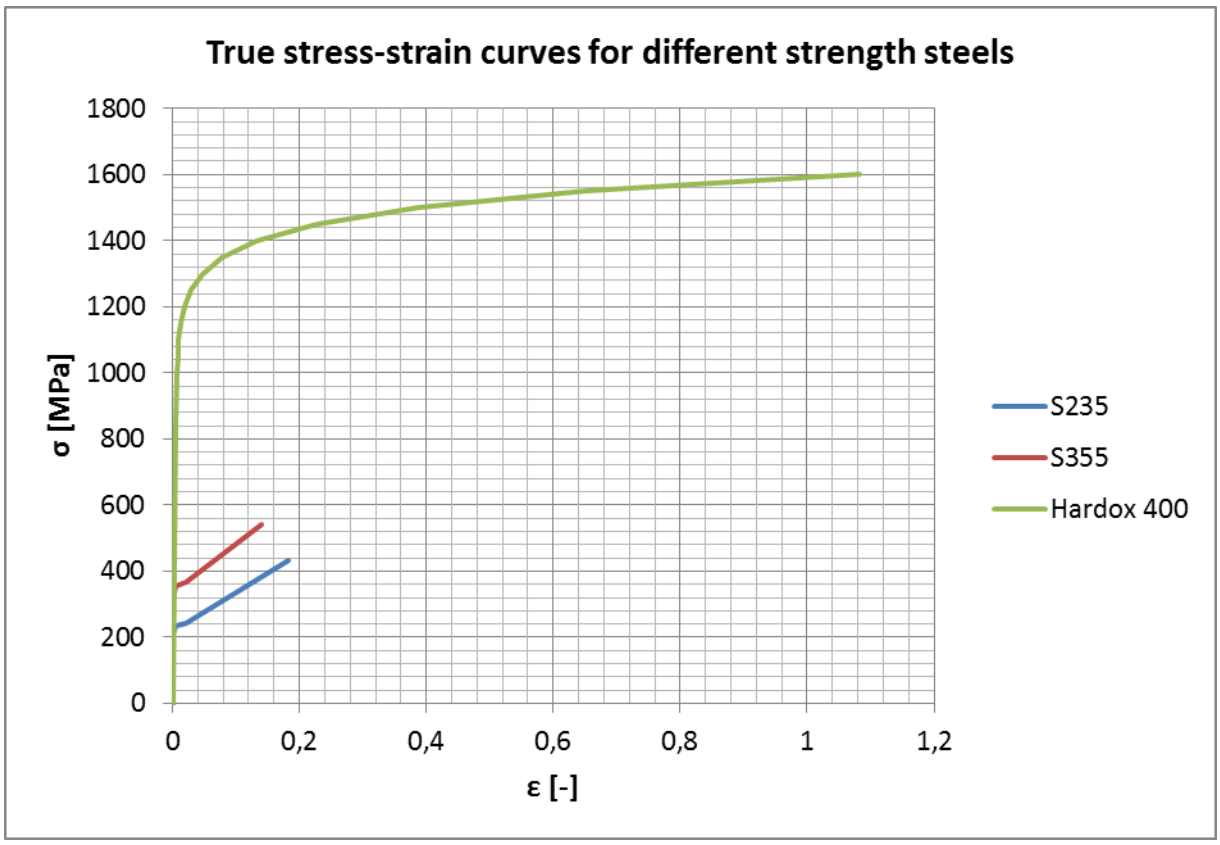

Figure 12: True stress vs. true strain curves

Considering the true stress-strain curves, the Hardox steel was expected to increase the energy dissipation capacity significantly.

4.3.2 Dynamic yielding

Large plastic deformations are expected when steel structures collide. High velocity impact will cause the structures to deform over a short amount of time, resulting in nonlinear material behaviour. The yield strength of a material is sensitive to the strain rate, so an adjustment of the static yield stress can be made to account for the dynamic effects (Paik, 2007). For instance, the yield strength of mild steel is expected to increase as the strain rate increases. The Cowper – Symonds constitutive equation is widely used, e.g. by Paik (2007) and Alsos & Amdahl (2009), and is shown in Eq. (39) (strain hardening is neglected).

$$\frac{\sigma_y^D}{\sigma_y} = 1 + \left(\frac{\dot{\varepsilon}}{C}\right)^{\frac{1}{q}} \tag{39}$$

σ_y^D is the dynamic yield stress, σ_y is the static yield stress, $\dot{\varepsilon}$ is the strain rate and C and q are the Cowper-Symonds coefficients. For mild steel, these coefficients were originally determined by tests to be C = 40.4 s^{-1} and q = 5 (Paik, 2007). Alsos & Amdahl (2009) suggests that the values of C should be greater for cases with large plastic deformations and high strain rates, and have obtained better results when the coefficients have values of C = 4000 s^{-1} and q = 5. DNV GL recommends the same values (C = 4000 s^{-1} and q = 5) for typical offshore steels if no other values are specified (DNV, 2013b). Paik (2007) also tabulates the coefficients for high tensile steel where C = 3200 s^{-1} and q = 5. As an initial configuration, the coefficients used in the Abaqus model for NV-NS and NV-36 steel were defined with C = 40.4 s^{-1} and q = 5. Based on the above, Hardox 400 steel was defined with C = 4000 $s^{-1}$and q = 5. Two sets of coefficients (listed in Table 5), and the case of neglecting strain rate effects, were tested in the sensitivity analyses.

Törnqvist (2003) discusses the uncertainties of strain rate adjustment in the material modelling. He argues that existing models are uncertain due to the difficulty of measuring the strain rate during tensile testing. As a tensile specimen is loaded, the strain rate will change over time. Further complication arises by the occurrence of necking, resulting in large differences in strain rate between the neck and the rest of the specimen. The measured values are often an average representation of the strain rate.

The Cowper-Symonds constitutive equation was applied in the numerical analysis, bearing in mind the uncertainties involved. Information on how to define the coefficients in Abaqus is found in the *Abaqus Analysis User's Manual* (Dassault Systèmes, 2012).

Table 5: Coefficients used for strain rate sensitivity analysis

C [s^{-1}]	q [-]
40.4	5
4000	5
No strain rate effects	

4.3.3 Damage properties

The elastic and plastic properties of the materials were compared with regards to true stress-strain curves. Strain rate effects were discussed, and were also included in the material modelling. Damage models are needed to describe the material behaviour further.

Looking back at the fracture models discussed in Section 3.2 and considering the information available, several choices had to be made with regards to the analyses. First of all, the choices became limited by the short list of fracture criteria available in Abaqus/Explicit. Some of the available models (e.g. Johnson-Cook (1985)) require testing and calibration to obtain the needed material parameters. Simple empirical models and their application were therefore investigated in the following.

Hogström (2012) argue that more simple failure models can be used with acceptable precision when assessing the failure of large structures. He points out the importance of good background knowledge in material modelling, especially when material degradation and fracture is relevant. This can be obtained by comparing numerical analyses with real life experiments for test specimens or structures of different scale (shown in Figure 13).

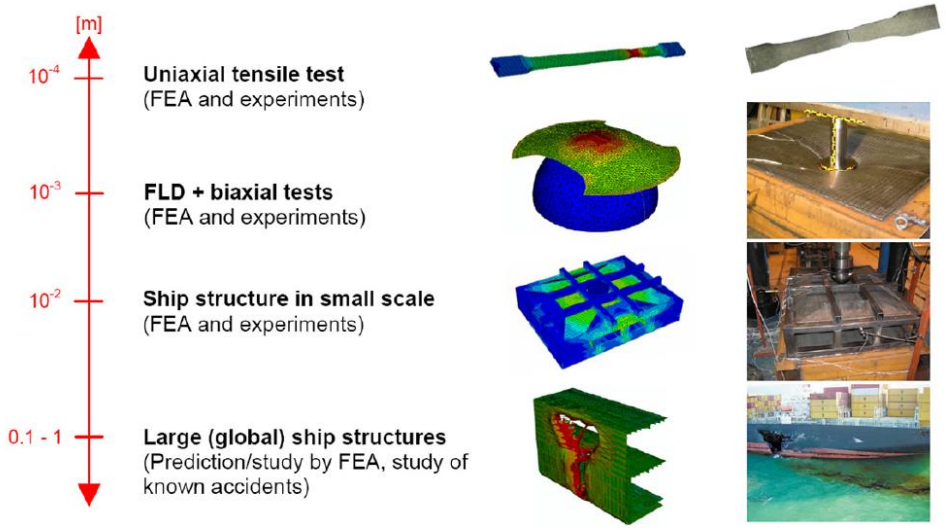

Figure 13: Numerical vs. experimental comparison methodology for different and size test specimens or structures (Hogström, 2012)

This approach has been taken by numerous scientists (Ehlers, 2010b; Hogström, 2012), and has resulted in models where the damage can be characterized by a fracture strain depending on finite element mesh size. Hogström has obtained fairly accurate results using Abaqus/Explicit with the following damage initiation models; shear failure, forming limit diagram (FLD) and forming limit stress diagram (FLSD) criteria. The most accurate results were obtained by using the shear damage criterion.

The shear criterion is a model that predicts the damage initiation caused by shear band localization (Dassault Systèmes, 2012). The model can be defined with varying complexity; from setting a constant equivalent plastic strain at damage initiation, to being dependent on shear stress ratio, strain rate and temperature. It is also possible to specify the damage evolution of the material. This model was considered well suited for the present analyses due to its simplicity, and ability to adapt according to which material parameters that are known.

In Figure 14 the model developed by Ehlers is shown. The steel used for the development of this model is Norske Veritas grade A (NVA) steel, which has an elastic modulus of 206 GPa, Poisson's ratio of 0.3 and the measured yield stress of 349 MPa (Ehlers, 2010b). This model was therefore considered appropriate for the NV-NS (S235) and NV-36 (S355) steels applied in the present study. However, sensitivity was tested as part of the parameter study in order to uncover any uncertainties in the fracture criterion.

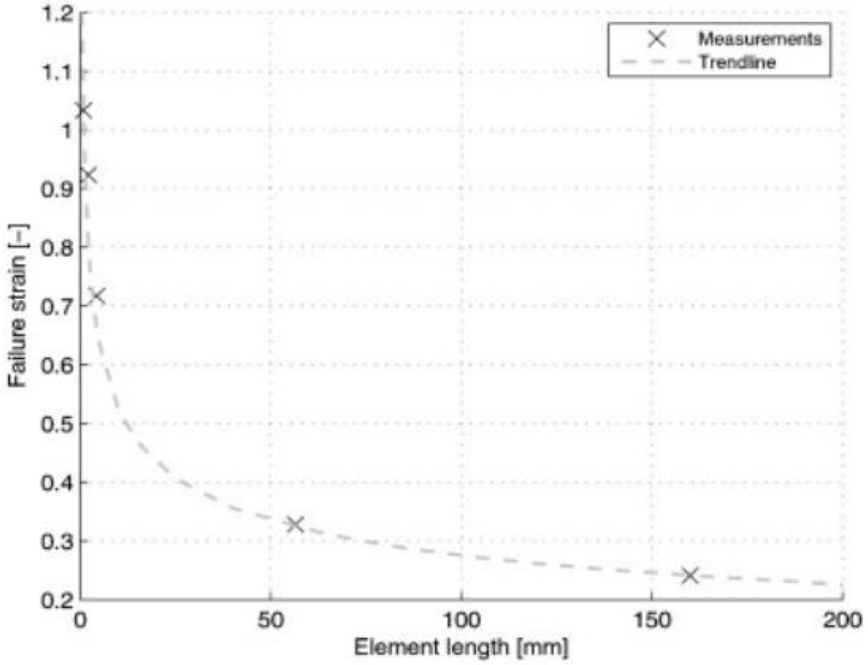

Figure 14: Failure strain vs. element length, NVA steel (Ehlers, 2010b)

No specific details were given in terms of fracture criterion for Hardox 400. Simply a value of fracture strain ε_f = 1.0, was recieved from Eriksson-Helle (2014, pers. comm., 24 March). This was used for the analysis, noting the uncertainty in the value.

4.4 Discretisation and Interaction

4.4.1 Element type

Shell elements are divided into two categories in Abaqus, and are explained in detail in the *Abaqus Analysis User's Manual* (Dassault Systèmes, 2012); conventional and continuum shell elements. Shell elements in general are defined as elements with a small thickness to characteristic length ratio (t/l << 1). For conventional shell elements the thickness is taken into account as a section property, and the geometry of the shell is a 2D flat plate. The degrees of freedom (DOF's) are displacement and rotational (6 DOF's in each node). The continuum shell element contains the thickness in the geometry so it is discretized as a 3D body. The degrees of freedom are translational only (3 DOF's in each node). The continuum shell elements can be used for any thickness, but may be inefficient and give very small stable time increments when used in Abaqus/Explicit. The geometrical properties of the two element types are compared in Figure 15.

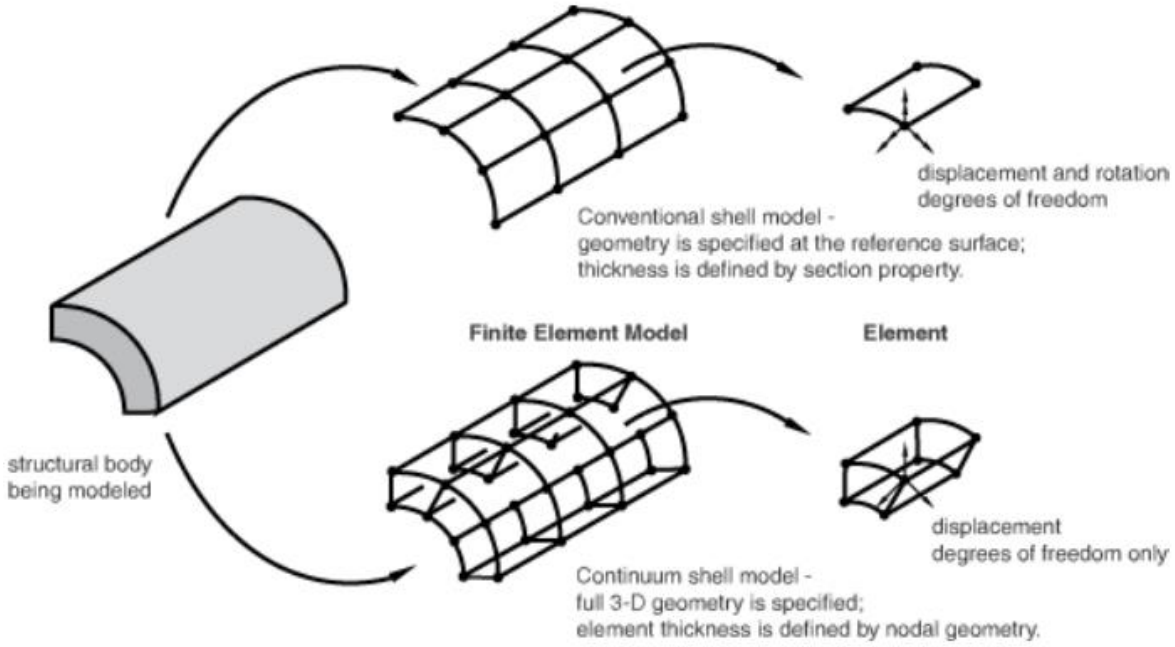

Figure 15: Conventional vs. continuum shell models (Dassault Systèmes, 2012)

The conventional shell elements can again be divided into three groups; Thin shell elements (according to Kirchoff shell theory), thick shell elements (according to Mindlin shell theory) and general-purpose shell elements. The thin and thick shell elements are only available in Abaqus/Standard (implicit theory), and are explained in detail in the *Abaqus Theory Manual* (Dassault Systèmes, 2012) and in chapter 7 of *Finite Element Modelling and Analysis of Marine Structures* (Moan, 2003).

The general-purpose shell elements are fit for all purposes, and are the only conventional shell elements available in Abaqus/Explicit. These elements allow thickness change as a function of in-plane deformation. The S4R shell element is a four-noded quadrilateral element that use uniformly reduced integration and has five section points in the thickness direction. This way membrane and shear locking is avoided. Hourglass modes are allowed to propagate over the mesh. All of these qualities make the S4R shell element very versatile. It also allows for large deformations with respect to the thickness. The S4R shell element was applied for most of the FE modelling, and the only element type used in the impact area of the deck. The corresponding three-noded triangular element (S3R) was used in transition areas between coarse and fine mesh.

4.4.2 Mesh

Mesh size is of great importance to display the correct load distributions and stiffness of the structure. In thesis the modelling of fracture was also of great importance. The onset of fracture was modelled using the Shear Criterion as explained in Section 4.3.3. Fracture occurs for a specified value of plastic strain depending on the element size. The modelling of fracture is then based on element deletion. All elements subjected to the critical plastic strain was removed (all stiffness was gone). This set requirements to the element size in the impact area.

A mesh refinement study was carried out, to see that fracture was modelled in a satisfying manner and the results converged. The initial configuration of the mesh refinement study was established by meshing the models according to DNV Classification Notes No. 31.3 *Strength Analysis of Hull Structures in Tankers* (DNV, 1999). These recommendations are based on the assumption that four-noded shell or membrane elements are used in the FE modelling together with beam or truss elements. 3-noded triangular shell elements should be refrained from unless they can improve mesh transitions (e.g. between coarse and fine mesh areas). This was in agreement with the element type chosen in Section 4.4.1. The following recommendations were used for the initial setup of the study:

- For web beams, three elements are recommended over the height;
- One element between longitudinal stiffeners;
- Two elements between transverse girders;
- For large brackets, the stiffener spacing may be appropriate as the element length

These guidelines were followed to the extent that they didn’t create poor mesh transitions in complicated structural intersections.

It is important to mention that this method is intended to enable the representation of correct stiffness and load distribution in the structure due to general design loads. The mesh density was therefore increased in the impact area to properly represent the plastic deformations and ultimately the fracture of the deck structure. Convergence was evaluated with respect to the force-displacement relation.

Since the models were generated separately, focus was set on meshing them as equal as possible. The differences in results were then solely dependent on the structural extent of the models. This was studied more closely when comparing BC's

For each model, six different mesh configurations were studied. The approximate element sizes and resulting fracture strain can be studied in Table 6.

Table 6: Mesh refinement setup for Model 1 and Model 2

Name	Characteristic element length [mm]	Fracture strain [-]
Run 1	300 (average)	0.21
Run 2	200	0.215
Run 3	100	0.27
Run 4	75	0.30
Run 5	50	0.34
Run 6	37.5	0.365

4.4.3 Contact formulation

A contact formulation had to be defined to the FE model. It was then possible to simulate an impacting object that could deform and possibly penetrate the deck model in a physical manner. The Interaction module in Abaqus/CAE was used to assign interaction types and properties. How to do this and what the different types and properties are, is explained in the *Abaqus/CAE User's Manual* (Dassault Systèmes, 2012). In this section a description of the General Contact formulation and assigned interaction properties are given.

The "General Contact" formulation is a simple way to define contact between areas of two or more models (feature edges, exterior faces and analytical rigid faces). This is due to the very few modifications needed, e.g. contact between all possible surface pairs are included in the formulation as a default. It is also possible to choose specific surface pairs, and formulate node-surface and surface-surface properties. Doing this can prevent any wrongful penetrations between parts, and help to reduce central processing unit (CPU) time by excluding untouched surfaces.

Abaqus has the master-slave concept built in, where the user chooses master and a slave surfaces on the interacting bodies. Slave surface nodes cannot penetrate a master surface, but nodes on a master surface can penetrate a slave surface. This is handled by the penalty enforcement algorithm. Slave nodes are prevented from penetrating the master surfaces by forces that depend on the penetration distance. An equal and opposite directed force is applied to the master surface. This method is further explained in the *Abaqus Analysis User's Manual* (Dassault Systèmes, 2012).The way parts in a model interact and how they are discretised (node-surface or surface-surface impact) determines how the user should choose the master and slave surfaces to avoid wrongful penetrations. This is also of importance to obtain the correct contact forces between the two colliding bodies. The master-slave concept is illustrated in Figure 16.

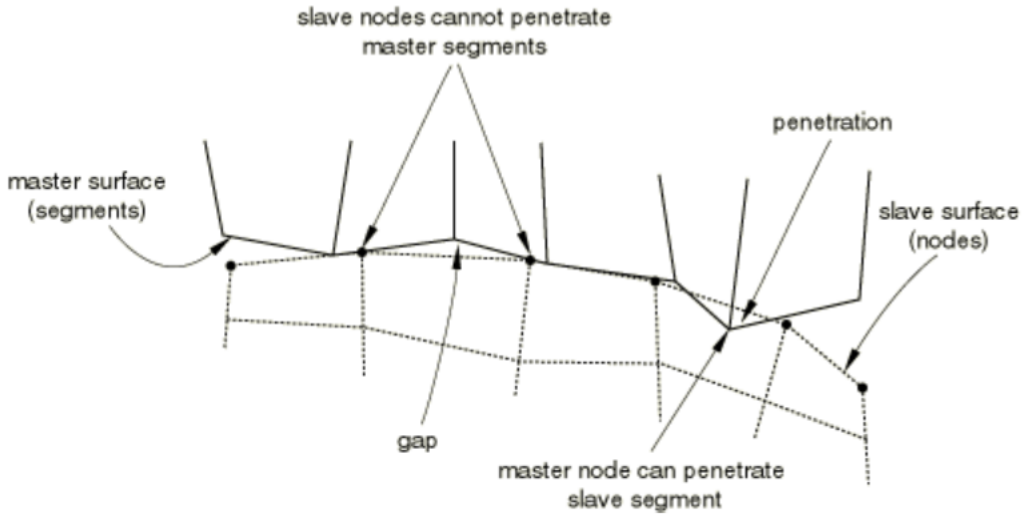

Figure 16: master – slave segment interaction (Dassault Systèmes, 2012)

Three main groups of interaction properties can be assigned to the General Contact formulation (mechanical, thermal and electrical). The different interaction properties are explained in detail in the *Abaqus/CAE User's Manual* (Dassault Systèmes, 2012). For an impact simulation, the most relevant properties are the normal and tangential behaviour.

The normal behaviour used for the container – deck interaction is set to "hard" contact (alternatives to this are explained in the *Abaqus/CAE User's Manual*). There is no contact pressure when there is no contact. When there is contact, any pressure possible is transmitted.

The tangential behaviour is simply described by a frictional formulation. Abaqus allows definitions ranging from a frictionless state to a "rough" frictional state (no sliding allowed).

Applied between the two extremes, is the basic *Coloumb* friction model which allows for relative sliding between contacting bodies after a certain value of traction stress τ_{max} is achieved. The maximum traction stress depends on the product of the friction coefficient μ (according to material type) and the contact pressure p between the contacting bodies. There are numerous ways of defining a friction formulation (static and kinetic friction coefficients, slip rate, temperature, etc.). The *Abaqus Analysis User's Manual* (Dassault Systèmes, 2012) is used as reference for further details on definition of frictional formulations.

Friction effects will naturally occur when two colliding objects slide relative to each other. Modelling the deck as frictionless was seen as a conservative (with regards to resistance force) but unphysical simplification. A friction formulation was therefore included in the parametric study, to see how resistance and energy dissipation is affected.

The friction coefficient should be decided based on material and relevant application. Törnqvist (2003) analysed energy dissipation in a ship double bottom due to stranding, using a friction coefficient of 0.3 for mild steel. Ehlers (2010b) also used a friction coefficient of 0.3 for analyses of ship side structures with regards to crashworthiness. The material used was NV A steel (as used in this thesis). Hogström (2012) analysed energy dissipation in ship sides due to ship collision. This was done for different types of ship sides. He argued that steel used for shipbuilding has a fairly rough surface with friction coefficient ranging between 0.1 and 0.6. He applied the friction coefficients of 0.1 and 0.3 in his analysis.

Based on these studies, a variation of friction coefficients were tested and compared to the initial frictionless state. These are listed in Table 7;

Table 7: Friction coefficients

Friction coefficient μ [-]
0.0 (initial)
0.2
0.3
0.4

4.5 Loads and Boundary Conditions

4.5.1 Load conditions

The values for initial load condition are presented in Table 8.

Table 8: Initial load condition

Drop Height [m]	Corresponding impact velocity [m/s]	Mass [kg]
5	9.9	24000 (20 foot container)

The mass of the container is based on the maximum cargo capacity added to the tare mass for a standard 20 foot container (FOREIGN TRADE ON-LINE™, 2013). This was the initial load condition used for Model 1 and Model 2 (see 4.1.2 and 4.1.3 respectively), and the basis for the numerical analyses.

According to Eq. (1) increasing the drop height is the only way to increase the impact velocity. As this most likely will increase the strain rate, also the yield strength should be increased (see Sec. 4.3.2). How this could influence the energy absorption of the deck was of great interest. The drop heights and corresponding impact velocities are listed in Table 9.

Table 9: Impact velocity

Drop height [m]	Corresponding velocity [m/s]
7.5	12.13
10	14.00

To model the worst case scenario of a dropped object load, impact angle is essential. Zhang (1999) performed extensive analyses to study the effect of impact angle, in cases of ship collisions and dropped objects. The latter was of course more relevant in the present study. A study was executed by Zhang (1999) where an object was dropped with different impact angles on a plate, and the critical impact energy was found. As expected, a perpendicular impact was the most critical as can be shown in Figure 17. The parameter values and method used can be found in chapter 4 in (Zhang, 1999).

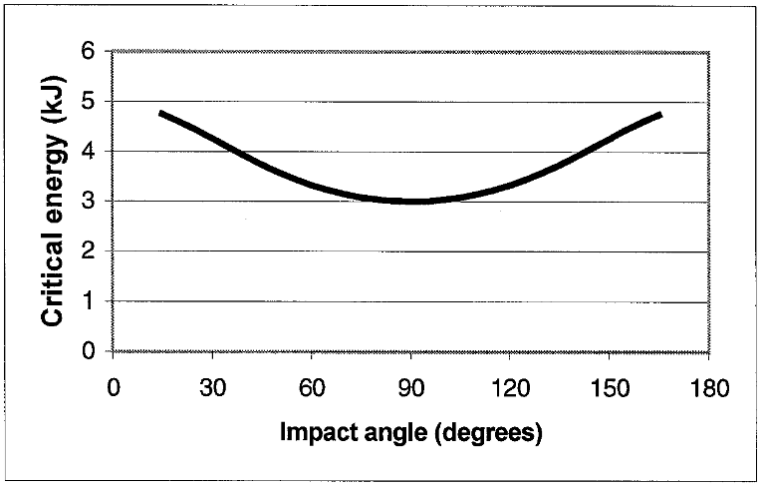

Figure 17: Critical energy vs. impact angle of dropped object (Zhang, 1999)

To model the worst possible impact scenario, the container was dropped edge-first (rotated as shown in Figure 18) on deck with an impact angle of 90°. For the main analyses the container was defined as an infinitely rigid shell, so the impact energy was absorbed exclusively by the deck.

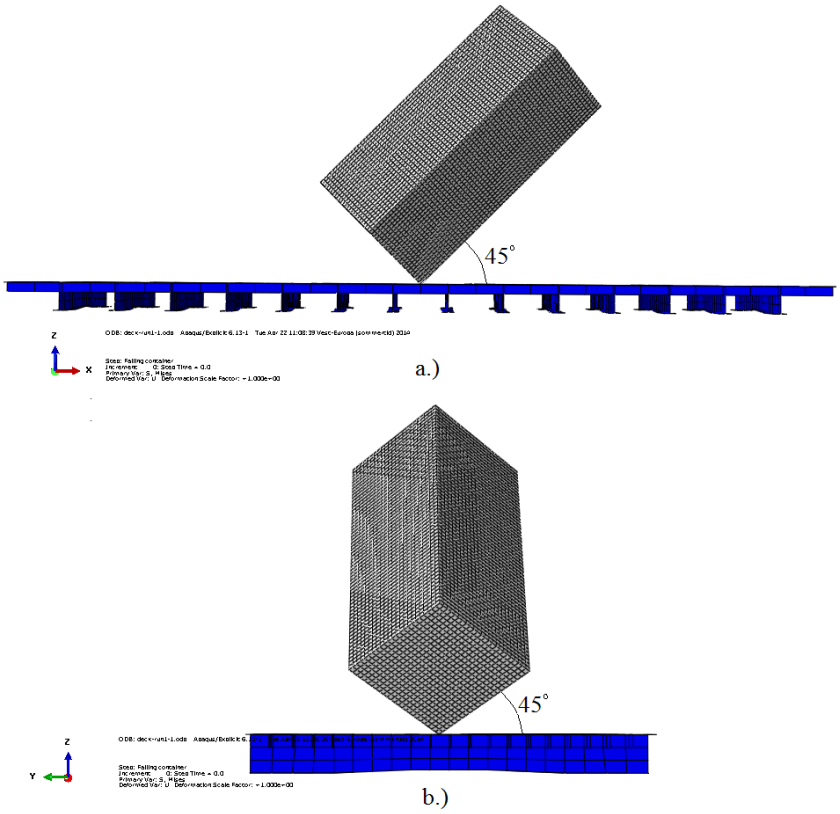

Figure 18: Container configuration in perspective a.) x-z-plane and b.) y-z-plane

The present study deals with the principle of total energy dissipation in the deck structure, commonly referred to as *Strength Design*. To study the realistic event of shared energy dissipation, a deformable container was also designed and tested. Hardox 400 steel was used, to compensate for the lack of corrugated walls (as this was not included). The model was discretised with a relatively large mesh density (sizes ranging between 37.5 – 75.0 mm) using conventional shell elements (as discussed in Sec. 4.4.1). The shell thickness was calculated based on the tare mass, mass density of steel and total surface area of the container model. This resulted in a shell thickness of approximately 4.40 mm.

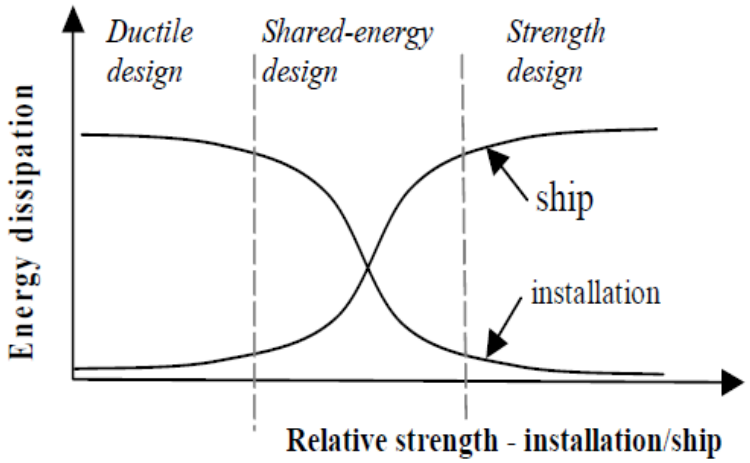

Figure 19: Energy sharing design principles (Moan, 2003)

4.5.2 Boundary conditions

Choosing the correct model extent and BC's was important to obtain accurate results. DNV (2013b) recommends the analyst to carry out sensitivity studies with regards to BC's, to check the validity of the model extent. The three following cases were tested;

- Model 1 with fixed edges (constrained in rotational and translational DOF's);
- Model 1 with simply supported edges (constrained in the translational DOF's);
- Model 2 with fixed edges.

The BC's were defined along the edge-nodes of the structure according to Figure 20 and Figure 21. The container was restrained in all DOF's except translation in z-direction (vertical). The x- and y-directions corresponded to the longitudinal and transverse directions of the ship respectively.

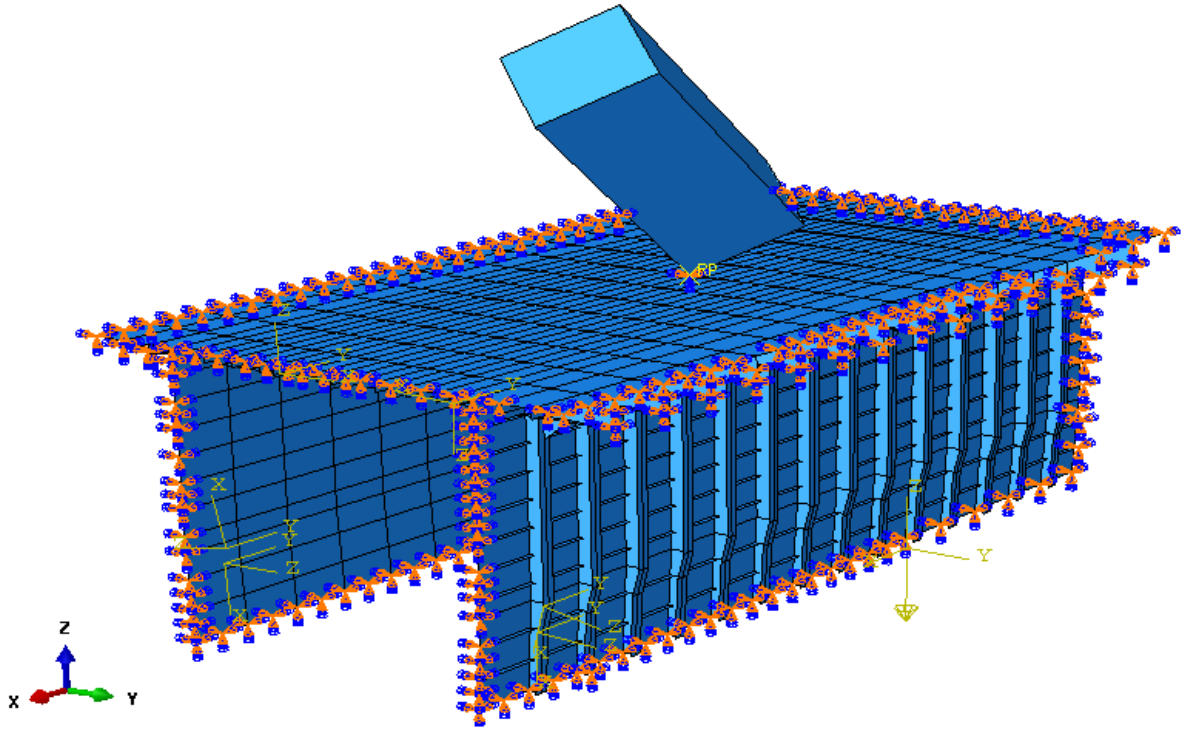

Figure 20: Model 1, fixed edges

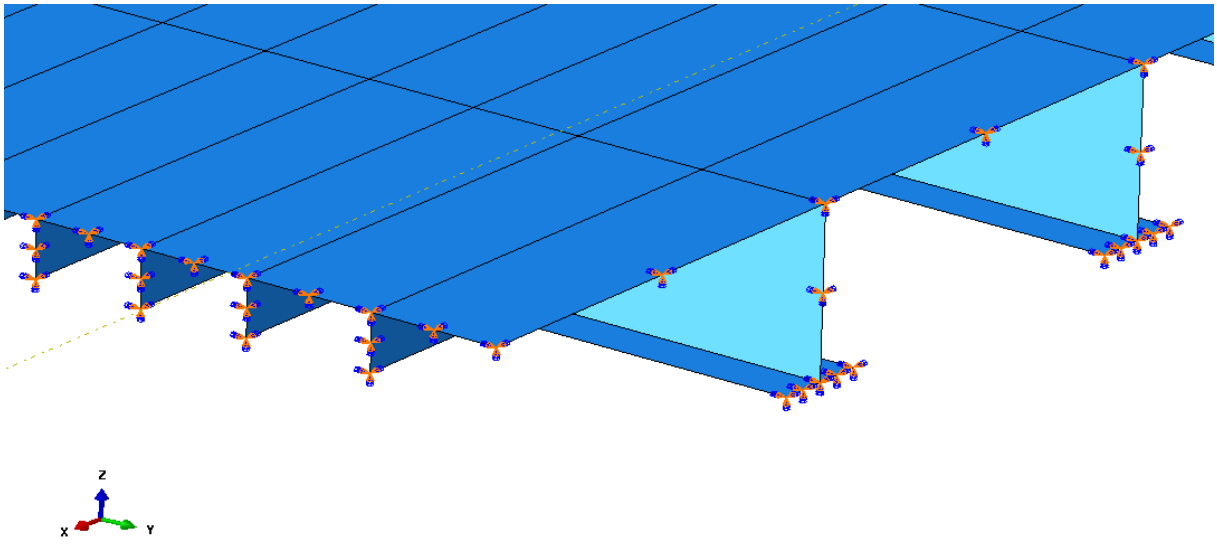

Figure 21: Model 2, fixed edges

4.5.3 Location of impact

Four different locations in the centre of the deck were compared with regards to critical energy absorption. These scenarios are specified relative to the deck structural members accordingly;

1. On web girder – stiffener intersection;
2. On web girder, between stiffeners;
3. Between web girders, on stiffener;
4. Between web girders and stiffeners.

The latter impact location was expected to display the most critical deformation of the deck.

4.6 Quantifying Critical Impact Energy

Co-supervisor Johnsen (2013, pers. comm., 23 September) defined the critical failure scenario to be when the falling object penetrates the deck. This was the basis for the numerical analysis, aiming to determine the critical impact energy to deck failure.

Firstly a convergence analysis with regards to mesh size and time increment size was executed. Parametric and comparative studies were subsequently carried out to determine the final configurations of the deck comparing steel types; NV-NS and NV-36 (as-built) vs. Hardox.

The parametric study (presented in Sec. 6.3) was carried out to investigate the following;

- Strain rate;
- Friction;
- Impact velocity;
- BC's, and;
- Fracture strain.

The first part of the Comparative study was carried out to investigate the critical energy dissipation to penetration in the following cases; using a deformable container model, and comparing impact locations (presented in Secs. 6.5.1 and 6.5.2 respectively).

Based on the above, final configurations were chosen. Energy dissipation to penetration of the deck model was analysed with as-built steel and Hardox steel. The difference in energy absorption formed the basis of discussions related to the application of Hardox steel in ship design.

5 Analytical Methods

A brief review of the interaction between hull structural members was made. Analytical methods to analyse the indentation resistance of structural members and predicting the dissipated energy from impact are discussed. The PSV deck structure (see Sec. 4.1.1) was assessed using these methods. Analytical results were compared (in Sec. 6.4) with the results obtained using Abaqus/Explicit.

5.1 Ship Structure

The lecture notes from the course *TMR 4167 Marine Technology 2 Part 1: Structural Analysis* (Amdahl, 2010) was used as reference in the following.

The hull of a ship is mainly designed to resist loads caused by hydrostatic pressure (buoyancy), own weight and cargo (gravity), and hydrodynamic loads (e.g. from waves, currents, etc.), among other. The plating of the hull (or the "skin") serves the purpose of keeping out water and transferring the external and internal loads to the "skeleton" of the hull; stiffeners, bulkheads and beams (web frames, girders and stringers). The loads propagate through panels (comprised of plates, bulkheads, stiffeners and beams) to the whole structure, forming the concept of the hull girder. This load propagation is shown schematically below.

$$Plates \rightarrow Stiffeners\ and\ bulkheads \rightarrow Beams \rightarrow Panels \rightarrow Hull\ girder$$

Understanding this is important to rightfully assess the resistance of the deck structure of a ship hull by analytical methods. The load propagation is illustrated on a tanker ship section in Figure 22.

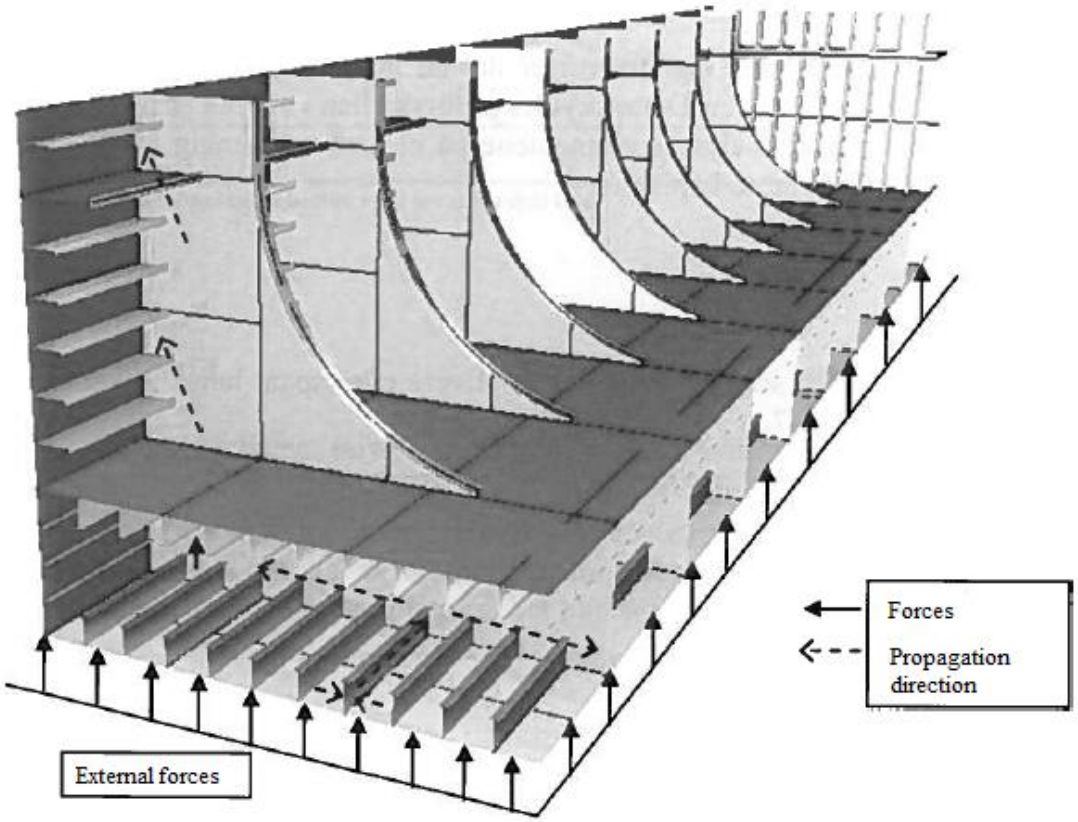

Figure 22: Load propagation in hull structural members (Amdahl, 2010)

An impacting container will do minor damage to the hull girder in total, but can do catastrophic damage to the plates, stiffeners, girders and at worst the cargo in close vicinity to the impact area. The example deck of the PSV used in this study comprised a deck plate, longitudinal bulkheads, longitudinal stiffeners and web frames. The damage extent was therefore closely related to the location of impact, e.g. on a web frame as opposed to in between two web frames. To properly predict the deck resistance analytically, all important load bearing effects were included. How this was done is discussed in the following.

5.2 Plastic Hinge Mechanism

A very simple method can be used to assess the structural resistance of an impact loaded panel, modelling the collapse of girders and stiffeners. Collapse is assumed to occur due to the growth of plastic zones. Elastic-perfectly plastic material is assumed (see Figure 23). When the zones become fully plastic, the beam collapses. This is commonly referred to as collapse by plastic hinge mechanisms. Søreide (1981) was used as reference.

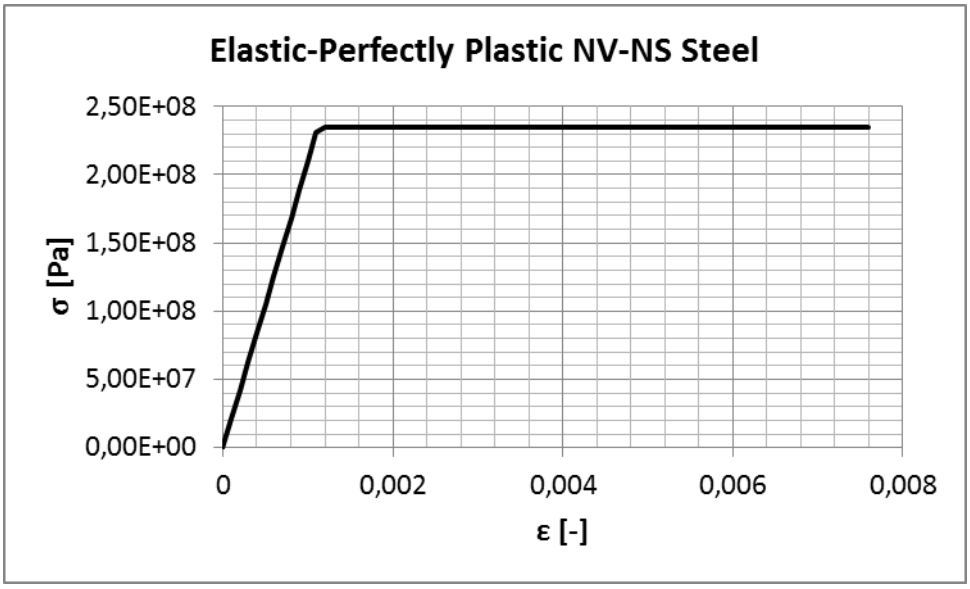

Figure 23: Elastic perfectly plastic stress-strain curve for NV-NS steel

In application to the present study, a panel of limited extent was modelled. Assumed measures were made based on the deck response observed from the numerical simulations. The contributions of internal energy from stiffeners and web girders within this area were summed; resulting in an analytical estimate for the deck resistance. The assumed impact area is shown in Figure 24. Effects from the deck plate were neglected for the sake simplicity. This could be included by using effective flanges contributing to the plastic moment capacity of the structural members.

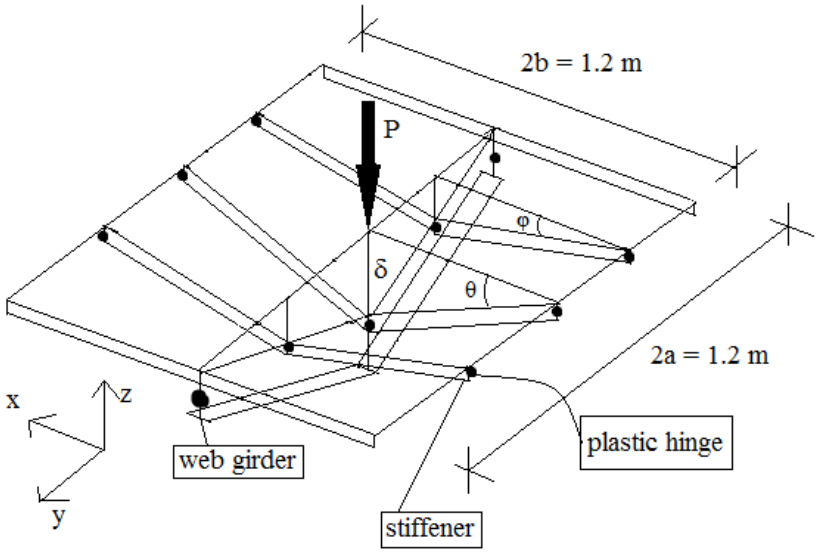

Figure 24: Plastic hinge development in simplified deck model

The stiffener and girder edges were assumed to have fixed BC's. This was considered fair with regards to the stiffeners being supported by the web girders in both edges. The BC's for the girder was, however, expected to give an overly stiff estimate.

Firstly the plastic bending moment capacity of a web girder and stiffener had to be calculated. Scantlings corresponded to the numerical model (listed in Appendix B). For a rectangular section with thickness *t* and depth *h*, the plastic bending moment capacity M_0 is;

$$M_0 = \frac{\sigma_y t h^2}{4} \tag{40}$$

For calculation of plastic moment capacity of other sections, reference was made to Codecogs (2014). As seen in Figure 24, the stiffener and girder deformations were governed by the indentation δ (inducing the rotations θ and φ) at the impact zone (girder-stiffener intersection). An expression for the total internal work E_i was deduced (*st* and *gi* denotes stiffeners and girders respectively);

$$E_i = E_{i,st} + E_{i,gi} = M_{0,st}(4\theta + 8\phi) + M_{0,gi}(4\theta) \tag{41}$$

$$\theta = \frac{\delta}{b} \; and \; \phi = \frac{\delta}{2b} \tag{42}$$

Finally the problem could be solved by equilibrium of external and internal work;

$$E_e = E_i \tag{43}$$

$$P_{cr}\delta = \frac{4\delta}{b}\left(2M_{0,st} + M_{0,gi}\right) \tag{44}$$

This resulted in an expression for the critical load to collapse P_{cr} of the simplified deck structure;

$$P_{cr} = \frac{4}{b}\left(2M_{0,st} + M_{0,gi}\right) \tag{45}$$

This model excludes the effect of fracture or in-plane crushing. The plastic hinge method was therefore expected to overestimate the critical force to collapse. Comparison with numerical results is presented in Section 6.4.1.

5.3 Crushing Resistance of Structural Members

5.3.1 Theory

Researchers such as Simonsen & Ocakli (1999), Zhang (1999), Hong & Amdahl (2008) have developed simplified methods to analytically determine the force-deformation relation of structural members when crushed by an indenter. These types of methods have proven to give good indication of the crushing resistance of structural members. This is seen by comparisons with experiments and numerical results obtained by using NLFEM programs (Simonsen & Ocakli, 1999; Hong & Amdahl, 2008; Haris & Amdahl, 2012). The models vary due to the proposed deformation patterns or folding patterns of the structural members. They are commonly referred to as "energy methods", "plastic methods" or "kinematic methods" and are based on the upper bound theorem (Hong & Amdahl, 2008). Elastic-perfectly plastic material behaviour is assumed. Interaction between structural elements is neglected. Energy dissipation is therefore added together for the contributing structural members. The instantaneous resistance of a web is found by solving for equilibrium between internal and external energy rates, by using Eq. (46);

$$P(\delta)\dot{\delta} = \dot{E}_i \tag{46}$$

$P(\delta)$ is the instantaneous resistance force, $\dot{\delta}$ is the in-plane indentation rate and $\dot{E}_i$ is the rate of absorbed strain energy. This internal energy dissipation rate is commonly divided into a membrane and a bending contribution.

In general the total structural strength can be characterised by the mean crushing force P_m, where the total dissipated energy E_{tot} is divided by the crushed distance $2H$, as shown in the following expression;

$$P_m = \frac{E_{tot}}{2H} \tag{47}$$

How this mean force is defined, differ between methods due to how the folding mechanism is described; specifically by the assumed development pattern of plastic hinge lines. A required parameter is therefore the plastic bending moment capacity in terms of thickness about the hinge line-directions, as expressed in Eq. (48).

$$M_0 = \frac{\sigma_0 t^2}{4} \tag{48}$$

M_0 is the plastic bending moment capacity (per unit length) and *t* characteristic thickness of the crushed member.

A less used parameter is the plastic membrane force capacity (per unit length). This is calculated by the following,

$$N_0 = \sigma_0 t A_d \tag{49}$$

A_d is the deformed area of the plate. The upper material limit of these methods is the flow stress σ_0, which can be calculated using Eq. (50).

$$\sigma_0 = \frac{\sigma_y + \sigma_u}{2} \tag{50}$$

Here σ_y is the yield stress, while σ_u is the ultimate tensile stress.

Obviously, the crushing distance will also be affected by the shape of the actual indenter. To account for this, an adjustment must be made to the theoretical crushing distance. This is done by using the effective crushing factor λ, that can be introduced to the mean crushing force in the following way;

$$P_m = \frac{E_{tot}}{\lambda 2H} \tag{51}$$

Hong & Amdahl (2008) present typical empirical values for λ; e.g. 0.7 for blunt objects and 1.0 for sharp objects. Based on this, the value was set to 1.0 for the present study, considering the container falling corner-first.

To adjust yield strength due to strain rate effects, the Cowper-Symonds constitutive equation (see Sec. 4.3.2) was used. An expression to approximate the strain rate is presented by Hong & Amdahl (2008), using the impact velocity *v*, the effective crushing factor λ and the crushing distance *H* as shown in Eq. (52);

$$\dot{\varepsilon} \approx \frac{v}{4\lambda H} \tag{52}$$

This can be inserted into Eq. (39) to obtain the dynamic yield stress.

Hong & Amdahl (2008) presented an extensive review of different simplified methods for calculating the resistance of structural members. Crushing resistance of beams and stiffened panels is the subject of discussion in the following.

5.3.2 Web girders

Most of the methods presented by Hong & Amdahl (2008) concern in-plane crushing of plates, which can be applied to web frames, girders, stringers and bulkheads/decks. These methods were of interest since the deck is supported primarily by transverse T-shaped web girders that are part of the web frames (see Appendix B for scantlings). These girders have a large span (6200 mm) between the bulkheads (see Figure 8), though this is compensated partially by using smaller stiffener spacing (300 mm as opposed to 600 mm which is typical for the rest of the ship) in addition to using S355 steel instead of the milder S235 steel (see Table 4 for comparison). Using the whole span of the girder in the calculations may therefore prove to give erroneous results if the crushing zone is limited to a small area in the middle of the girder. As an initial setup, the effective span was therefore reduced to a value of 1.20 m to be consistent with the frame spacing.

Two simplified methods are presented and were compared, where the following references were used;

- *Experiments and theory on deck and girder crushing* by Simonsen & Ocakli (1999);
- And *Crushing Resistance of web girders in ship collision and grounding* by Hong & Amdahl (2008).

This was believed to be a more scientific approach, than applying one method exclusively. Simonsen and Ocakli (1999) verified their method with experiments using very thin plated structures (1 mm). They did not originally take into account the effective crushing factor. This was later introduced by Hong & Amdahl (2008), who by doing this obtained reasonable predictions of the crushing resistance when comparing the method with larger scale experiments. Hong & Amdahl (2008) further developed a new method that was intended to capture the characteristics of a girder during crushing. This model showed good correlation with experiments.

Analytical formulae of the two methods were used here. For consistency, notations were used according to Hong & Amdahl (2008). In Eq. (53) we see the expression for instantaneous resistance force proposed by Simonsen & Ocakli (1999);

$$\frac{P(\delta)}{M_0} = \frac{3b}{H\sqrt{1-\left(1-\frac{\delta}{4H}\right)^2}} + \frac{22H}{bt}\delta \tag{53}$$

Here δ is the indentation, b is the half-span and t is the thickness of the girder. The crushing wavelength is $4H$, where H is determined by;

$$H = 0.377 b^{\frac{2}{3}} t^{\frac{1}{3}} \tag{54}$$

, and the mean resistance force is calculated by;

$$\frac{P_m}{M_0} = \frac{18.72}{\lambda}\left(\frac{b}{t}\right)^{\frac{1}{3}} \tag{55}$$

The idealised folding pattern is shown in Figure 25, where it is shown that the deformation is developed by eight plastic hinge lines.

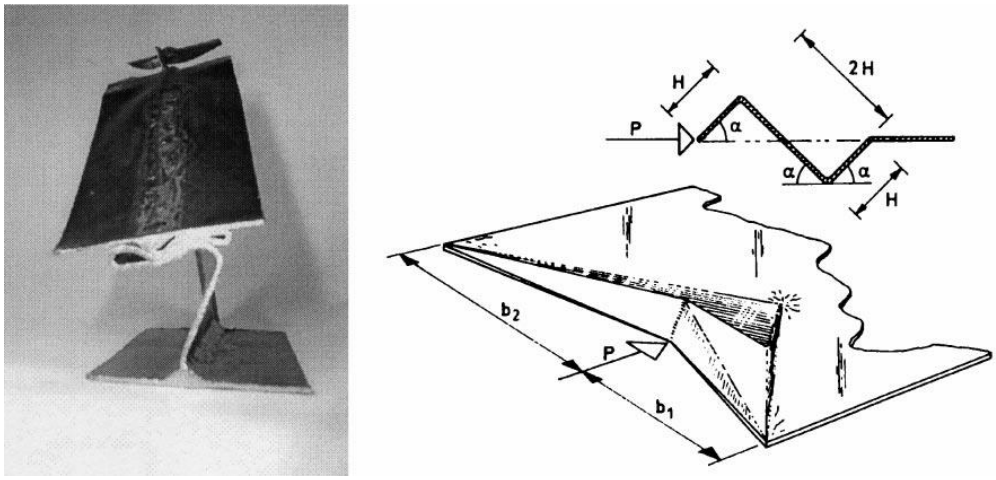

Figure 25: Crushed girder (left) compared with the idealised deformation model (right) by Simonsen & Ocakli (1999)

This can be compared with a similar folding mechanism suggested by Hong & Amdahl (2008), seen in Figure 26.

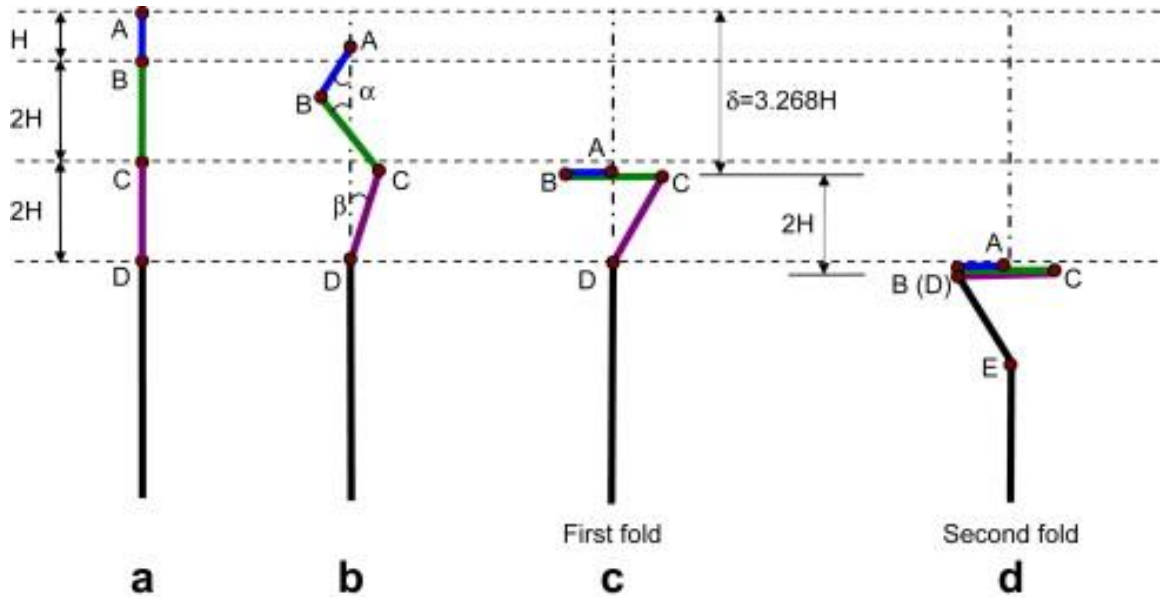

Figure 26: Idealised folding pattern by Hong &Amdahl (2008)

Both models display a deformation pattern with two folds, but the latter has an assumed deformation depth of 5*H* instead of the depth 4*H*.

The deduction of the following analytical formulae in addition to formulae used to predict the resistance for subsequent folding can be studied in *Crushing Resistance of web girders in ship collision and grounding* by Hong & Amdahl (2008). The wavelength *H* can be found by;

$$H = 0.395 b^{\frac{2}{3}} t^{\frac{1}{3}} \tag{56}$$

The mean crushing force is found using;

$$\frac{P_m}{M_0} = \frac{17.0}{\lambda}\left(\frac{b}{t}\right)^{\frac{1}{3}} \tag{57}$$

Finally the instantaneous crushing force can be calculated for the first fold (valid up to case c in Figure 26), using the following expression;

$$P(\delta) = \frac{1.2 M_0 b}{H\sqrt{1-\left(1-\frac{0.3\delta}{H}\right)^2}}\left(2 + \frac{1-\frac{0.3\delta}{H}}{\sqrt{3+\left(1-\frac{0.3\delta}{H}\right)^2}}\right) + \frac{5.56 N_0 H \delta}{b} \tag{58}$$

5.3.3 Stiffened plates

Additional strength is provided to the deck by the stiffeners and plates. This can be accounted for by using similar expressions as shown in the previous. Zhang (1999) proposed a simplified method to determine the resistance of a plate, impact loaded by different ship bow shapes. The raked bow formulation (as shown in Figure 27) is chosen for this thesis bearing in mind the collision configuration used (as shown in Figure 18).

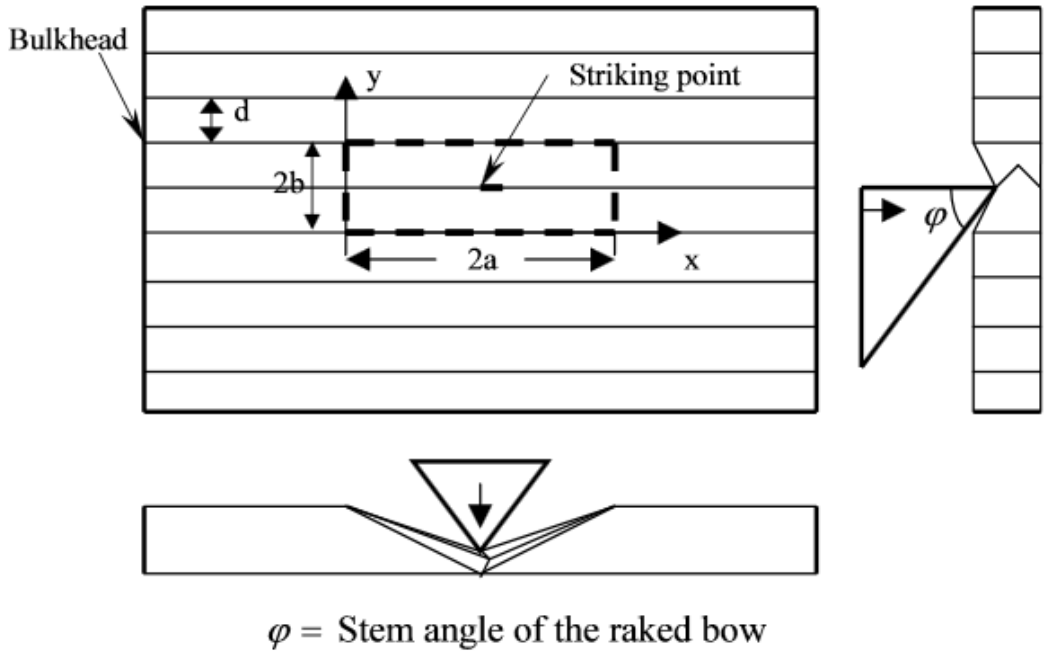

Figure 27: Raked bow impacting a ship side (Zhang, 1999)

The following expression is the used to calculate the instantaneous resistance of the crushed panel.

$$P(\delta) = \frac{4}{3}\frac{2}{\sqrt{3}}\sigma_0 t_p \delta \left(\frac{d}{a} + \frac{a}{d}\right) \tag{59}$$

This can be used in the case of a container dropped on deck, where d is the frame spacing, t_p is the plate thickness while $2a$ and $2b$ are the plate dimensions. The plate dimensions will then be chosen according to the frame spacing and the effective span ($2b$ in Sec. 5.3.2) of the crushed girder. Haris & Amdahl (2012) argue that the stiffeners can be included (to the membrane strength) by using equivalent plate thicknesses in x - and y-direction (t_{px} and t_{py} respectively), where the stiffener area is smeared over the plate. This depends on the

orientation of the stiffeners, i.e. longitudinal stiffeners will only contribute the equivalent longitudinal thickness. The expression is then adjusted as follows.

$$P(\delta) = \frac{8}{3\sqrt{3}}\sigma_0 ad\left(\frac{t_{px}}{d^2} + \frac{t_{py}}{a^2}\right)\delta \tag{60}$$

5.3.4 Total resistance

An analytical representation of the deck resistance was made by including all the relevant contributions from the different structural members. This involved predicting how the deck would deform and how the structural members interacted. Haris & Amdahl (2012) show how, by defining an impact area comprising of different structural members that contribute according to position relative to the impacting object (in their case for different bow shapes). A numerical study is made to analyse the different contributions. Based on this, weight factors are defined for each member and multiplied to their mean crushing resistance. All contributions are finally summed to get the total structural resistance during impact.

The main focus of the current study was to analyse the response of the deck structure by numerical studies. A more involved analytic study could be carried out as further work. These methods were therefore applied in a simple manner.

The deformation pattern was predicted to occur within an area of 1.2x1.2 m (in the deck centre) similar to what was assumed in the plastic hinge method (shown in Figure 24). Two scenarios with regards to the location of the crushing force were analysed using simplified formulae. These corresponded to scenario 1 and 3, presented in Section 4.5.3. A comparison of the resistance and energy absorption could then be made (presented in Sec. 6.4.2). The contribution factors are displayed in Table 10 and Table 11.

Table 10: Contribution factors for structural members, Scenario 1

Scenario 1	Total contribution factor
Web girder	1.0
Plate (1.2x1.2 m)	1.0
Stiffeners	2.0

Table 11: Contribution factors for structural members, Scenario 3

Scenario 3	Total contribution factor
Plate (1.2x1.2 m)	1.0
Stiffeners	2.0

How the contribution factors were chosen, can be shown in Figure 28;

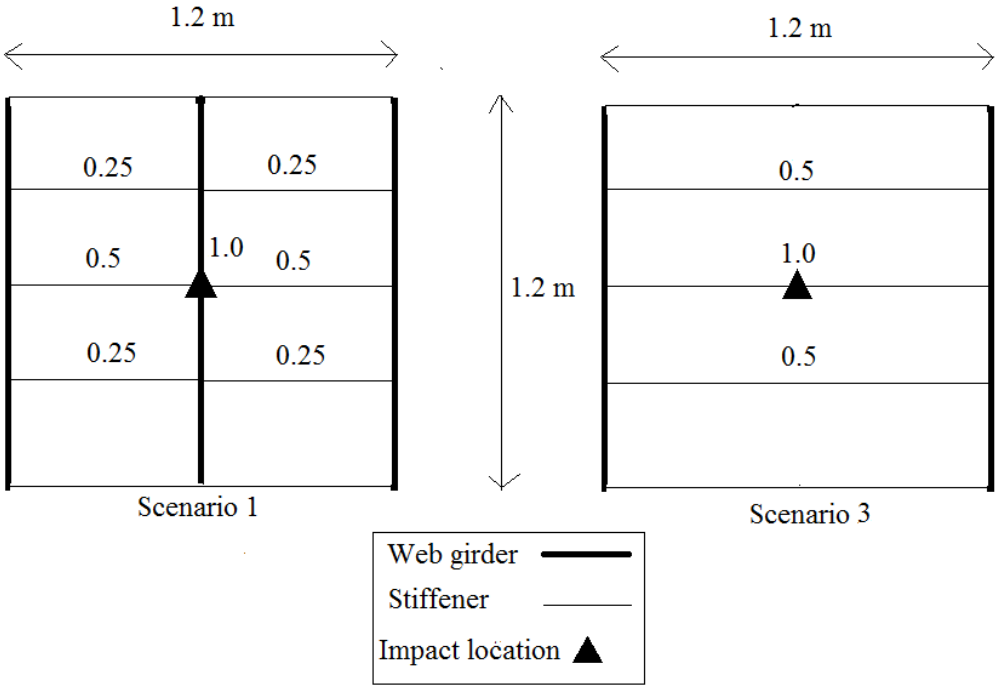

Figure 28: Contribution factors of relevant structural members

6 Results

The methods presented in Sections 4 and 5 were applied to analyse the resistance of the deck structure (above an LNG fuel tank) when crushed by a container. The resistance can be described by the force (working in the opposite direction of the container) in relation to the indentation (depth of deformation). The force was defined by the vertical contact force between the container and the deck. The indentation was measured at the impacting corner of the container (shown in Figure 29). The absorbed energy was quantified by integrating the resistance force over the indentation.

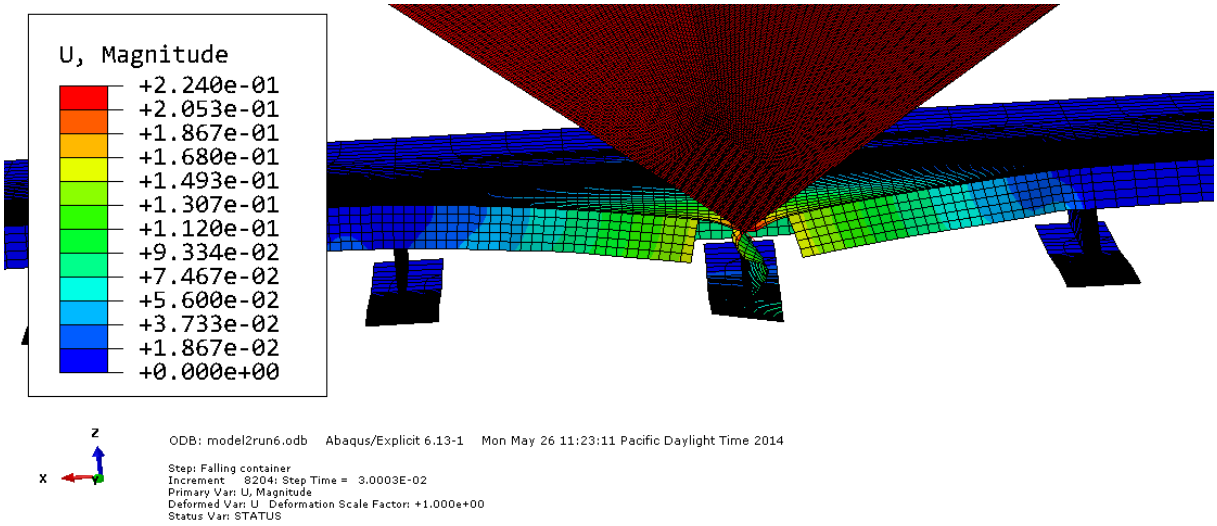

Figure 29: Indentation U [m] of deck (model is cut in half)

Correctness of the FE-solution was tested by executing convergence tests with respect to mesh and time increment size. Parametric studies based on sensitivity of results due to effects from strain rate, friction, impact velocity, BC's and fracture strain were subsequently conducted. Analytical results were compared with numerical results. Finally, the deck penetration resistance was tested with regards to critical energy absorption from impact. Firstly, the results were validated according to the following.

6.1 Validation of Results

Abaqus allows for a large number of output variables to be gathered. To find the deck resistance force, the history output variable “total force due to contact pressure” was chosen for the vertical force direction. To validate this, the user also sourced the acceleration and displacement of the container and calculated the force manually. As seen in Figure 30, the results show perfect correlation. This was more time efficient, since unnecessary calculations were avoided. Also, the results displayed the load history when contact was present, regardless of the force-direction.

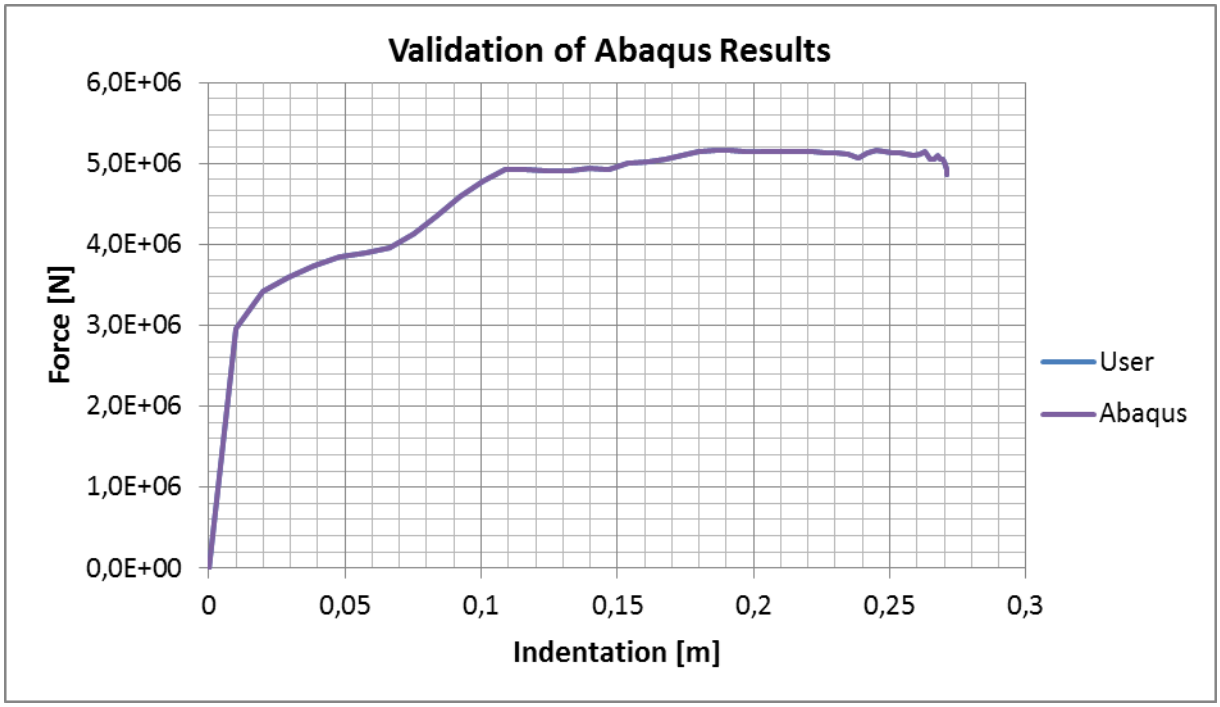

Figure 30: Validation of Abaqus results

6.2 Convergence Studies

Abaqus/Explicit was used as solver in the numerical analysis. Here the time increments are calculated automatically based on the smallest element size (as explained in Sec. 4.2). A convergence study was therefore carried out for the solution over time, by scaling the automatically generated time increments with 0.5 and 0.25. A mesh refinement study was aditionally carried out to obtain a satisfying level of convergence. This was also of importance to the representation of fracture.

The time domain of the analysis was chosen to be 0.2 seconds, which proved to be a reasonable time for the models to settle after impact. The time domain was split into 200 evenly spaced intervals for sourcing of result variables. This was believed to give a nice representation of results over time.

6.2.1 Mesh refinement study

The element sizes were reduced to naturally fit into the dimensions of the structural elements. It turned out to be important to show care when choosing the smaller element sizes. This was because the thickness was scaled down when the element length to thickness ratio became too small for the contact algorithm to handle. Erroneous results were obtained due to a significant reduction in stiffness which further induced fracture at an early stage of the indentation. This happened when the element size was set to 32.5 mm in the impact area. Increasing the element size to 37.5 mm eliminated this problem.

The results from the refinement test are presented in Figure 31 (force vs. indentation) and Figure 32 (absorbed energy vs. indentation). It is important to mention that the material parameters were based on the engineering stress-strain curve. Due to limited time, this error was not corrected in the mesh refinement study. This was however corrected for the remaining simulations.

The force-indentation relation for Run 1 turned out to be very discontinuous due to coarse meshing, and was therefore left out of the representation. Otherwise, results reached a satisfying level of convergence from Run 5 to Run 6. Hence an element size of 37.5 mm was chosen for the remaining simulations.

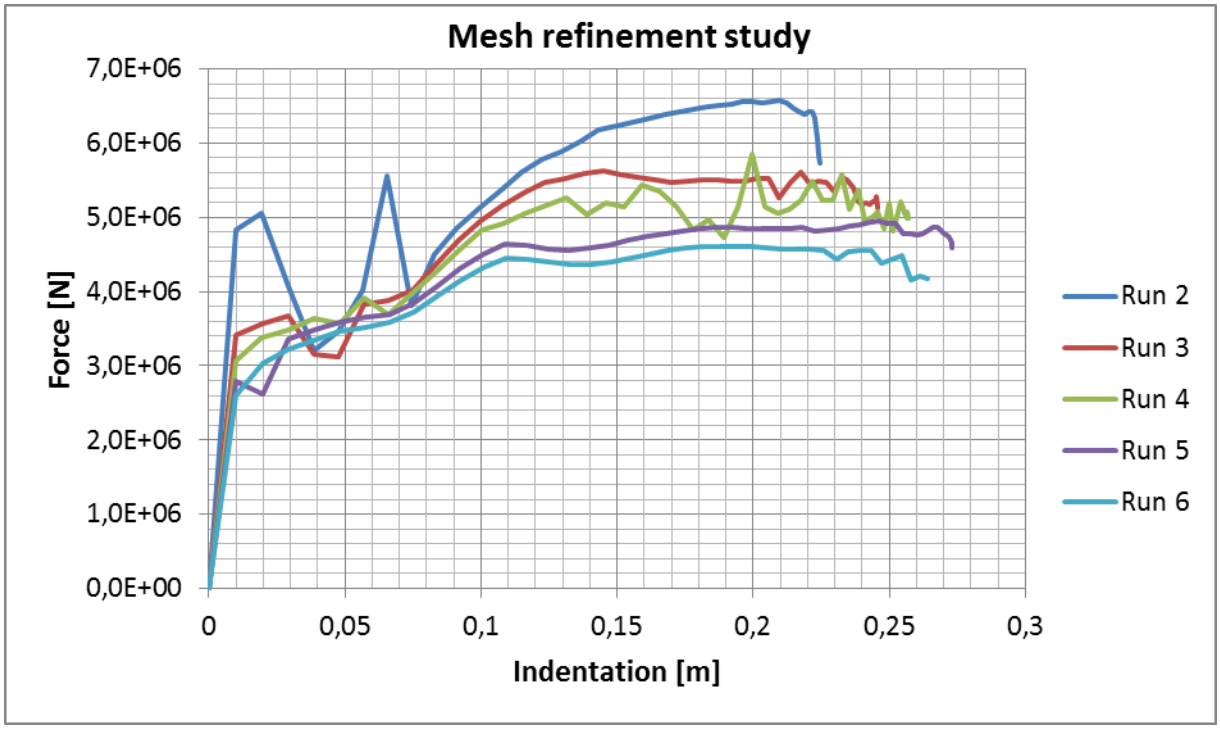

Figure 31: Mesh refinement study, force vs. indentation

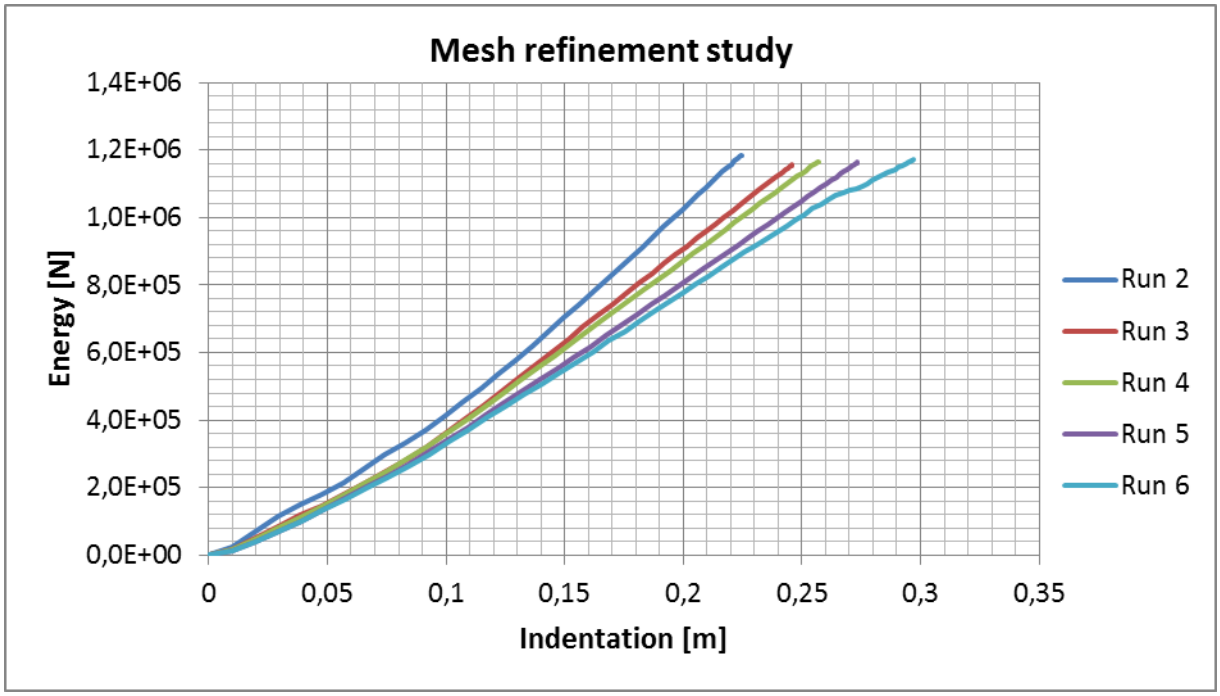

Figure 32: Mesh refinement study, energy vs. indentation

The maximum deflection of the deck is shown for Run 6 (with true stress-strain parameters) in Figure 33. Some of the following response mechanisms were observed;

- In-plane folding of web girder;

- Perpendicular indentation of deck plate;
- Transverse deflections of longitudinal stiffeners.

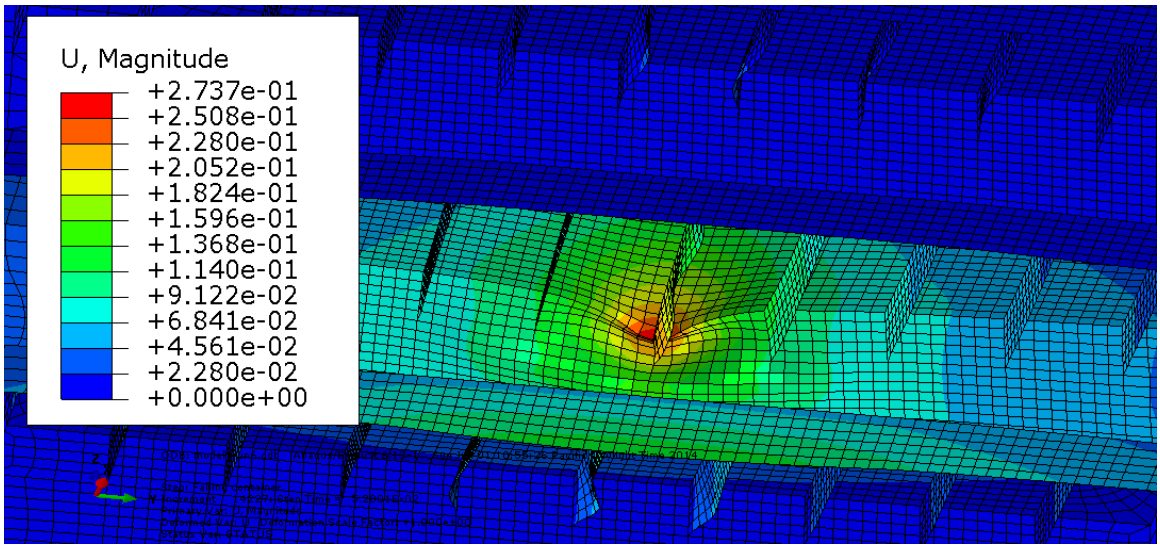

Figure 33: Maximum indentation U [m], Initial run

6.2.2 Time increment size

Convergence was also checked in terms of scaling the automatically determined stable time increment (as explained in 4.2). Scale factors of 0.50 and 0.25 were applied. The results are shown in the Figure 34 and Figure 35.

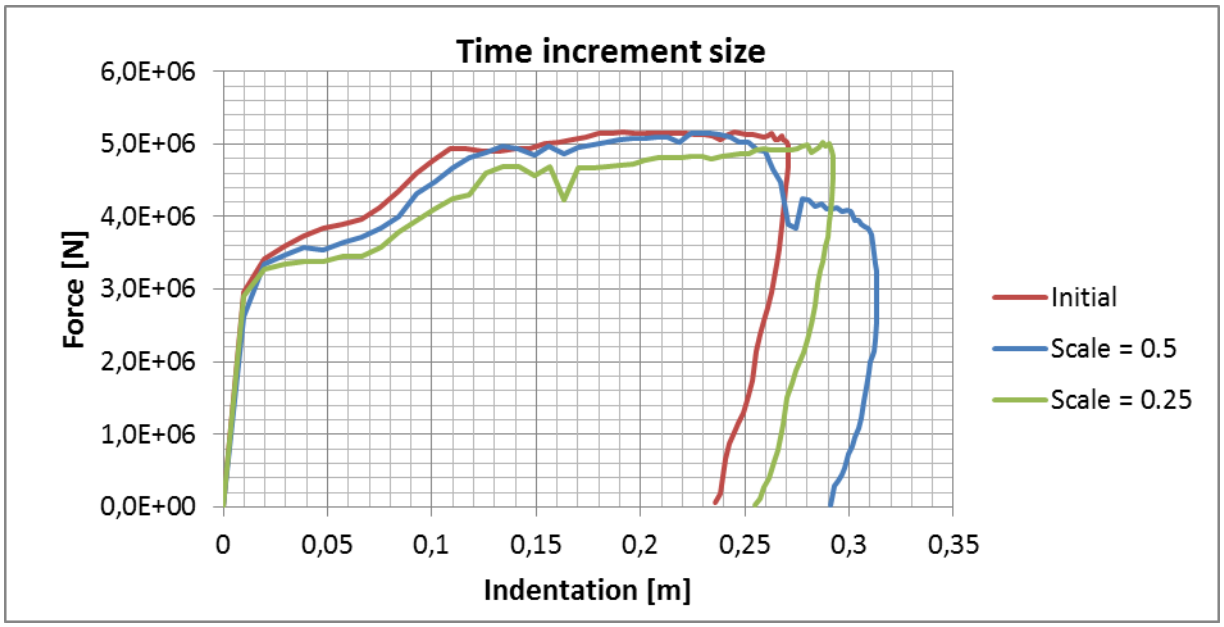

Figure 34: Time increment size, force vs. indentation

Displayed is a difference in resistance and indentation. Initially the structural strength seemed to decrease with the decreased scale value. Looking more closely, the resistance at fracture was lowest for a scale value of 0.5. The sources of uncertainty were not found. The energy curves showed better correlation, although a slight decrease in energy absorption vs. indentation was found by decrease of time scale.

The time scale was chosen to be 0.5, as this provided the worst fracture resistance. This study was, however, carried out after the parametric studies. The updated time scale was consequently used merely in the final comparison study, presented in Section 6.5.3.

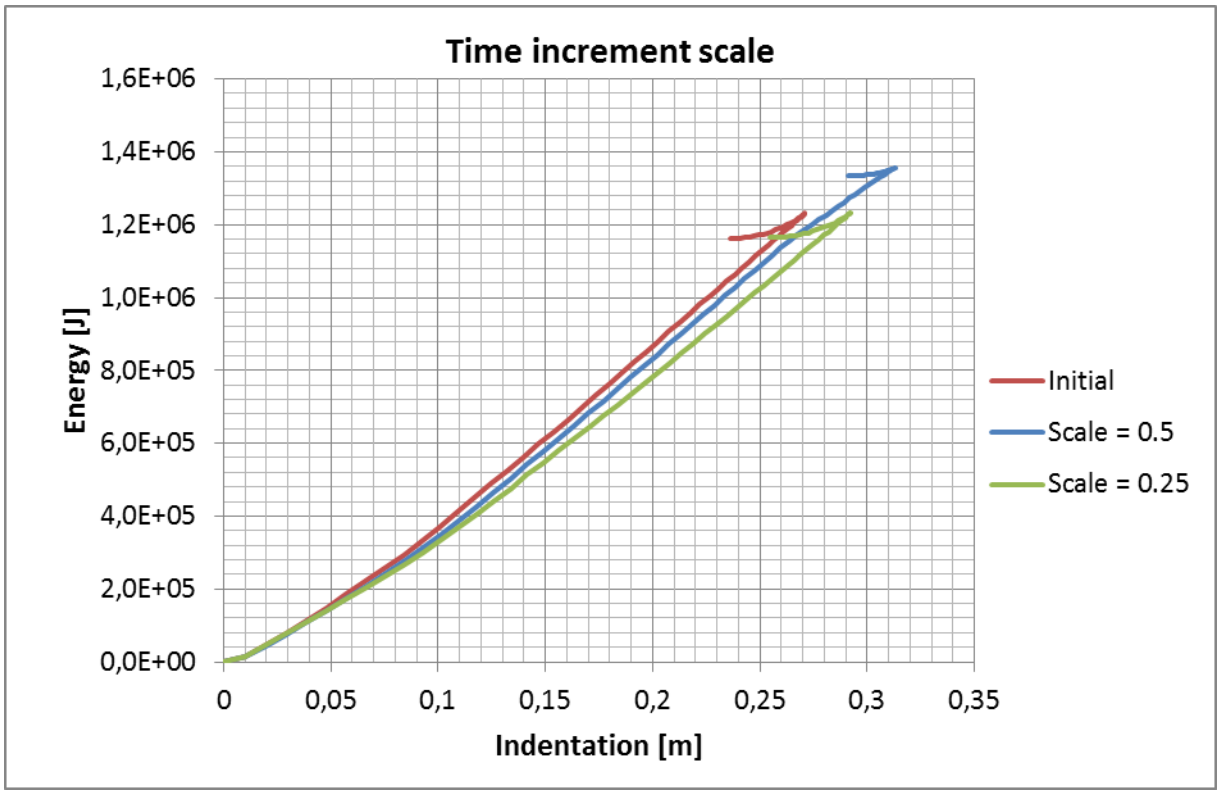

Figure 35: Time increment size, energy vs. indentation

6.3 Parametric Studies

Presented in the following are the results obtained from the parametric studies carried out in Abaqus/Explicit. The force-indentation curve obtained for the case of a container dropped from 10 m is compared to the observed deformation mechanisms during impact. This is presented in Appendix C**,** to get a better understanding of the force-indentation curves presented in the following.

6.3.1 Strain rate

The changes in deck resistance due to varying application of the Cowper-Symonds equation were analysed. The results are shown in Figure 36 and Figure 38.

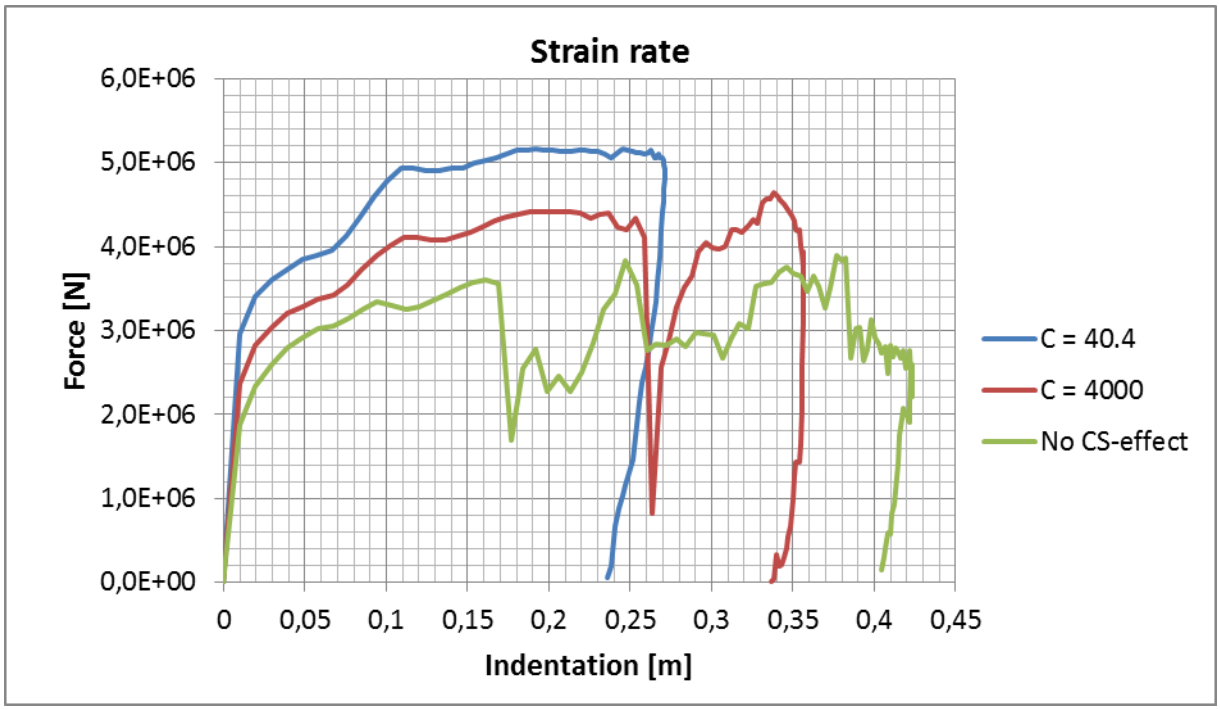

Figure 36: Strain rate, force vs. indentation

Significant changes were obtained, in terms of resistance force and energy dissipation to penetration. The final indentation of the deck also differed enormously; approximately by 0.17 m between neglecting strain rate effects and using the initial values for the Cowper-Symonds equation. The following deformation modes were observed, seen in Figure 37; penetration of deck plate, folding and rupture of web girder, transverse deflections and rupture of stiffeners. This can be compared with the displayed deformations in Figure 33.

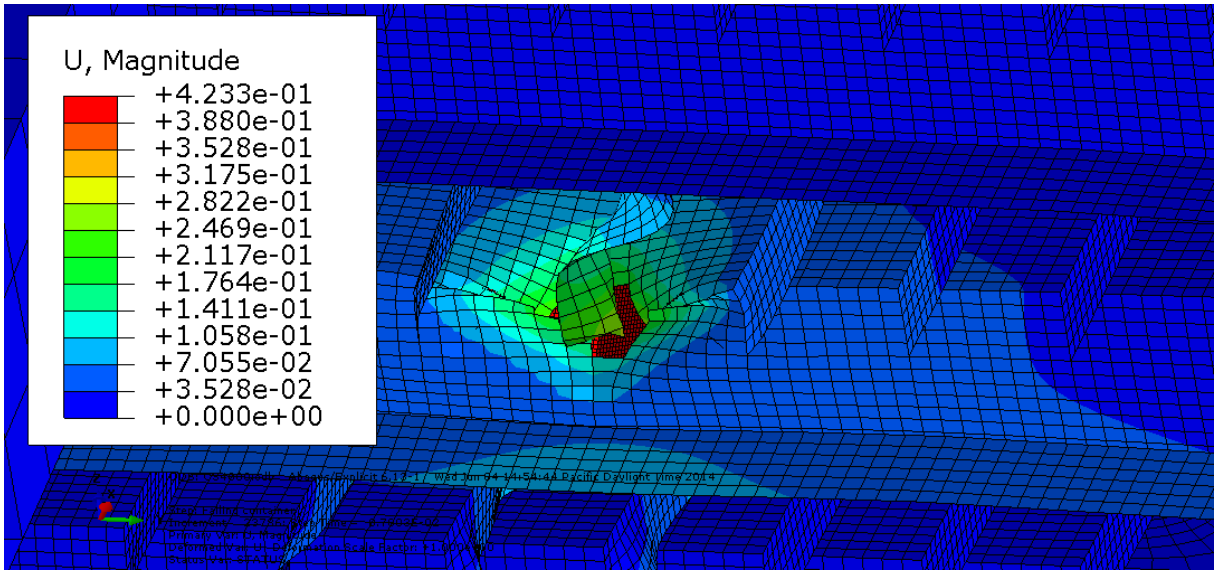

Figure 37: Deck response when strain rate effects are neglected

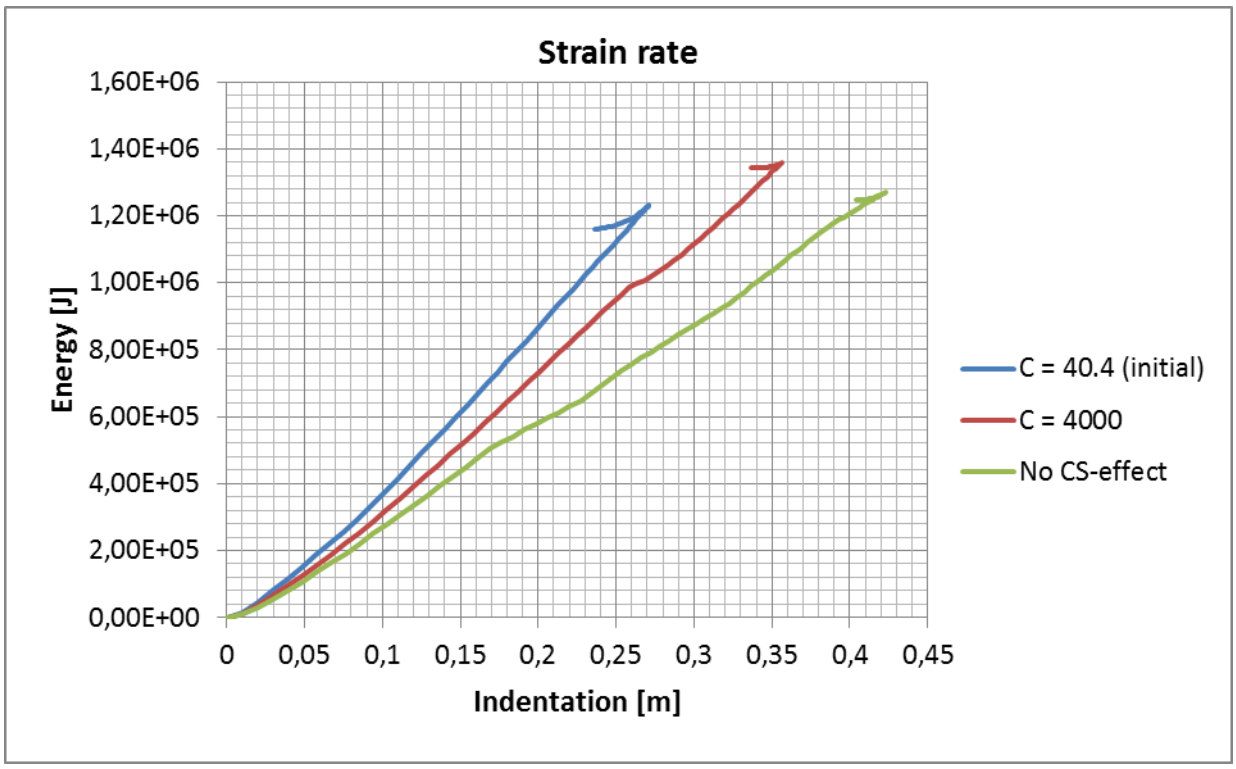

Figure 38: Strain rate, energy vs. indentation

6.3.2 Friction

Results for different friction coefficients are seen in Figure 39 and Figure 40.

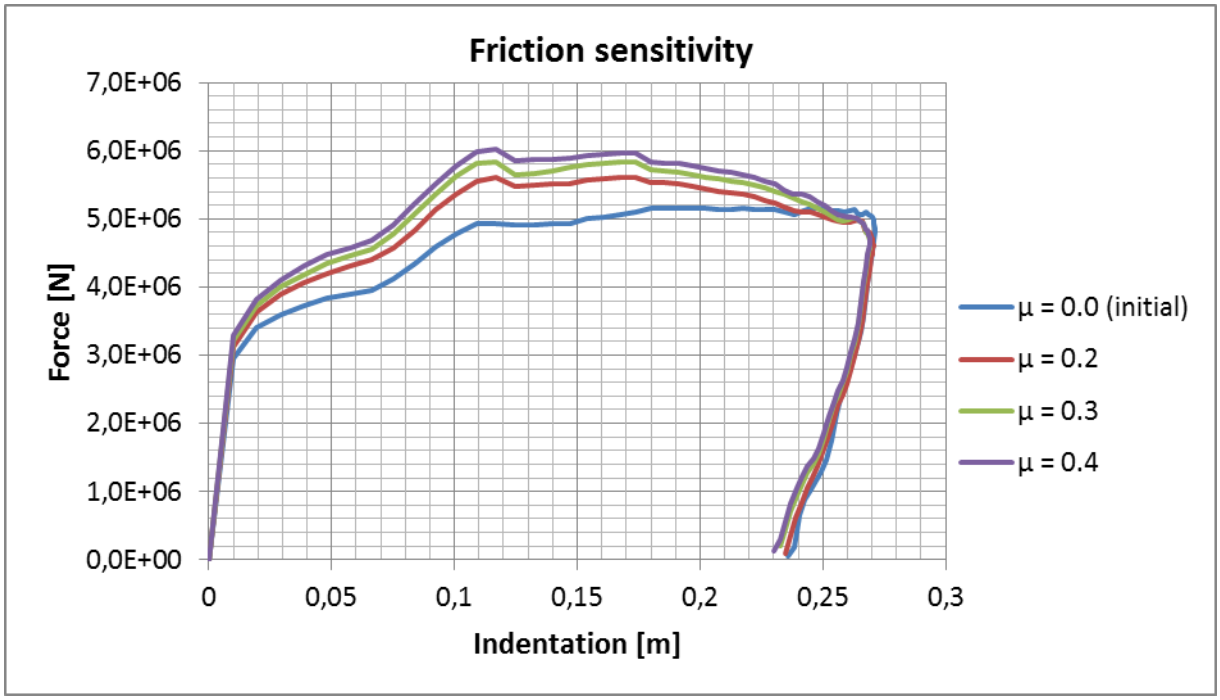

Figure 39: Friction, force vs. indentation

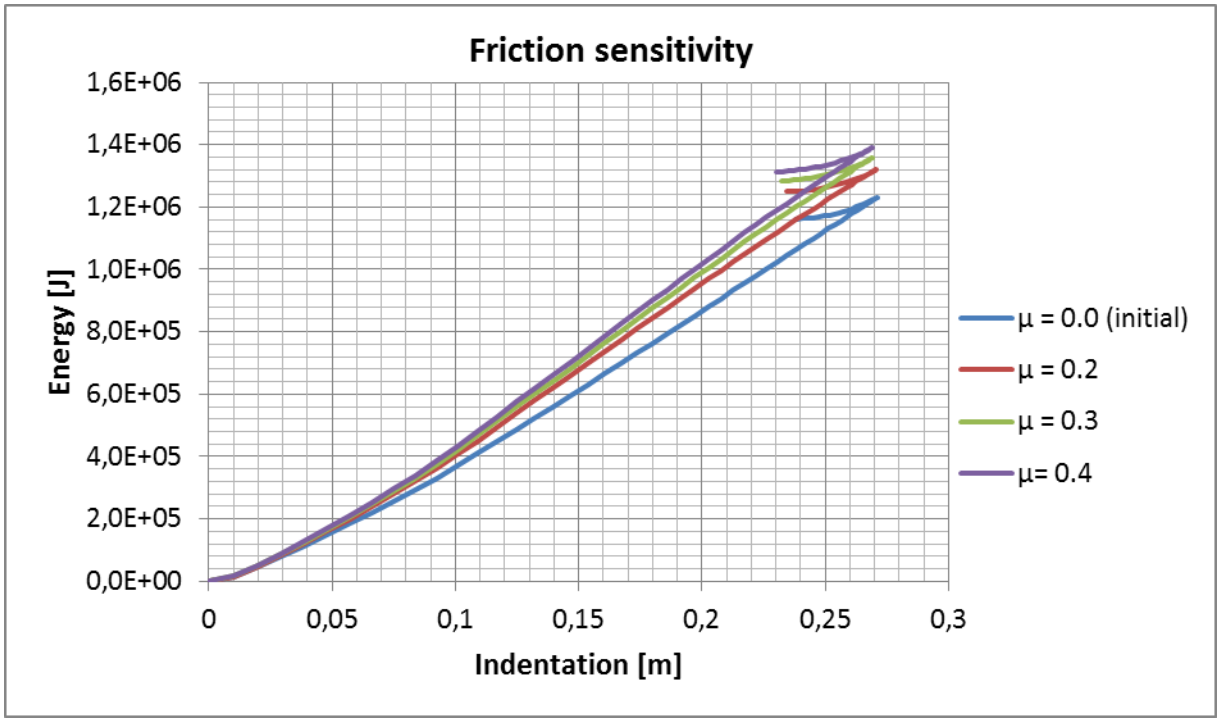

Figure 40: Friction, energy vs. indentation

The effect of friction was noticeable in the results. There were, however, minor differences in the increase of friction dissipation between the coefficients compared to the total dissipated energy in a frictionless state;

Table 12: Increase of total energy dissipation due to friction

Friction coefficient μ [-]	Increase of energy dissipation due to friction [%]
0.2	7.22
0.3	10.41
0.4	13.08

Based on this and earlier work (referenced in Section 4.4.3), a friction coefficient of 0.3 was introduced to the final configuration.

6.3.3 Impact velocity

Three different drop heights were tested to analyse the effect of increased velocity. The results are displayed in in Figure 41 and Figure 42.

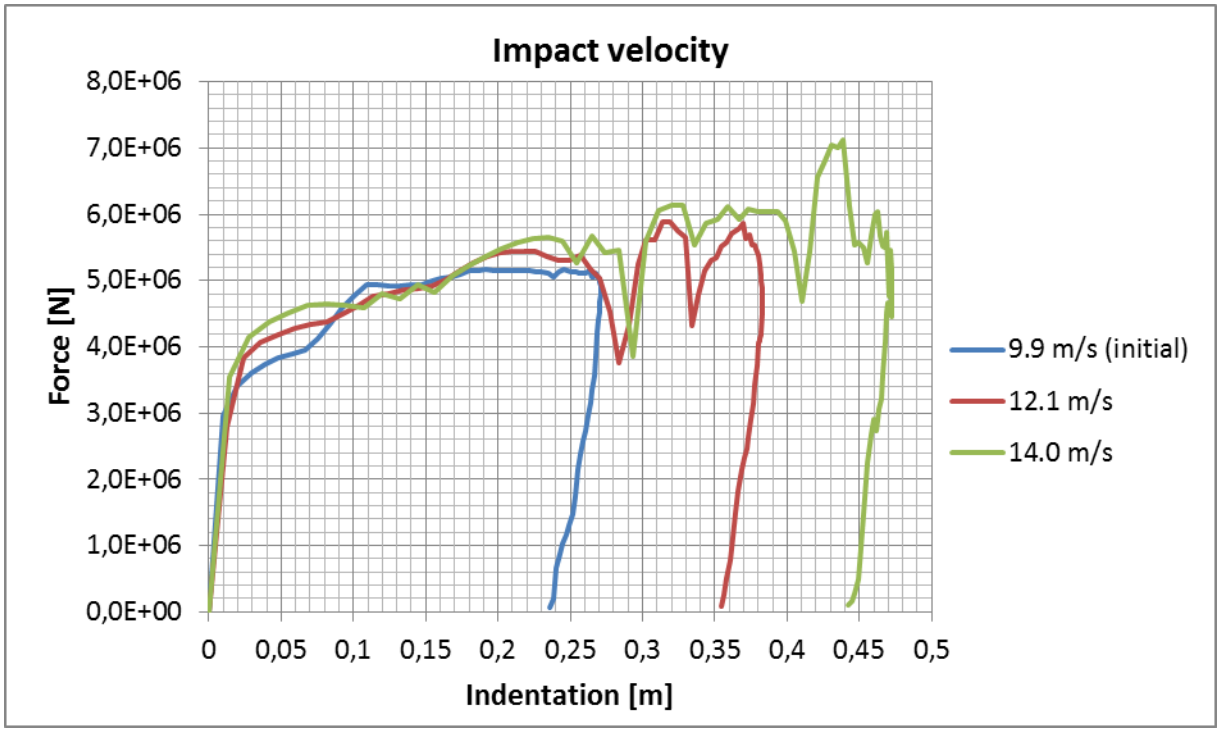

Figure 41: Impact velocity, force vs. indentation

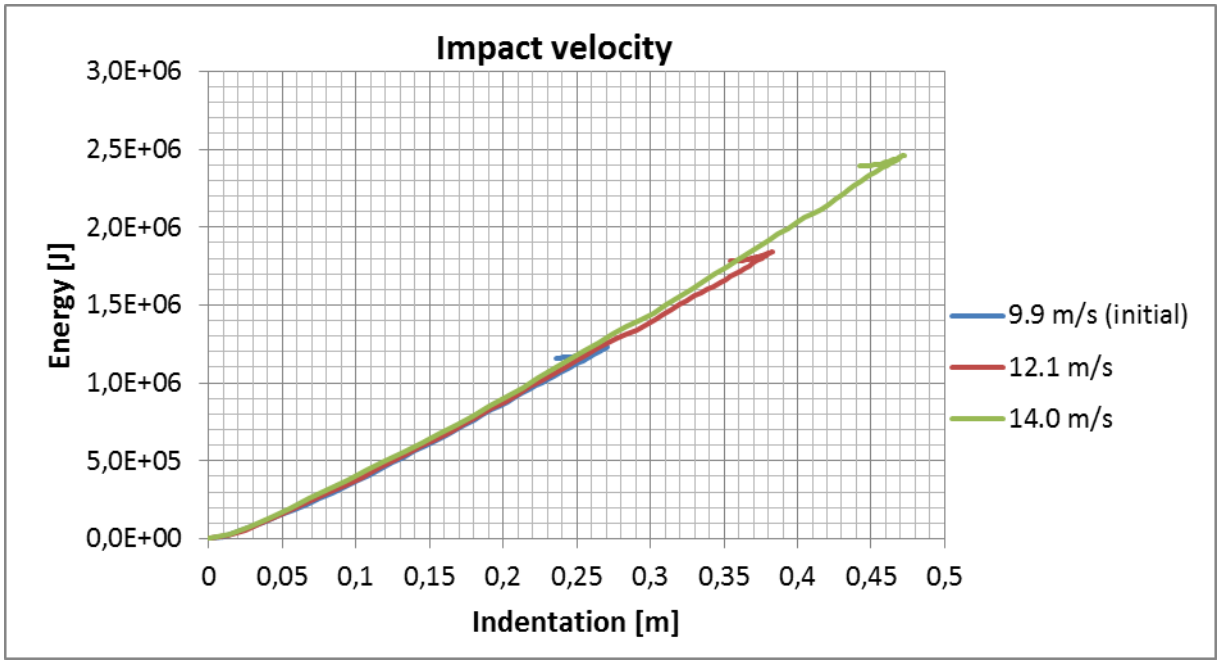

Figure 42: Impact velocity, energy vs. indentation

The deck resistance force increased with container velocity during the initial faces of the impact. Also the critical indentation to penetration increased between the two velocities of 12.1 m/s and 14.0 m/s. Other than that, the force-indentation curves correlated well. The slight differences in strength were seen to be caused by strain rate effects, as the same trend was not apparent when the container mass was increased (increasing impact energy, without increasing velocity) corresponding to a 40 foot container with a mass of 30.5 tonnes (see Figure 43).

A small increase in energy absorption in relation to indentation was obtained. This was measured by sourcing the dissipation energies at the indentation of approximately 0.271 m (corresponding to the maximum indentation for velocity v = 9.9 m/s). The increase (in percentage) was calculated, and is presented in Table 13;

Table 13: Increase in energy dissipation due to increased impact velocity

Impact velocity [m/s]	Dissipated energy [MJ]	Increase [%]
9.9	1.23	-
12.1	1.25	1.9
14.0	1.28	4.3

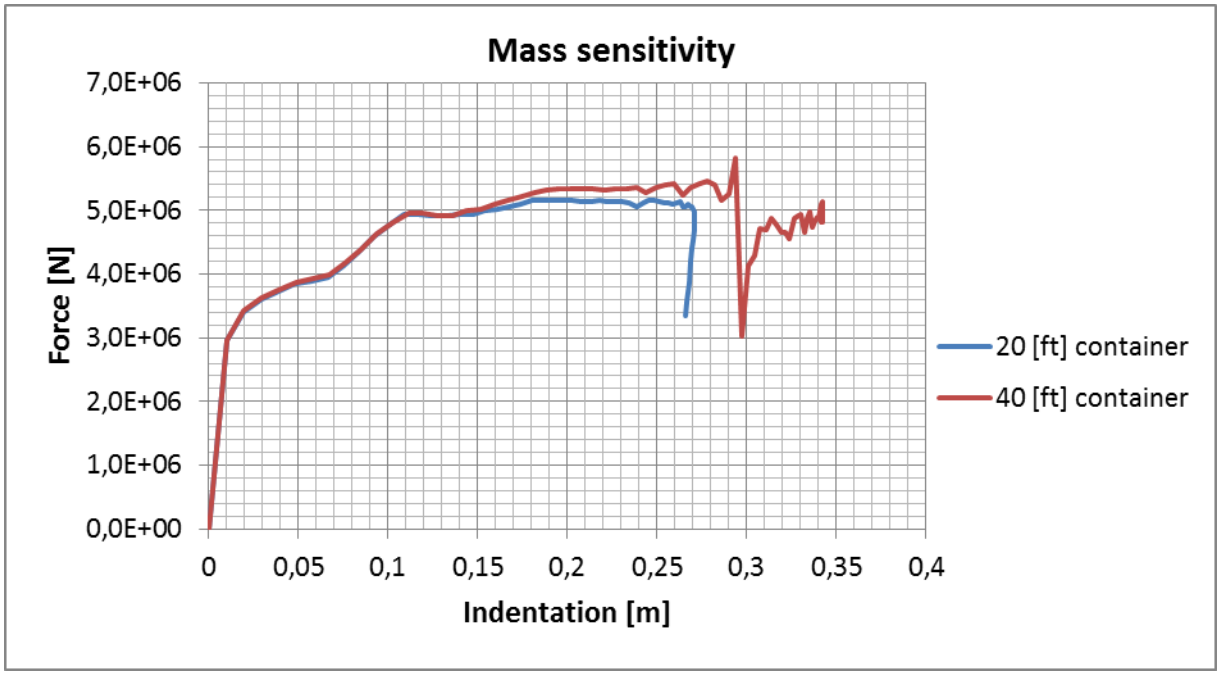

Figure 43: Container mass, force vs. indentation

6.3.4 Boundary conditions

A sensitivity study was carried out for Model 1 and Model 2 in terms of BC's. BC's were chosen as described in Section 4.5.2. The structural resistance of deck Model 1 and Model 2 are shown in Figure 44.

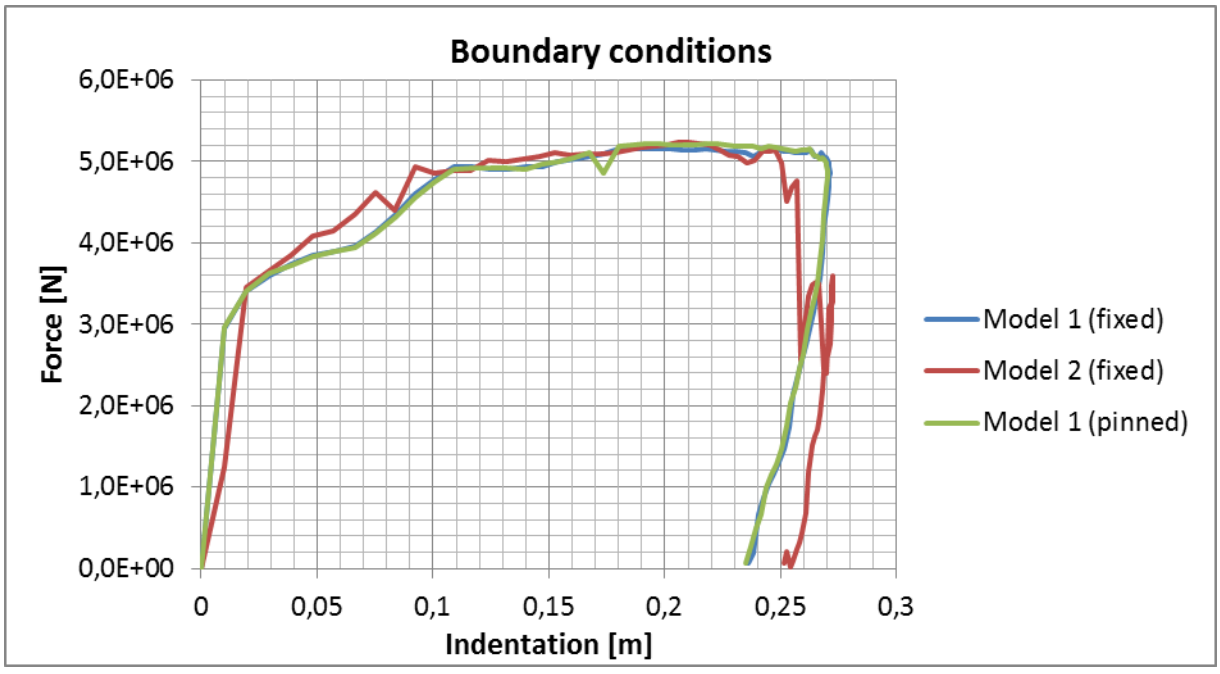

Figure 44: BC's, force vs. indentation

Changing the boundary conditions from fixed to simply supported edges (pinned) for Model 1 introduced negligible changes to the resistance of the structure.

Comparison of Model 2 and Model 1, however, showed noticeable differences in terms of penetration resistance; the deck was penetrated in Model 2, not Model 1. This was seen for indentations larger than 0.25 m. Difference in resistance was also obtained in the early stages of the impact simulations, up to an indentation of 0.1 m. The models correlated well otherwise.

Energy dissipation from the BC sensitivity analysis is shown in Figure 45.

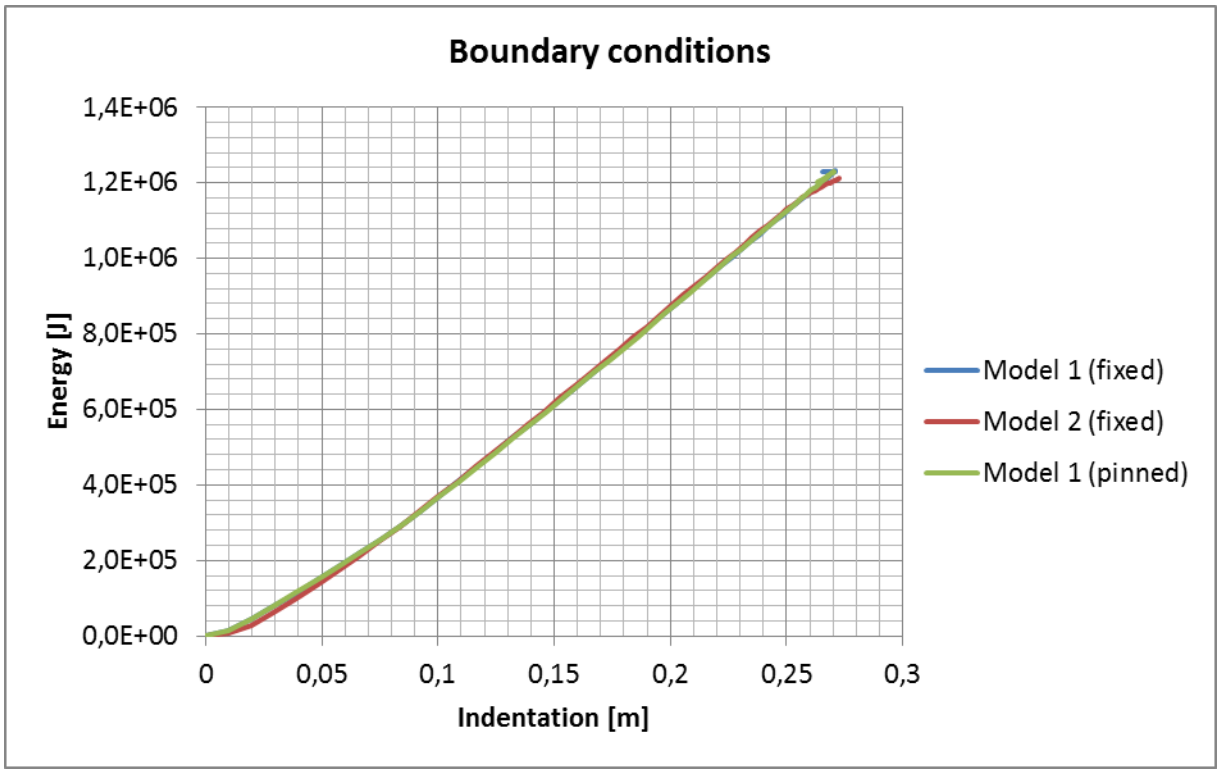

Figure 45: Boundary conditions, energy vs. indentation

Changing BC's showed little to no effect on Model 1 with regards to energy absorption. Results correlated well between Model 1 and Model 2.

Based on the above, a choice was made to use Model 1 with fixed BC's for all the analyses.

6.3.5 Fracture strain

Uncertainty in the applied fracture criterion (explained in Sec. 4.3.3) was studied. The results are shown in Figure 46 and Figure 47.

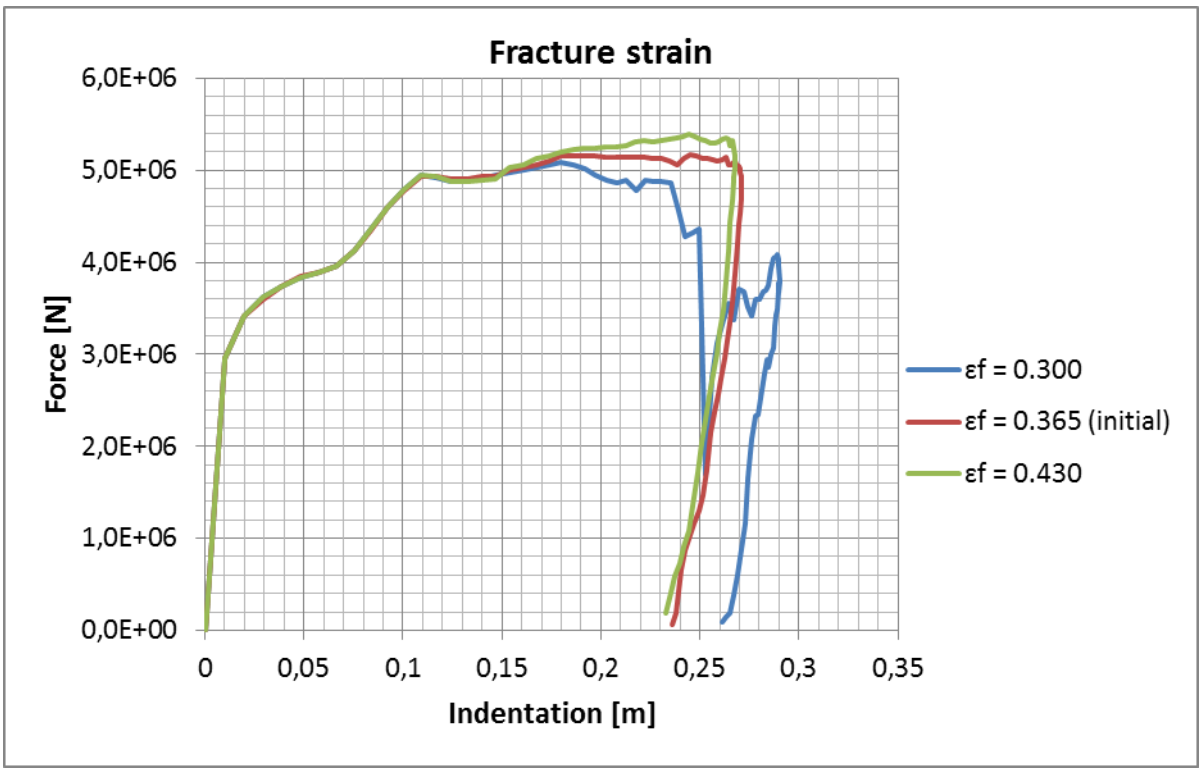

Figure 46: Fracture strain, force vs. indentation

The obtained results showed interesting changes in material behaviour in relation to fracture strain. The applied empirical model shown in Figure 14 correlated well with the present study, as the plotted strain to failure becomes increasingly uncertain for increased element lengths. This was seen by comparing the initial fracture strain with;

- The increased strain value ε_f = 0.43 corresponding to finer FE mesh, resulting in an insignificant difference in resistance force vs. indentation, and;
- The decreased strain value ε_f = 0.30 corresponding to coarser FE mesh, resulting in a significant difference in resistance and indentation due to fracture.

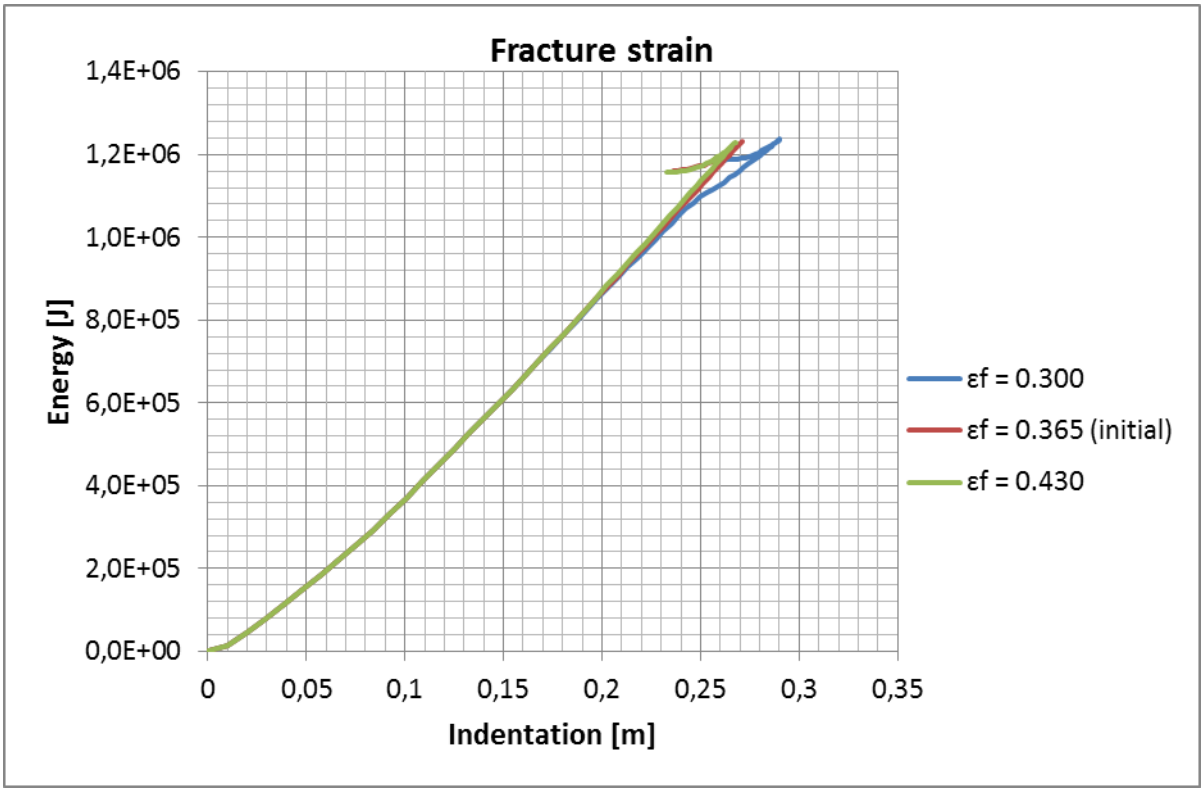

Figure 47: Fracture strain, energy vs. indentation

6.4 Analytical Studies

6.4.1 Plastic hinge theory

Plastic hinge theory was used to determine the collapse force of a simplified deck model, shown in Figure 24. The procedure presented in Section 5.2 was carried out. The collapse force estimate (indentation independent) is compared with numerical results in Figure 48.

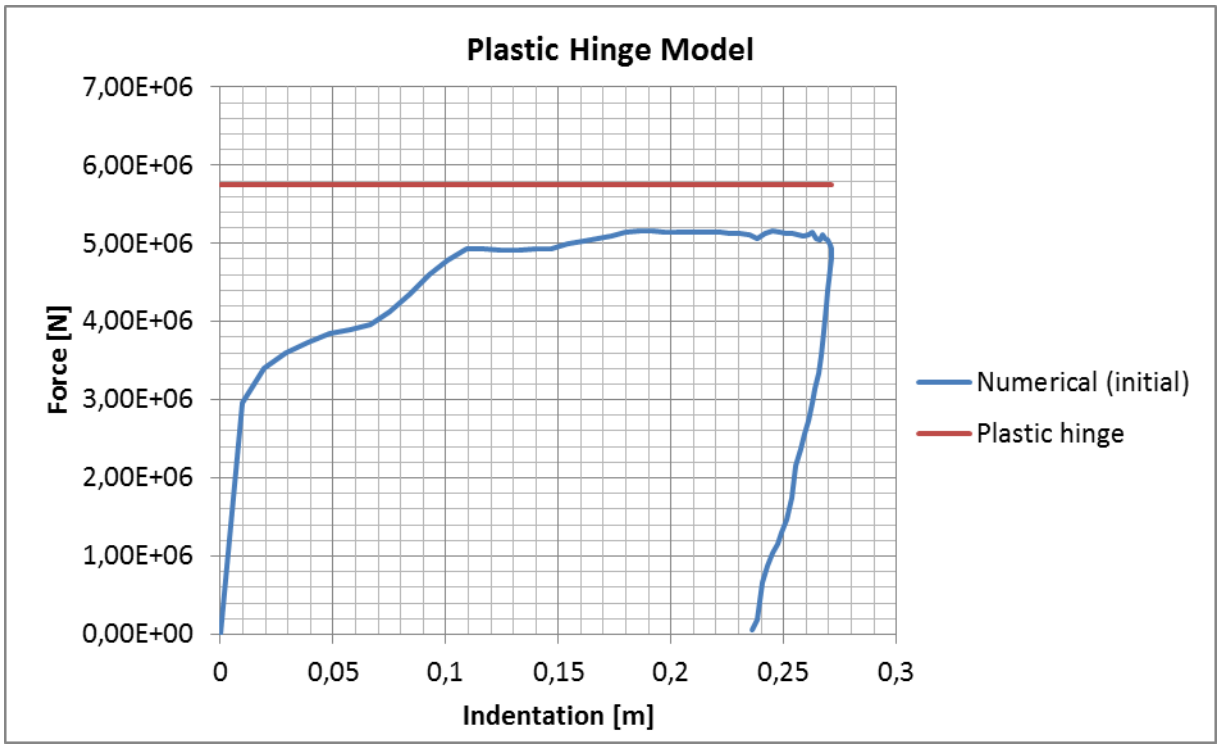

Figure 48: Collapse force of simple deck model, plastic hinge theory

The collapse force obtained using plastic hinge theory was approximately P = 5.75 MN. This shows a general overestimation of the resistance force when compared with numerical results.

6.4.2 Crushing mechanism

More involved analytical methods were used to study the deck resistance, based on crushing mechanisms as described in Section 5.3. Comparisons between numerical and analytical results were made, displayed in Figure 49 and Figure 50.

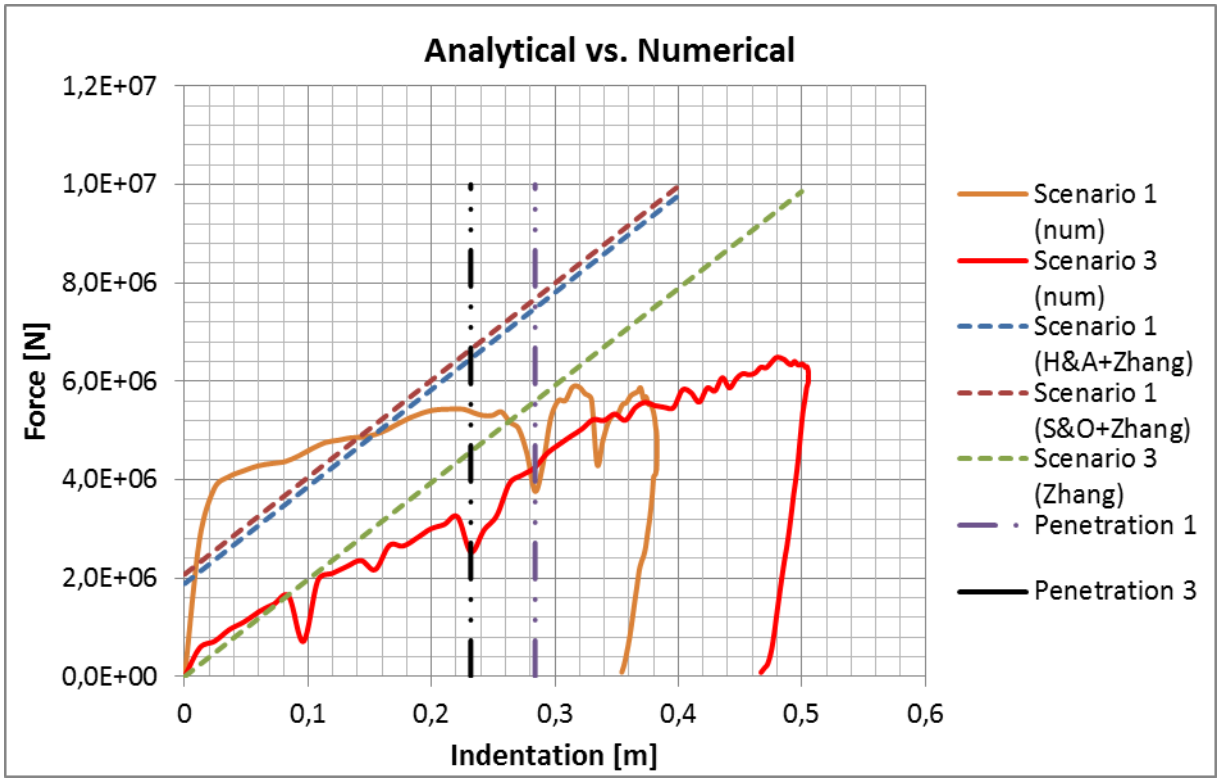

Figure 49: Analytical vs. numerical solution, Scenarios 1 and 3

Shown above are the resistance force-indentation relations for Scenarios 1 and 3. Numerical results (num) were compared with analytical calculations (H&A – Hong &Amdahl (2008), S&O – Simonsen & Ocakli (1999) and Zhang (1999)). Also included was the indentation at penetration for Scenarios 1 and 3 (Penetration 1 and Penetration 3 respectively) from the numerical simulations.

In the analytical calculations, the following forces were determined;

- The results obtained from the web girder crushing methods, were based on the mean crushing force (H&A using Eq. (57) and S&O using Eq. (55)). These results differed slightly; the S&O estimate ($P_m \approx 2.08$ MN) was 10 % larger than the H&A estimate ($P_m \approx 1.89$ MN). Both methods were used in the calculation of resistance for Scenario 1.
- The stiffened deck plate resistance was linear dependent on the indentation (as expressed in Eq. (60)). This was used for both load scenarios.

Poor representation of the force-indentation relation was made with the analytical solution of Scenario 1. There was however slight agreement between the numerical and analytical solution in Scenario 3, at least for an indentation up to approximately 0.11 m.

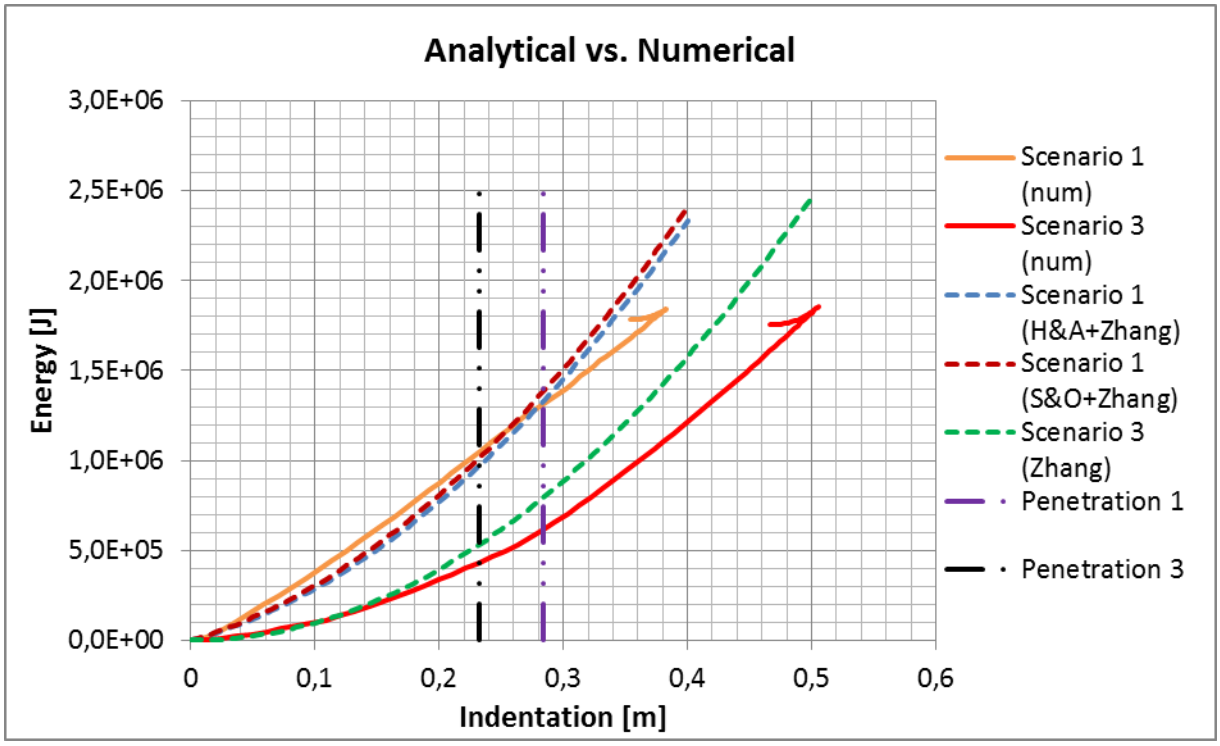

Figure 50: Analytical vs. numerical, Scenarios 1 & 3

In terms of energy dissipation comparison for Scenario 1, results correlated well before penetration. After penetration however, the energy curves spread out. The S&O estimated energy absorption showed better agreement with numerical results at indentations before penetration. The H&A estimate however gave a closer estimate of the energy absorption at penetration

The analytical results from load scenario 3 overestimated the energy dissipation compared to numerical results.

The above observations were made by comparing the curves, and calculating the difference (in percentage), presented in Table 14.

Table 14: analytical vs. numerical results in terms of energy vs. indentation at deck penetration

Scenario	Indentation [m]	Analytical [MJ]	Numerical [MJ]	Difference [%]
1 (H&A)	0.28	1.30	1.31	-1.05
1 (S&O)	0.28	1.36	1.31	+3.12
3	0.23	0.52	0.43	+20.1

The local deck response from load Scenario 1 was studied at the occurrence of deck penetration. Deformations are displayed in Figure 51. Half the deck model and the container were removed for better visualisation in b. The transverse web girder positioned below the location of impact showed failure by folding, which agrees well with the proposed models. The transverse extent of folding was mainly noticeable between the longitudinal stiffeners positioned at $\pm$ 0.30 m from CL. The longitudinal stiffener at CL was fractured by the impact.

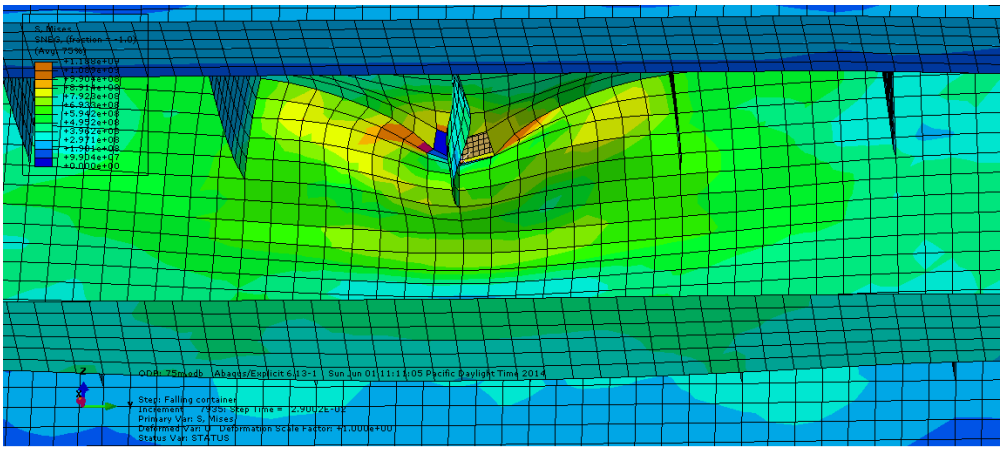

a.)

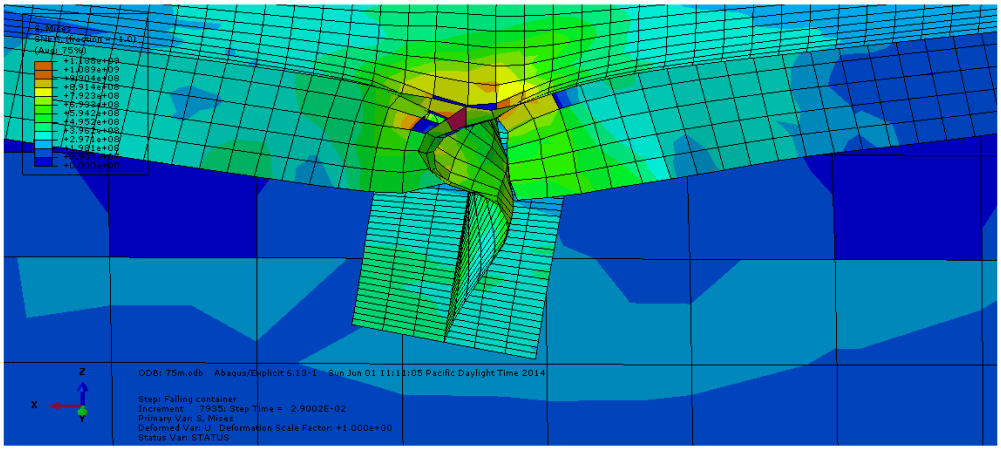

b.)

Figure 51: Deck response in Scenario 1, direction of view; a.) longitudinal; b.) transverse

6.5 Comparative Studies

6.5.1 Deformable container

To keep the study conservative, the container was assumed to be infinitely rigid. For comparison, the container was re-modelled using 4.4 mm thick Hardox 400 steel plating, thus being able to deform. This showed tremendous changes in the results seen in Figure 52 and Figure 53.

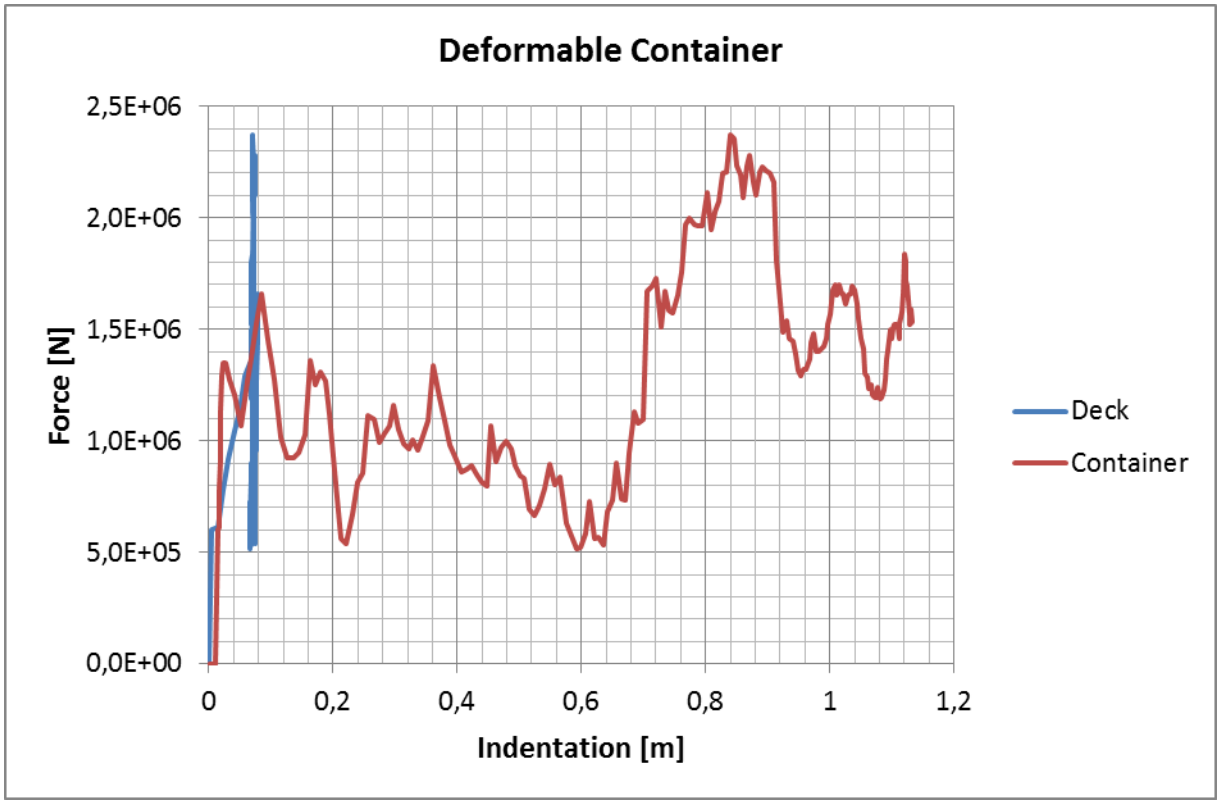

Figure 52: Deformable container, force vs. indentation

The deck was barely deformed compared to the container, which was completely crumbled by the impact (see Figure 54). Energy was absorbed mainly by the container, corresponding to a decrease of energy absorption in the deck by 93 %.

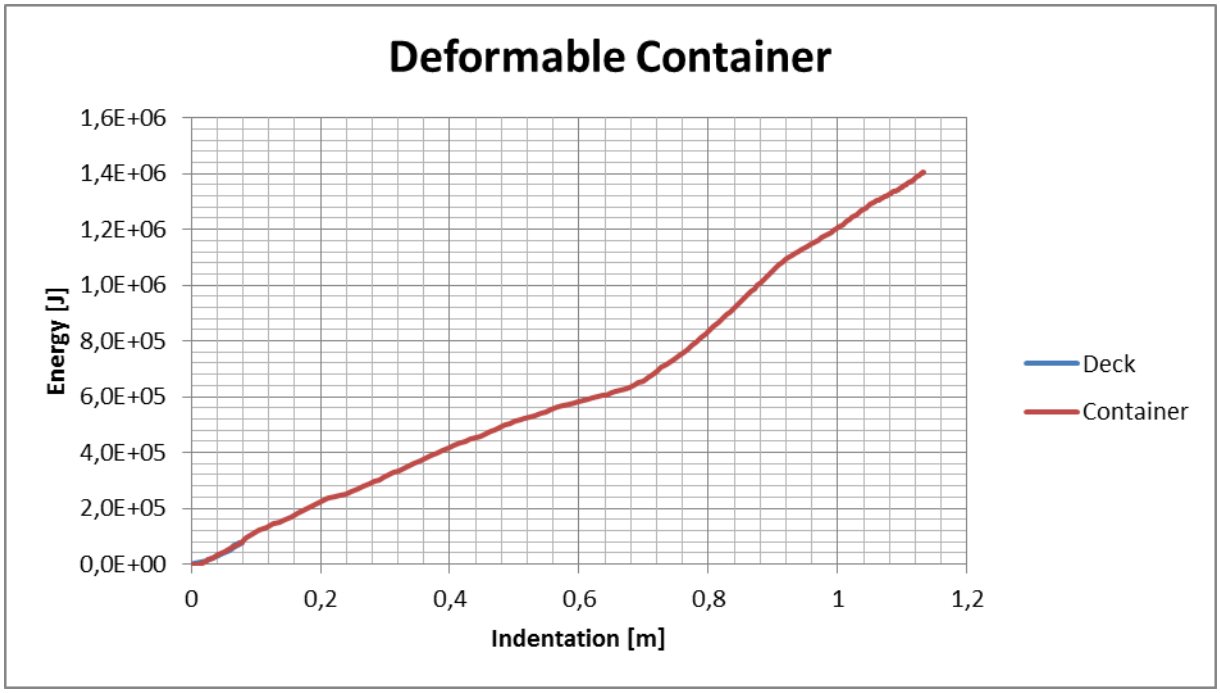

Figure 53: Deformable container, energy vs. indentation

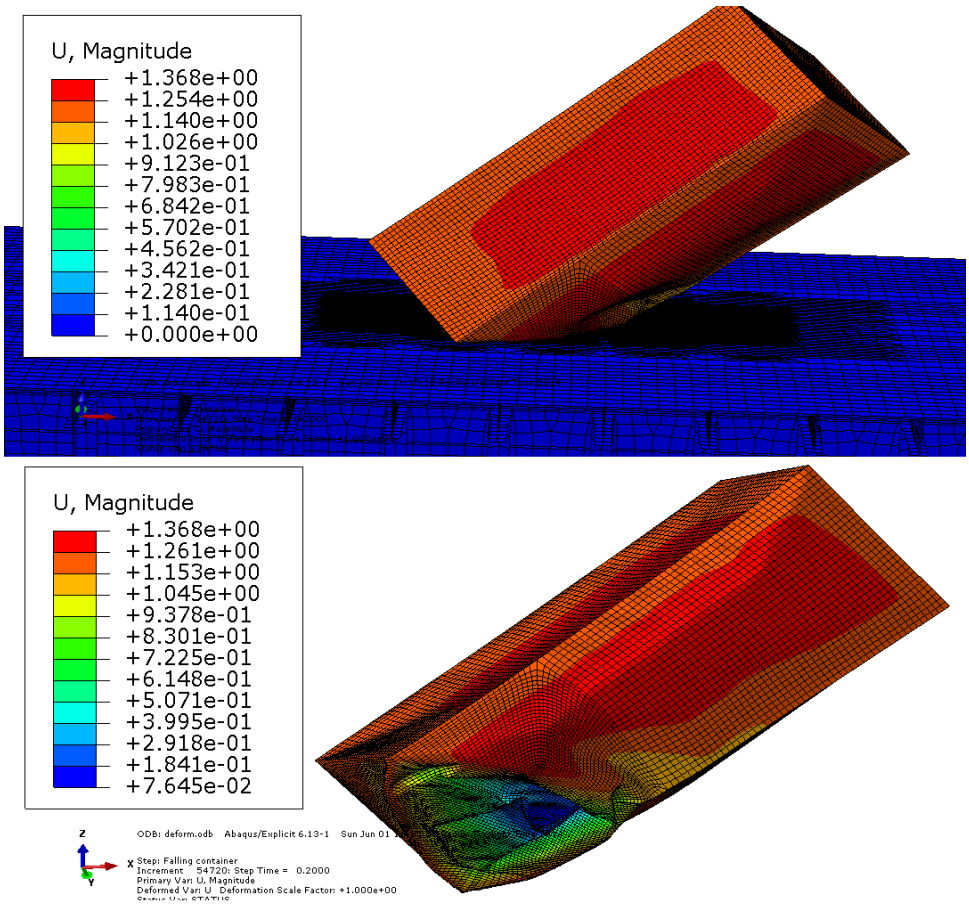

Figure 54: Deformed container (Hardox 400 shell plate)

6.5.2 Location of impact

The following study was carried out to assess the critical energy dissipation to penetration of the deck. Since penetration wasn't an issue in the initial run, the drop height of the container was increased (to 7.5 m) to inflict penetration in all four scenarios. The comparisons are seen for deck resistance and energy absorption in Figure 55 and Figure 56.

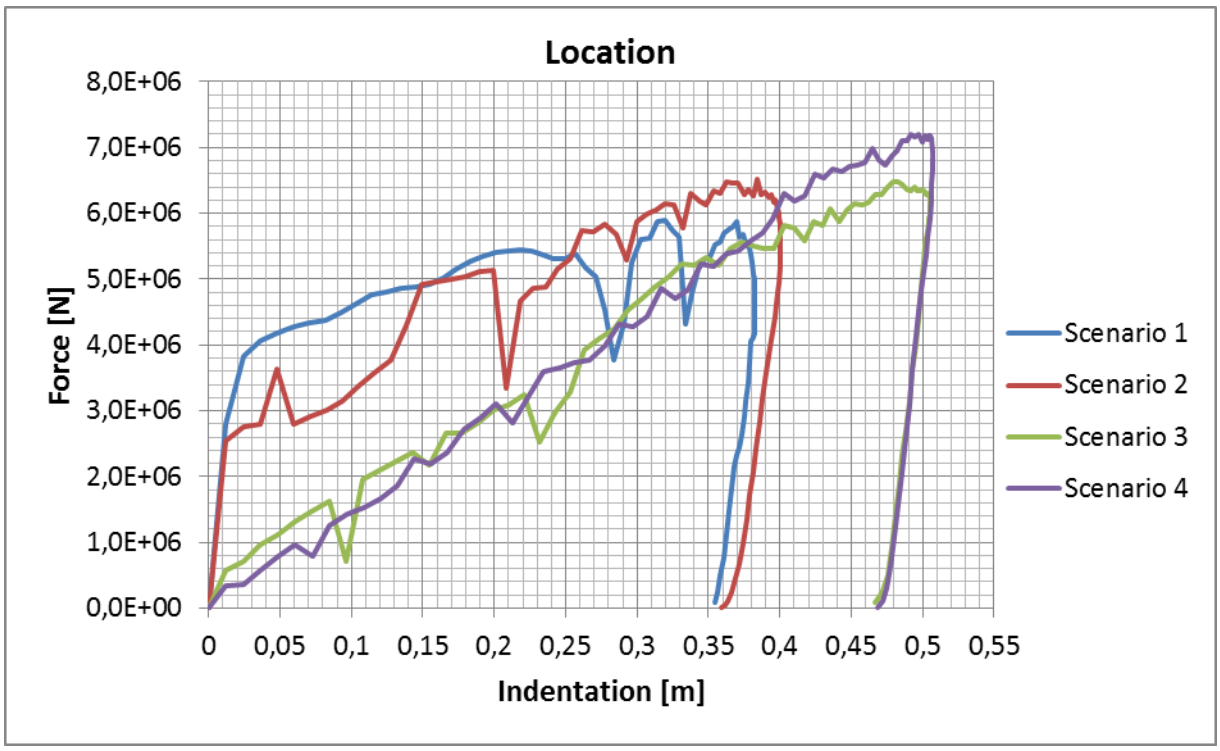

Figure 55: Location, force vs indentation

As expected, the critical energy to penetration was larger for Scenario 4. The deformations in Scenario 4 displayed tripping of stiffeners and deep indentation and rupture of deck plate.

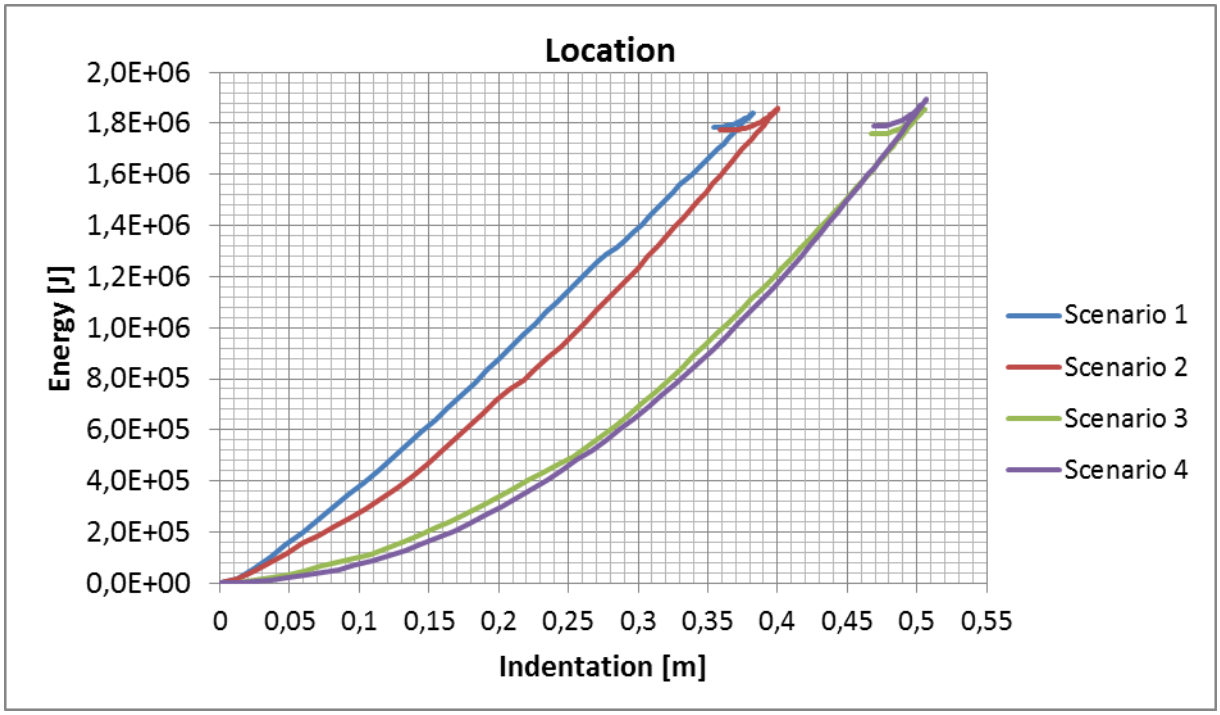

Figure 56: Location, energy vs. indentation

6.5.3 Steel type

Based on the convergence and parametric studies, final configurations were defined to compare resistance and energy absorption of the deck structure; using as-built steel vs. Hardox 400 steel parameters (as presented in Sec. 4.3). The specified (or changed) parameters are shown in Table 15.

Table 15: Parameter values for steel type comparison study

Parameter	Value
Time increment scale [-]	0.50
Cowper-Symonds constants	C = 4000 1/s, q = 5
Friction coefficient μ [-]	0.30
Mass of container [kg*10^3]	58.0
Impact velocity [m/s]	9.90

Increasing kinetic energy at impact was conservatively provided by increasing container mass, instead of impact velocity (to eliminate strain rate effects).Scenario 4 was chosen in terms of impact location (see Sec. 4.5.3).

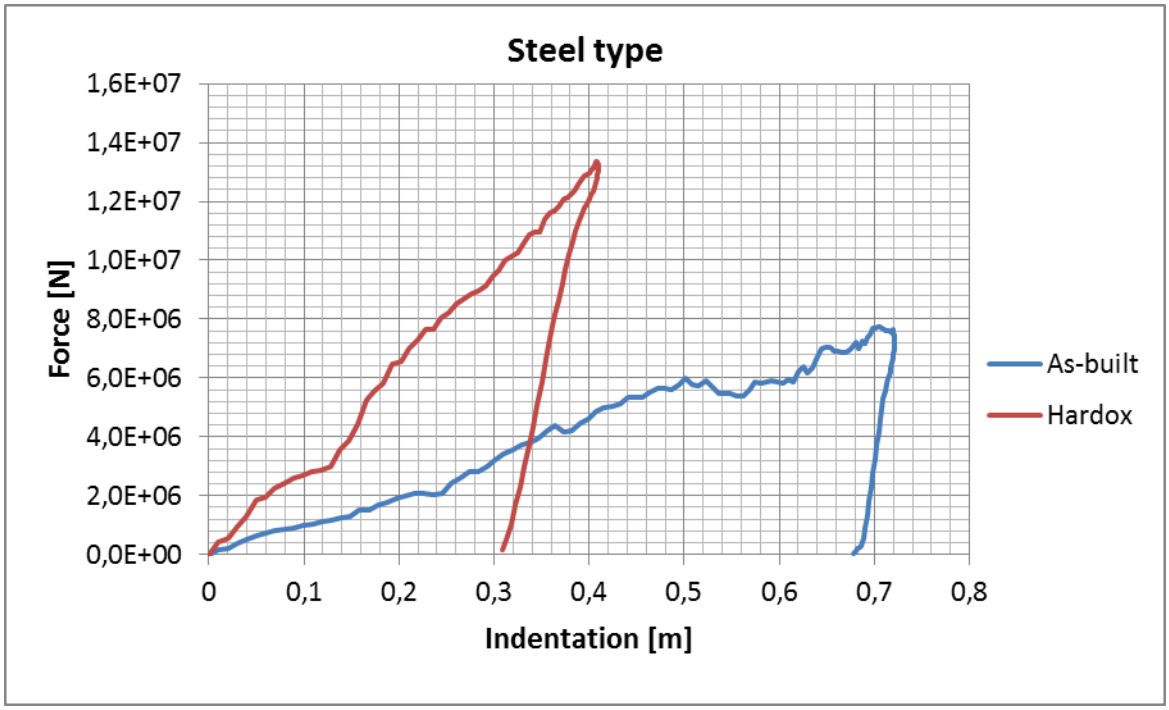

Figure 57: Steel type, force vs. indentation

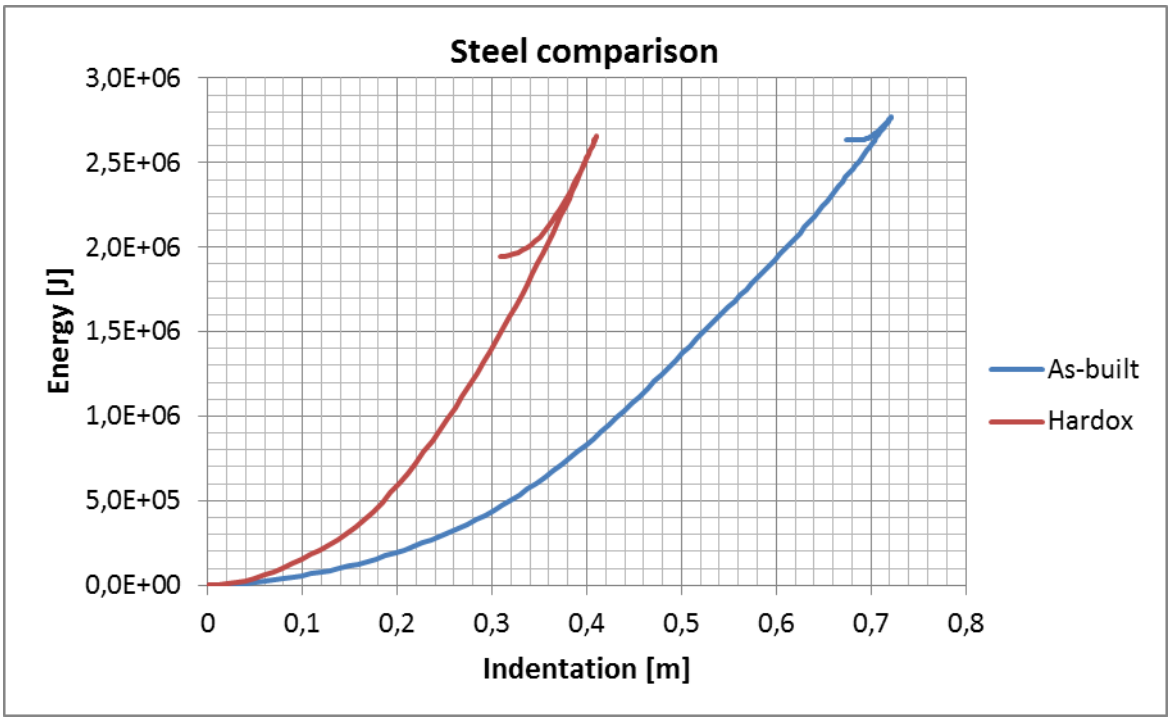

Figure 58: Steel type, energy vs. indentation

The specific values for critical energy dissipation to deck penetration were compared, and are presented in Table 16. The absorbed energy capacity to failure was increased by approximately 822 %.

Table 16: Final results, comparison of steel type

Parameter	NV-NA & NV-36 (as-built)	Hardox 400
Critical energy dissipation[MJ]	0.29	2.66
Indentation at first penetration [mm]	250	410
Max. indentation [mm]	722	410

The obtained value of indentation for the as-built configuration showed that the container not only penetrated the deck, but also impacted the LNG-fuel tank. This was seen by comparing the maximum indentation to the top point of the tank located 0.7 m below 1st deck (as displayed in Transversal Section #64 in Appendix DAppendix C). The critical energy dissipation to LNG-tank impact was shown to be 2.59 MJ for the as-built configuration.

7 Discussion

The scope of the thesis was restricted to the assessment of PSV deck penetration capacity by nonlinear FEA for the as-built and Hardox steel configurations. The critical energy to penetration was quantified based on the proven worst case scenario (see Sec. 6.5.2); assuming an infinitely rigid dropped object impacting the deck panel centre in between stiffeners and girders.

The final results showed an expected increase in penetration capacity using Hardox steel. This was based on comparing the received and assumed Hardox material parameters listed in Appendix A with the material parameters for conventional steels presented in Section 4.3. Parameters chosen for sensitivity analysis were considered well chosen based on the discovered uncertainties (in Sec. 6.3).

The FE solution converged in a satisfying manner by mesh refinement, although the initial runs (with coarser mesh) provided overestimated results considering resistance to failure. It is fair to assume that this was related somewhat with the applied fracture criterion developed by Ehlers (2010b). He showed similar trends when using the fracture criterion in the simulation of a stiffened plate subjected to a conical punch. Compared with experiments, a slight overestimation of the resistance force to fracture was obtained, by using 40 mm element length as opposed to 4 mm. The stable time increment was also tested for convergence. Less satisfying results were obtained in differences of resistance force to fracture. This source of uncertainty remained unsolved. Further investigation of the time increment scaling should be made, for instance by searching for similar problems in previous studies.

The uncertainty in strain to fracture of Hardox steel was unspecified in dependence of FE mesh and other important parameters discussed in Section 3.2. No measurable data from the present study can support or discard a fracture strain of $\varepsilon = 1.0$.

SSAB claims the following characteristics of Hardox steels in their web pages; “It can take heavy blows without being deformed”, “It will resist cracks if subjected to plastic deformation” and “If a local crack should occur it will resist propagation” (SSAB, 2014). All

of these were found in the numerical results. In terms of workability, Hardox steel allows for welding with other steel types, free bending and roll-bending, hot and cold cutting, and machining. In other words, it is safe to assume that Hardox is compatible with conventional steels in terms of welding. Based on this, it can be possible to combine steel types for increased strength and lighter design.

Above all were the uncertainties due to material strain rate dependence. As expected, applying the Cowper – Symonds constitutive equation in the material formulation resulted in a significant increase in yield strength. The coefficients (C = 40.4 s^{-1} and q = 5) used for the initial configuration were considered unsuitable based on the previously presented (in Sec. 4.3.2), and conservatism.

To avoid any foregone conclusions, consequences from increasing structural stiffness (e.g. by changing material type or structural scantlings) should be evaluated. Alsos & Amdahl (2009) conducted panel penetration experiments, showing how contradictive material behaviour can be when dealing with ductile steels. They showed that increasing stiffeners or their dimensions, led to more localised deformations which in turn led to initiation of fracture at a decreasing level of energy absorption. Designing a structure to resist large deformations, may therefore pose unwanted weaknesses in terms of accidental load capability. Sometimes it is better to design a structure to be flexible (allowing for large plastic deformations) rather than stiff (posing weaknesses to sudden collapse or fracture), e.g. in the case of ship collision where penetration can result in flooding of hull compartments. This statement can be reversed by discussing the present study. A shallow penetration is more desired than a deep indentation, if the latter scenario causes damage to the LNG-fuel tank and the former does not.

This contradiction awakens the imagination to numerous thoughts on how to design hull structural components in the most diverse and functional way. What comes to mind are the seemingly endless possibilities of optimizing hull strength concerning structural scantlings, material properties, hull shape, load scenarios, etc. Various factors have been studied, e.g. by Ehlers (2010b) who conducted analyses to optimise ship sides for crashworthiness by testing different striking locations and numerous combinations of stiffeners per strake.

With this in mind, the comparison study presented in the current thesis is too narrow in proving whether Hardox steel provides for a better deck material.

Estimates of resistance force and energy dissipation were obtained using analytical methods. The plastic hinge method (presented in Sec. 5.2) provided poor representation of the deformation mechanisms in the PSV deck model, compared to the numerical model. It was discarded from further application as it overestimated the load capacity significantly. Folding mechanisms gave far better estimates and physical understanding, particularly in relation to the resistance of web girders subjected to in-plane loading. Evaluating the expressed plastic moment capacity (in Eq. (48)) in correlation with the two presented methods (in Sec. 5.3.2), it is apparent that the web thickness is a governing parameter in estimation of girder resistance. Hence, a study could be made on the advantages or disadvantages of increased girder thickness. Perhaps it's possible to obtain an even greater moment capacity by introducing stiffeners (vertical or horizontal) that are welded to the girder webs.

Finally, it is necessary to mention the principle of shared energy design as opposed to strength design. This was exemplified by using a deformable container in the FE simulation. This provided a tremendous amount of decrease in energy absorption; maximum energy dissipation was reduced by approximately 93 % in comparison with the rigid configuration. It's safe to say that this container design did not pose any threat to the deck. Even though it doesn't contribute to quantifying energy capacity of the deck, it reminds us that a dropped object load can come in all kinds of shapes, sizes, masses and velocities (e.g. as punctuated in the Introduction).

8 Conclusion

Based on the comparison of steel types, Hardox steel can be recommended for further investigation and possible application in ship design. It was shown (in Sec. 6.5.3) that the increase in penetration capacity was of significance using the obtained material parameters, and that it provided protection for the LNG-tank (as opposed to the as-built deck) in the proven worst case scenario. Further material definition should, however, be obtained to confidently predict a specific energy capacity to deck failure; including a well-documented fracture criterion and strain rate dependence.

The element length-related fracture criterion was considered well suited in prediction of fracture for the as-built steel configuration, and is recommended for further use. The Cowper-Symonds coefficients should be given values of C = 4000 and q = 5, based on previous studies by Alsos & Amdahl (2009), recommendations by DNV (2013b) and supporting evidence of these from the results in Section 6.3.1.

Based on the previous, the following can be recommended for future studies;

- Conduct (or obtain results from) tensile tests with Hardox steel specimens, with specific interest in the strain to fracture and strain rate sensitivity.
- Conduct drop tests on a deck model constructed with Hardox steel vs. conventional ship building steels. Compare with numerical results (e.g. obtained from the present study) using nonlinear FEA.
- Investigate possible statistics on the load – response relation due to dropped object loads, primarily to investigate damage extent of impacted vs. impacting structure. This is of specific interest due to the observed deformation of the container model in the present study.
- Optimisation of the PSV deck structural scantlings to minimise response due to dropped object loads; of particular interest is the effect of increasing web thickness or using additional vertical and/or horizontal stiffeners along girder webs to increase crushing resistance. This is of interest based on the shown correlation of folding mechanisms between analytical and numerical results.

- Analyse the aftermath following a dropped object load scenario with attention to hull strength. A specific study could deal with different location scenarios (as studied in the present thesis), comparing the criticality of diminished strength between stiffened deck plate and web girders.

9 Bibliography

Alsos, H. S. & Amdahl, J., 2009. On the resistance to penetration of stiffened plates, Part I - Experiments. *International Journal of Impact Engineering,* 36(6), pp. 799-807.

Alsos, H. S., Amdahl, J. & Hopperstad, O. S., 2009. On the resistance to penetration of stiffened plates, Part II: Numerical analysis. *International Journal of Impact Engineering,* 36(7), pp. 875-887.

Amdahl, J., 2010. *TMR 4167 Marine Technology 2, Part 1: Structural Analysis (Lecture Notes).* 3rd ed. Trondheim: Department of Marine Technology.

ASTM International, 2014. *ASTM E10 - 12 Standard Test Method for Brinell Hardness of Metallic Materials.* [Online]
Available at: http://enterprise.astm.org/filtrexx40.cgi?+REDLINE_PAGES/E10.htm
[Accessed 25 May 2014].

Berge, S., 2006. *Fracture Design of Welded Structures.* Trondheim: Marine Technology Centre.

Blikom, L. P., 2013. *Basics of LNG safety - DNV GL Blog.* [Online]
Available at: http://blogs.dnvgl.com/lng/2013/03/basics-of-lng-safety/
[Accessed 30 May 2014].

Bonora, N., 1997. A Nonlinear CDM Model for Ductile Fracture. *Engineering Fracture Mechanics,* 58(1), pp. 11-28.

Codecogs, 2014. *Plastic Theory of Bending - Materials - Engineering Reference with Worked Examples.* [Online]
Available at: http://www.codecogs.com/library/engineering/materials/plastic-theory-of-bending.php
[Accessed 3 June 2014].

Dassault Systèmes, 2012. *Abaqus 6.12 Online Documentation.* [Online]
Available at: http://www.tu-chemnitz.de/projekt/abq_hilfe/docs/v6.12/
[Accessed 13 May 2014].

Dassault Systémes, 2014. *Abaqus/CAE - Dassault Systémes.* [Online]
Available at: www.3ds.com/products-services/simulia/portfolio/abaqus/abaqus-portfolio/abaquscae/
[Accessed 16 May 2014].

DNV GL, 2014. *DNV GL Annual Report 2013,* Høvik: DNV GL AS.

DNV GL, 2014. *Sesam GeniE.* [Online]
Available at: http://www.dnv.com/services/software/products/sesam/sesam_genie/index.asp
[Accessed 17 May 2014].

DNV, 1999. *Classification Notes 31.3: Strength Analysis of Hull Structures in Tankers.* Høvik: Det Norske Veritas.

DNV, 2010. DNV-RP-C204: Design against Accidental Loads. In: *Recommended Practice.* Høvik: Det Norske Veritas.

DNV, 2012b. DNV-OS-C102: Structural Design of Offshore Ships. In: *Offshore Standards.* Høvik: Det Norske Veritas.

DNV, 2013a. DNV-OS-A101: Safety Principles and Arrangements. In: *Offshore Standards.* Høvik: Det Norske Veritas.

DNV, 2013b. DNV-RP-C208: Determination of Structural Capacity by Non-linear FE analysis Methods. In: *Recommended Practice.* Høvik: Det Norske Veritas.

DNV, 2013c. *Sesam User Manual GeniE Vol. III, Modelling of Plate/Shell Structures.* Høvik: Det Norske Veritas Software.

DNV, 2014. Gas Fuelled Ship Installations. In: *Rules for Classification of Ships.* Høvik: Det Norske Veritas.

Ehlers, S., 2010a. Strain and stress relation until fracture for finite element simulations of a thin circular plate. *Thin-Walled Structures,* 48(1), pp. 1-8.

Ehlers, S., 2010b. A procedure to optimize ship side structures for crashworthiness. *Proceedings of the Institution of Mechanical Engineers, Part M: Journal of Engineering for the Maritime Environment,* 224(1), pp. 1-11.

Fish, J. & Belytschko, T., 2007. *A First Course in Finite Elements.* 1st ed. Chichester: John Wiley & Sons Ltd..

FOREIGN TRADE ON-LINE™, 2013. *FOREIGN TRADE ON-LINE™.* [Online]
Available at: http://www.foreign-trade.com/reference/ocean.cfm
[Accessed 16 May 2014].

Haris, S. & Amdahl, J., 2012. An Analytical model to assess a ship side during a collision. *Ships and Offshore Structures,* 7(4), pp. 431-448.

Hogström, P., 2012. *RoPax Ship Collision – a Methodology for Survivability Analysis,* Gothenburg: Department of Shipping, Division of Marine Design, Chalmers University of Technology.

Hong, L. & Amdahl, J., 2008. Crushing resistance of web girders in ship collision and grounding. *Marine Structures,* 21(4), pp. 374-401.

Johnson, G. R. & Cook, W. H., 1985. Fracture Characteristics of Three Metals Subjected to Various Strains, Strain rates, Temperatures and Pressures. *Engineering Fracture Mechanics,* 21(1), pp. 31-48.

Moan, T., 2003. *TMR 4190 Finite Element Modelling and Analysis of Marine Structures.* Trondheim: Department of Marine Technology, NTNU.

Oil & Gas UK, HSE, 2009. *Accident Statistics for Offshore Units on the UKCS 1990-2007,* s.l.: Oil & Gas UK.

Paik, J. K., 2007. Practical techniques for finite element modeling to simulate structural crashworthiness in ship collisions and grounding (Part I: Theory). *Ships and Offshore Structures,* 2(1), pp. 69-80.

Rice, J. R. & Tracey, D. M., 1969. On the Ductile Enlargement of Voids in Triaxial Stress Fields. *Journal of the Mechanics and Physics of Solids,* 17(3), pp. 201-217.

Simonsen, B. C. & Ocakli, H., 1999. Experiments and theory on deck and girder crushing. *Thin-Walled Structures,* 34(3), pp. 195-216.

SSAB, 2011. *SSAB.* [Online]
Available at:
http://www.ssab.com/Global/Hardox/Datasheets/en/151_HARDOX_400_UK_Data%20Sheet.pdf
[Accessed 8 May 2014].

SSAB, 2014. *Hardox.* [Online]
Available at: www.hardox.com
[Accessed 7 May 2014].

Søreide, T. H., 1981. Beams under Transverse Loading. In: *Ultimate Load Analysis of Marine Structures.* Trondheim: Tapir, pp. 2.1-2.69.

Tvergaard, V., 1981. Influence of voids on shear band instabilities under plane strain conditions. *International Journal of Fracture,* 17(4), pp. 389-407.

Tvergaard, V. & Needleman, A., 1984. Analysis of the Cup-cone Fracture in a Round Tensile Bar. *Acta Metallurgica,* 32(1), pp. 157-169.

Törnqvist, R., 2003. *Design of Crashworthy Ship Structures, PhD Thesis,* Kongens Lyngby: Technical University of Denmark.

Weck, A., n.d. *Fracture & Femtosecond Research Ottawa Group.* [Online]
Available at: http://www.weck.ca/index.php?mode=7
[Accessed 16 May 2014].

Wärtsilä, 2013. *Offshore Support Vessels - From Design to Operation.* [Online]
Available at: http://www.wartsila.com/file/Norway/1278540320899a1267106724867-wartsila-sp-b-wartsila-offshore-osv.pdf
[Accessed 31 May 2014].

Zhang, S., 1999. *The Mechanics of Ship Collision, PhD Thesis,* Lyngby: Technical University of Denmark.

Appendix A: Hardox Steel Parameters

Hardox 400	
***E* [GPa]**	205
$\boldsymbol{\varepsilon_f}$ **[-]**	1.0
***ν* [-]**	0.3 (assumed)
$\boldsymbol{\rho}$ **[kg/m^3]**	7850 (assumed)
True strain [-]	**True stress [MPa]**
0	0
0,0041463	850
0,006988	1000
0,008142	1050
0,0099859	1100
0,0131398	1150
0,0187237	1200
0,0287276	1250
0,0465915	1300
0,0781454	1350
0,1330893	1400
0,2272532	1450
0,3861071	1500
0,650011	1550
1,0819249	1600

Appendix B: Structural Scantlings used in Sesam GeniE

Structural member type	Dimension [mm]
Web spacing	1200
Inner Deck (distance from CL: 0 mm – 3100 mm)	
Deck plate thickness	14
Stiffener spacing	300 – 350
Web beam height	550 – 600
Web beam thickness	15
Web beam flange width	250
Web beam flange thickness	25
Stiffener height	200
Stiffener thickness	9
Outer Deck (distance from CL: 3100 mm – 4900 mm)	
Deck plate thickness	12
Stiffener spacing	500 – 600
Web beam height	600
Web beam thickness	15
Web beam flange width	200 – 250
Web beam flange thickness	20 – 25
Stiffener height	220
Stiffener thickness	11.5

Bulkheads (2400 mm – 9000 mm ab.BL)	
Plate thickness (7500 mm – 9000 mm ab.BL)	10
Plate thickness (2400 mm – 7500 mm ab.BL)	6.5
Web beam height	250 – 350
Web beam thickness	10 – 12
Web beam flange width	150
Web beam flange thickness	12 – 15
Stiffener height	100
Stiffener thickness	8

Appendix C: Deck Deformation Mechanisms

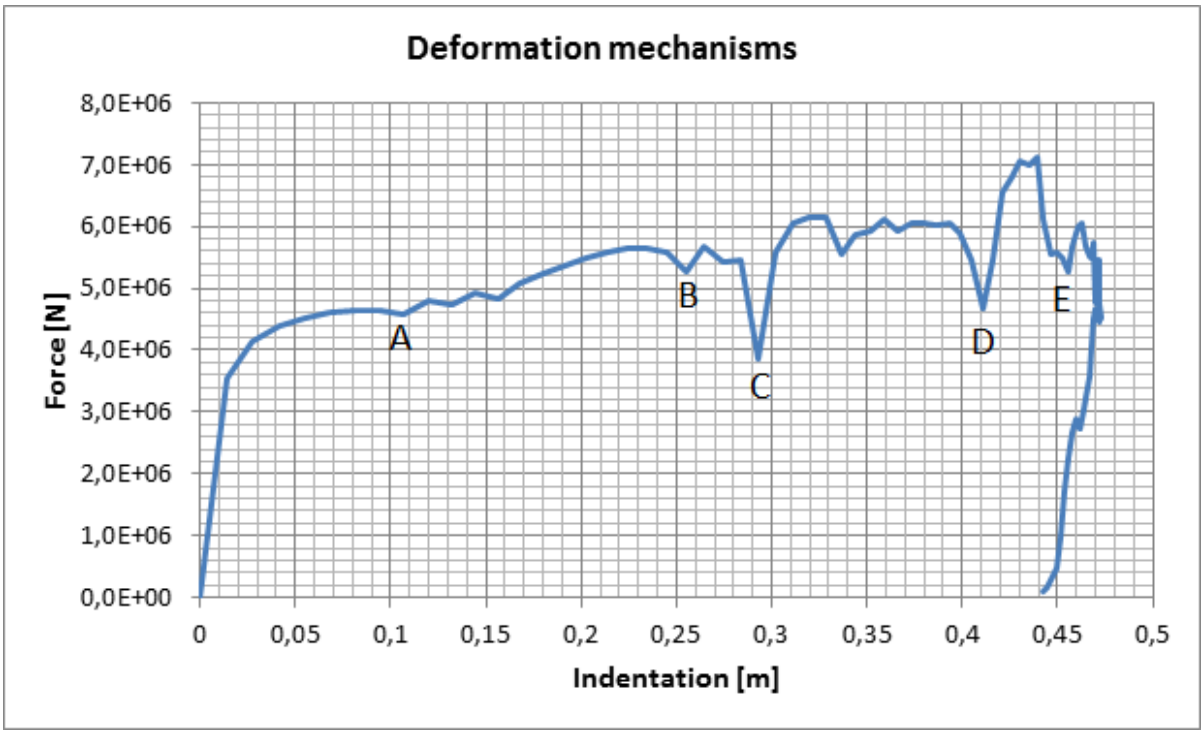

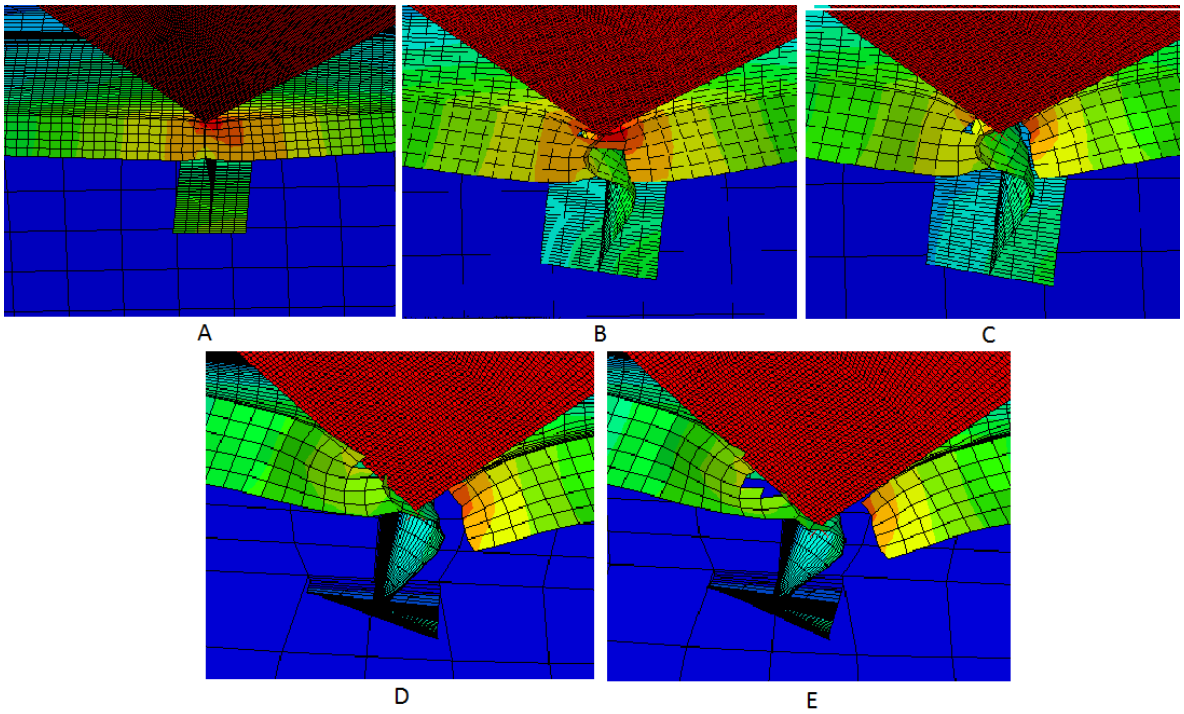

Appendix D: Structural Drawings

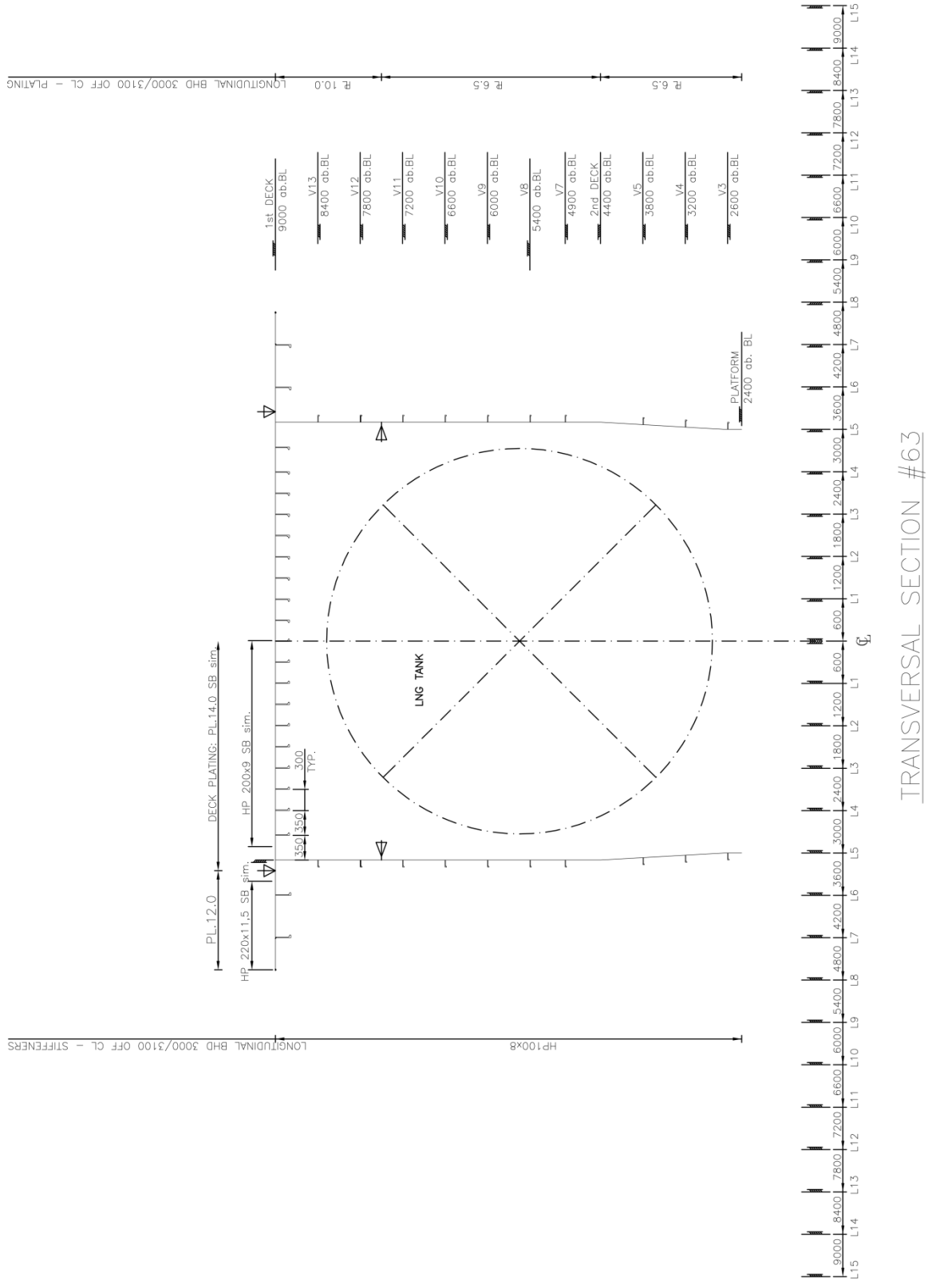

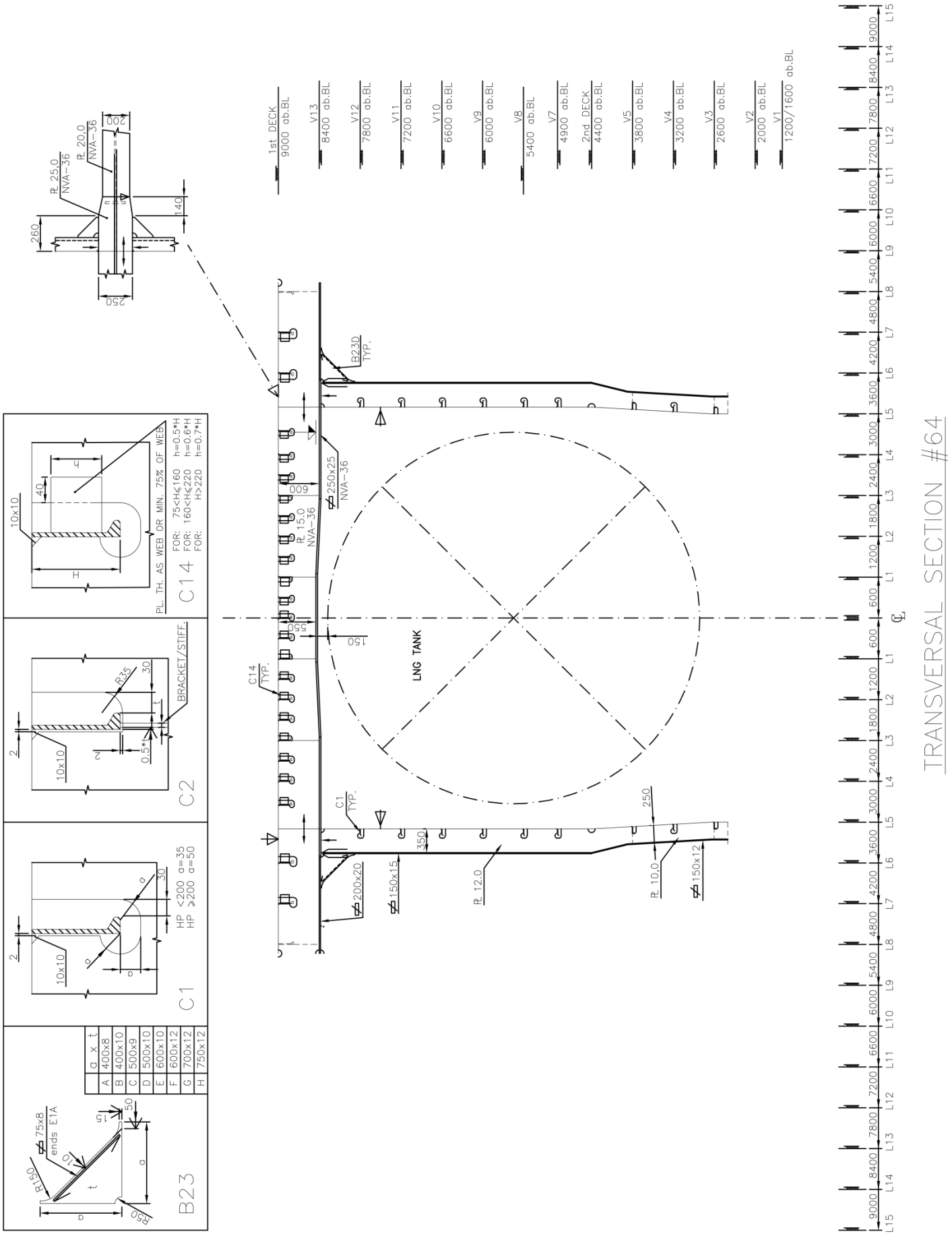
TRANSVERSAL SECTION #64
1st DECK 9000 ab.BL
V13 8400 ab.BL
V12 7800 ab.BL
V11 7200 ab.BL
V10 6600 ab.BL
V9 6000 ab.BL
V8 5400 ab.BL
V7 4900 ab.BL
2nd DECK 4400 ab.BL
V5 3800 ab.BL
V4 3200 ab.BL
V3 2600 ab.BL
V2 2000 ab.BL
V1 1200/1600 ab.BL
LNG TANK
B23D TYP.
C14 TYP.
C1 TYP.
250x25 NVA-36
R 15.0 NVA-36
200x20
150x15
150x12
R 12.0
R 10.0
R 25.0 NVA-36
R 20.0 NVA-36
B23
C1
C2
C14
BRACKET/STIFF.
PL. TH. AS WEB OR MIN. 75% OF WEB
FOR: 75<H≤160 h=0.5*H
FOR: 160<H≤220 h=0.6*H
FOR: H>220 h=0.7*H
HP <200 a=35
HP ≥200 a=50
a x t
A 400x8
B 400x10
C 500x9
D 500x10
E 600x10
F 600x12
G 700x12
H 750x12

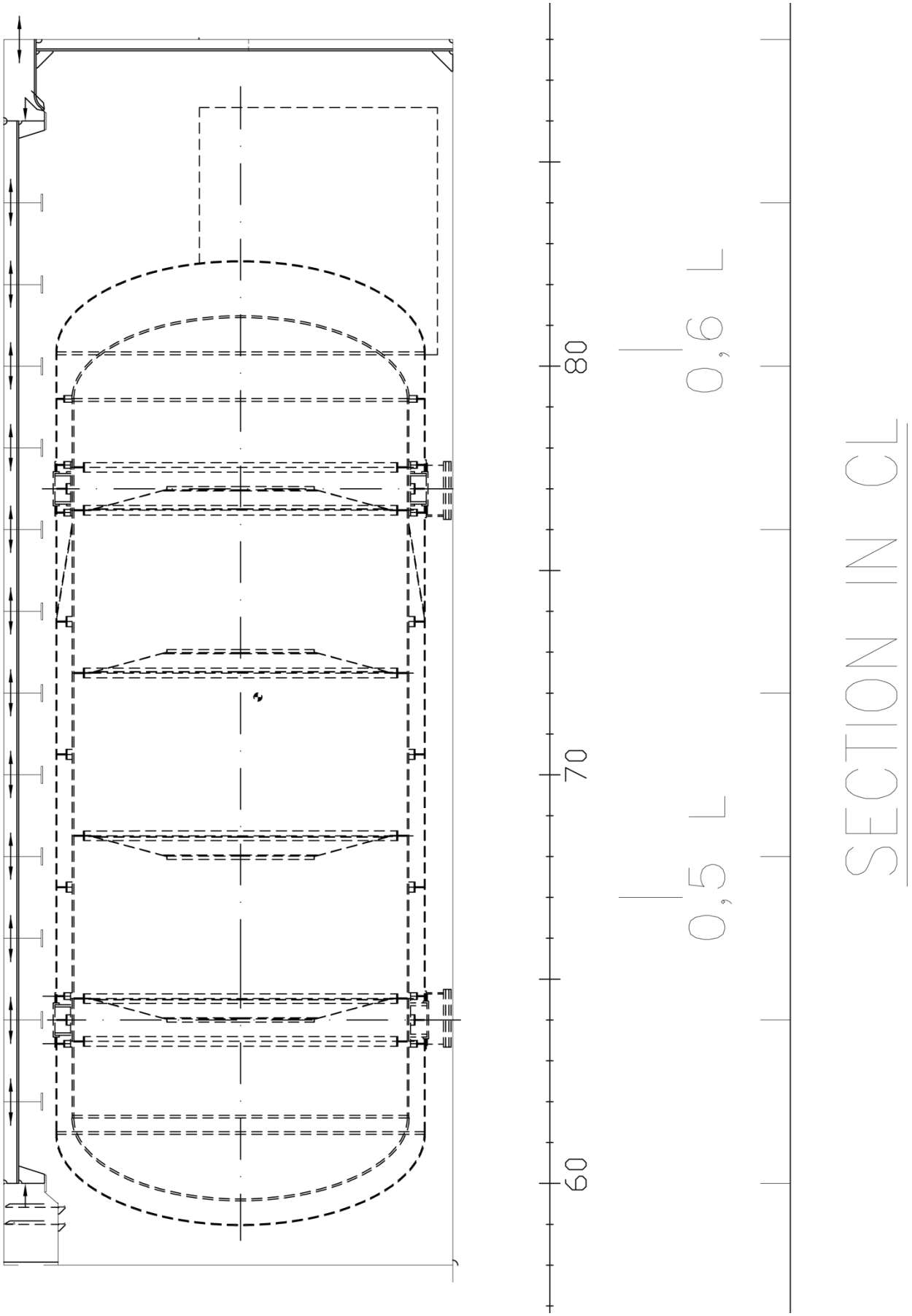
80
70
60
0,6 L
0,5 L
SECTION IN CL